UCLA

Structural & Geotechnical Engineering

Seismic Compression of Soils with Variable Levels of Fines Content and Fines Plasticity

Final Report

Jonathan P. Stewart
Pendo M. Duku
Daniel H. Whang

University of California, Los Angeles
Department of Civil and Environmental Engineering
5731 Boelter Hall
Los Angeles, California 90095-1593

Sponsor:
United States Geological Survey (USGS)

UCLA - SGEL
Report - 2007/01
March 2007

Seismic Compression of Soils with Variable Levels of Fines Content and Fines Plasticity

by

Jonathan P. Stewart, Pendo Duku and Daniel H. Whang
Department of Civil and Environmental Engineering
University of California, Los Angeles

A report on research conducted under Contract No. 05HQGR0050 by University of California, Los Angeles with funding provided by the United States Geological Survey (USGS)

USGS Report 2007

March 2007

ABSTRACT

Seismic compression is defined as the accrual of contractive volumetric strains in unsaturated soils during strong shaking from earthquakes, and has been recognized as a major cause of seismically induced damage (i.e., Stewart et al., 2001, 2004; Wartman et al., 2003). As a result, there has been an increasing demand within the engineering profession for seismic compression analysis procedures as evidenced by the California Geological Survey's (CGS) recent requirement that analysis of seismic compression be included as part of the design process for critical projects such as school and hospital structures (CGS, 2004). However, existing methods for estimating seismic compression susceptibility (Tokimatsu and Seed, 1987 and Stewart and Whang, 2003) are limited in their applicability because they only apply for a few specific soil characteristics.

A state-of-the-art cyclic simple shear apparatus was developed to facilitate soil testing to address this problem. The device is capable of applying multi-directional earthquake loading to soil specimens. This device, herein termed the Digitally Controlled Simple Shear (DC-SS) apparatus is capable of reproducing sinusoidal and broadband command signals across a wide range of frequencies and amplitudes. The device has limited control capabilities for very small command displacements (less than approximately 0.005 mm). The small-deformation limitation results from noise introduced to the control system from analog-to-digital conversion of feedback signals. We demonstrate that bi-directional command signals can be accurately imparted with minimal cross-coupling, which results from an innovative multiple-input, multiple-output digital control system.

Using the DC-SS apparatus, we investigate the volume change of 14 clean sands subjected to cyclic loads. We examine the effects of compositional and environmental factors on the vertical strain at 15 uniform shear strain cycles and on the cycle-to-cycle variation of vertical strain. The compositional factor found to principally affect seismic compression susceptibility was relative density (D_R). Compositional factors found to not significantly affect cyclic volume change include gradation parameters (mean grain size, uniformity coefficient), particle angularity, soil fabric, mineralogy, and void ratio "breath" e-e_{min}. An environmental factor found to affect seismic compression susceptibility was confining stress, with volumetric strains decreasing with increasing stress. Based on these findings, an empirical model is developed to represent the

major trends of the data for application in engineering practice, which improves upon an earlier model that is based on a much smaller database and which does not account for the aforementioned environmental factors.

Additionally, we investigate seismic compression of non-plastic silty sands by testing eight materials that span a range of fines content ($10 \leq FC \leq 50\%$). The tests are performed using artificial mixtures of sand-silt mixtures prepared to a range of relative compaction (*RC*) and degree-of-saturation (*S*). The silt is comprised predominantly of quartz and is truly non-plastic (i.e., unmeasureable plastic limit) with liquid limit <~ 17. We make significant new findings with respect to saturation and fines content. The effect of intermediate saturation ($S \approx 30\%$) decreases vertical strains relative to values for dry or high saturation ($S \geq 60\%$); this condition appears to be related to high matric suction in materials with intermediate saturation. On the other hand, increasing FC increases seismic compression susceptibility for a fixed relative compaction. This finding is strongly dependent on the non-plastic nature of the fines, and previous studies suggest an opposite trend for soils with plastic fines.

We investigate the seismic compression of soils with plastic fines by testing five materials which span a range of plasticity index (PI = 0 – 33). These materials are tested at a range of relative compaction (*RC* = 80 – 92%) and saturation (*S* = 50 – 90). The primary factors that affect seismic compression of soils with plastic fines are as-compacted saturation (*S*) and relative compaction (*RC*), plasticity index (PI), and pseudo-overconsolidation from ageing. Vertical strain decreases with increase in relative compaction and plasticity index. Vertical strains are significantly smaller for materials compacted on the dry side of the line of optimums than materials compacted on the wet side due to a clod-like fabric that forms on the dry side that is absent on the wet side. Ageing of medium to high plastic soils leads to pseudo-overconsolidation (*OC*) which significantly reduces the seismic compression susceptibility of the *OC* soil relative to an otherwise similar normally consolidated (*NC*) soil.

ACKNOWLEDGMENTS

Support for this work was provided by the U.S. Geological Survey (USGS), Department of the Interior, under USGS award No. 05HQGR0050. The views and conclusions contained in this document are those of the authors and should not be interpreted as necessarily representing the official policies, either expressed or implied, of the U.S. Government.

The authors would like to thank the following individuals who provided materials that were of assistance in this research program: Nirun Tungkongphanit of URS Consultants and Debanik Chaudhuri of Exponent Consultants. We acknowledge the technical assistance to the laboratory testing program provided by Patrick Smith of Fugro West Consultants, and the supportive work of graduate students Mathew Moyneur and Lisa Coyne.

TABLE OF CONTENTS

ABSTRACT ..... **ii**

ACKNOWLEDGMENTS ..... **iv**

TABLE OF CONTENTS ..... **vi**

LIST OF FIGURES ..... **x**

LIST OF TABLES ..... **xiii**

1 INTRODUCTION **1**

1.1 Compacted Structural Fills 1

1.2 Observed Behavior of Structural Fills during Earthquakes 2

1.3 Motivation and Objectives of Present Study 8

2 DIGITALLY CONTROLLED SIMPLE SHEAR APPARATUS FOR DYNAMIC SOIL TESTING **11**

2.1 Introduction 11

2.2 Physical Description of DC-SS Device 13

2.3 DC-SS Control System 19

2.4 DC-SS System Performance 22

2.4.1 Sinusoidal Tracking 23

2.4.2 Broadband Command Signal Tracking 27

2.5 Example Test Result for Dry Clean Sand 32

2.6 Summary and Conclusions 33

3 VOLUMETRIC STARINS OF CLEAN SANDS SUBJECTED TO CYCLIC LOADS **35**

3.1 Introduction 35

3.2 Soils Tested 38

3.3 Laboratory Equipment and Test Protocols 40

3.4 Test Results 42
3.4.1 Form and Parameterizations 42
3.4.2 Effects of Relative Density 45
3.4.3 Effects of Saturation, Loading Frequency and Compositions 49
3.4.4 Effects of Overburden Pressure 52
3.4.5 Effects of Stress History 56
3.4 Discussion and Conclusion 57

4 SEISMIC COMPRESSION OF NON-PLASTIC SILTY SAND 59

4.1 Introduction 59
4.2 Soils Tested 60
4.3 Laboratory Testing and Equipment Protocols 61
4.4 Results of Cyclic Simple Shear Tests 62
4.4.1 Form and Parameterization of Results 62
4.4.2 Effect of Density 64
4.4.3 Effect of Saturation 65
4.4.4 Effect of Fines Content 68
4.4.4.1 Overview and Concept of Limiting Fines Content 68
4.4.4.2 Seismic Compression Test Results and Interpretation 70
4.4.4.3 Comparison to Previous Studies 72
4.4.5 Effect of Number of Cycles 73
4.5 Conclusions 74

5 PLASTIC AND NON-PLASTIC SOILS 77

5.1 Introduction 77
5.2 Literature Review 77

5.3 Testing Performed in Present Research 83
5.3.1 Testing Protocols 83
5.3.2 Soils Tested 83
5.4 Test Results 88
5.4.1 Test Results for Fine-Grained Plastic Soils 88
5.4.2 Seismic Compression of Pseudo-Overconsolidated (Aged) Soils 92
5.5 Summary and Recommendations 96

6 SUMMARY 99
6.1 Scope of Research 99
6.2 Research Findings and Recommendations 100

REFERENCES 103

LIST OF FIGURES

Figure 1.1 Typical geometries of compacted fills 2

Figure 1.2 Site locations where fill movements caused significant damage during Northridge earthquake 3

Figure 1.3 Schematic showing typical damage to fill slope 5

Figure 1.4 Plan view of subdivision showing fill and cut zones and locations of damaged water pipes and structures 7

Figure 2.1 Schematic of the UCLA DC-SS Device 15

Figure 2.2 (a) Photograph of the UCLA DC-SS; (b) a close view of the tri-post frame, top adaptor plate, and LVDT to measure settlement (c) specimen confined by a wire-reinforced membrane covered at the top and bottom by caps which fit in the recess on the top and bottom adaptor plates 15

Figure 2.3 Tripartite plot demonstrating the theoretical limitations of the UCLA DC-SS device 18

Figure 2.4 Layout of the different elements of the UCLA DC-SS device 20

Figure 2.5 Controller architectures for (a) independent PID controller, and (b) MIMO-PID controller 21

Figure 2.6 Sinusoid tracking of cyclic displacement amplitudes = 0.2 and 0.012 mm at f = 1 Hz for shearing along one axis at a time and noise level with pump on and off (MIMO controller) 23

Figure 2.7 Variation of normalized root mean square of tracking errors for uni-directional shaking with (a) displacement amplitude and (b) loading frequency 25

Figure 2.8 Normalized root mean square of tracking errors on baseline axis for varying frequencies of excitation on perpendicular axis (PID and MIMO-PID controllers 27

Figure 2.9 Reproduction of recorded history for shearing on one axis at a time (i.e., without interaction effects; MIMO-PID controller) 29

Figure 2.10 Distribution of values of noise feedback signal with pump on and zero command signal (D_N) along with normal probability distribution fit to the data 30

Figure 2.11 Normalized root mean square of tracking errors for uni-directional and multi-directional broadband command signals of different amplitude. Multi-directional command is with both PID and MIMO-PID control 31

Figure 2.12 Comparison of vertical strains of a clean sand confined at 101.3 kPa to a comparable relative density. Soil was sheared uni-directionally and bi-directionally, respectively 33

Figure 3.1 Comparison of Silver and Seed (1971) and Youd (1972) test results for clean sands tested under strain-controlled conditions 37

Figure 3.2 Gradation curves for the fourteen tested sands 39

Figure 3.3 Typical cyclic simple shear test results (Silica No. 2 Sand, D_R = 60%, and S = 0% 43

Figure 3.4 Volumetric strain material models summarizing test results, (a) $\varepsilon_{v,N=15}$ versus γ_c relationship and (b) $\varepsilon_v/\varepsilon_{v,N=15}$ versus N 45

Figure 3.5 Relationship between slope parameter b and D_R, where b is from the simultaneous regression of slope and intercept parameters reported in column A of Table 3.3 46

Figure 3.6 Relationship of intercept parameter a and D_R; where a is from regression with b = 1.1, column B of Table 3.3 47

Figure 3.7 (a) Residuals of $\varepsilon_{v,N=15}$ versus γ_c, and (b) the distribution of the normalized residuals with COV = 0.34 48

Figure 3.8 (a) Comparison of data to model for D_R = 60%. (b) Plot of mean model prediction compared to previous study of Silver and Seed (1971) at D_R = 45, 60, and 80%. 48

Figure 3.9 Trend of slope parameter (R) versus D_R 49

Figure 3.10 Results of testing that demonstrates the lack of effect of saturation and loading frequency on vertical strains from seismic compression 50

Figure 3.11 Results of testing that demonstrates data trends with respect to (a) method of sample preparation, (b) D_{50} (mean diameter), (c) C_u (coefficient of uniformity), (d) S_{avg} (average shape factor), and (e) (e - e_{min}). 51

Figure 3.12 (a) Effect of overburden pressure on vertical strains from seismic compression of Silica No. 2 sand at D_R = 60-63%; (b) Overburden correction factor $K_{\sigma,a}$ derived using the data from (a); (c) mean power law fits for two sands at two D_R levels; and (d) recommended overburden correction factor derived from combined data with error term. 53

Figure 3.13 (a) Equivalent values of *CSR* for different shear strain levels in strain-controlled tests; (b) effective K_σ values at N = 1 and 15; (c) comparison of results to previous studies 55

Figure 3.14 *OCR* effect for Silica No. 2 with baseline σ_v = 1.0 atm (a) at D_R = 60-63%, (b) at D_R = 80-82%, and (c) *OCR* effect for Silica No. 2 at D_R = 60-63% and σ_v = 0.5 atm. 57

Figure 4.1 Volumetric strain model (Vulcan 50-50 mix) 64

Figure 4.2 Effect of density on Vulcan 50-50 mix at S = 30% 65

Figure 4.3 Effect of saturation on Vulcan 50-50 mix(a) *RC* = 87% and (b) *RC* = 92% 66

Figure 4.4 Variation of normalized seismic compression with saturation 67

Figure 4.5 Variation of matric suction and shear modulus with saturation 68

Figure 4.6 Index void ratios at *RC* = 87% for (a) Vulcan and (b) Silica No. 2 host sands 70

Figure 4.7 Effect of silt content on compression behavior of Vulcan host sand 71

Figure 5.1 Relationship between shear strain and vertical strain at N = 10 cycles for fill material at Jensen Filtration Plant 78

Figure 5.2 The effect of w on settlement a low plasticity clay for N = 3, 10, and 40 cycles 79

Figure 5.3 Seismic compression test results for low-plasticity silty sand 82

Figure 5.4 Seismic compression test results for medium-plasticity clayed sand 82

Figure 5.5 Grain size distribution for the tested plastic clay soil 84

Figure 5.6 Results of Atterberg limits tested for the clayed sand 85

Figure 5.7 Modified Proctor compaction curve for the clayed soil 85

Figure 5.8 Grain size distribution for Westlake materials tested 86

Figure 5.9 Atterberg test for Westlake materials with USCS classification shown in parenthesis 87

Figure 5.10 Compaction curves for Westlake materials tested together with ZAV (Zero Air Voids) curve and LOO (Line Of Optimum) 87

Figure 5.11 (a) Effect of plasticity index on seismic compression, (b) saturation dependence for PI = 15 soil, and (c) saturation dependence for PI = 27 soil 89

Figure 5.12 Seismic compression of Westlake A confined at 0.25 atm compacted to RC = 88% at S = 65% 89

Figure 5.13 Seismic compression of Westlake B1 confined at 0.50 atm compacted to RC = 88% at S = 89% 90

Figure 5.14 Seismic compression of Westlake B2 confined at 0.50 atm compacted to different RC at different S 91

Figure 5.15 Seismic compression of Westlake C confined at 0.25 atm compacted to RC = 82% at S = 75% 91

Figure 5.16 Material A (a) static consolidation and (b) seismic compression test results 93

Figure 5.17 Material B2 (a) static consolidation and (b) seismic compression test results 94

Figure 5.18 Effects of ageing on seismic compression of plastic soils 95

Figure 5.19 Seismic compression behavior of fine grained soils with measurable plasticity ... 97

LIST OF TABLES

Table 1.1 Damage statistics for subdivisions as function of site condition. Indicated are numbers (and percentages in parentheses) of lots within each site category with different damage levels 6

Table 3.1 Indices of soils tested in published and unpublished studies 36

Table 3.2 Soil indices for current study (Saturation [S = 0%]) 39

Table 3.3 Volumetric strain material model ($\varepsilon_{v,N=15}$) regression constants for all sands tested 46

Table 3.4 Parameters used for evaluating overburden effects 52

Table 3.5 Parameters used for evaluating stress history 56

Table 4.1 Soils tested 61

Table 5.1 Soil indices and test conditions 84

Table 5.2 Test results for materials tested to investigate the effects of ageing 95

1 INTRODUCTION

1.1 COMPACTED STRUCTURAL FILLS

Structural fills are earth structures that are placed to create level building pads for building construction. In hillside areas, these fills are generally constructed in wedge shapes and placed along hillsides (as shown in Figure 1.1a) or are placed in canyons (Figure 1.1b).

There are a number of processes that can lead to deformations of compacted structural fills. Static, long-term processes include hydro-compression, consolidation, and slope creep (e.g., Lawton et al., 1989; Brandon et al., 1990). Seismic processes include seismic slope instability and seismic compression (e.g., Stewart et al., 2001). Deformations resulting from the above processes can be damaging to the building structures, and hence engineers generally design fills so as to minimize future ground deformations. Such analysis procedures are well developed for static processes (e.g., Houston et al., 1988 for hydro-compression), but significant work remains to be done before reliable ground deformation analysis procedures can be developed for seismic applications.

The focus of our research is on seismic compression, which is defined as volumetric strain accumulation in unsaturated soil during earthquake shaking. Seismic compression only occurs in compacted fills whose voids are not fully filled with water (unsaturated); when such soils experience seismically induced shear deformations, the soil grains tend to settle into a denser configuration.

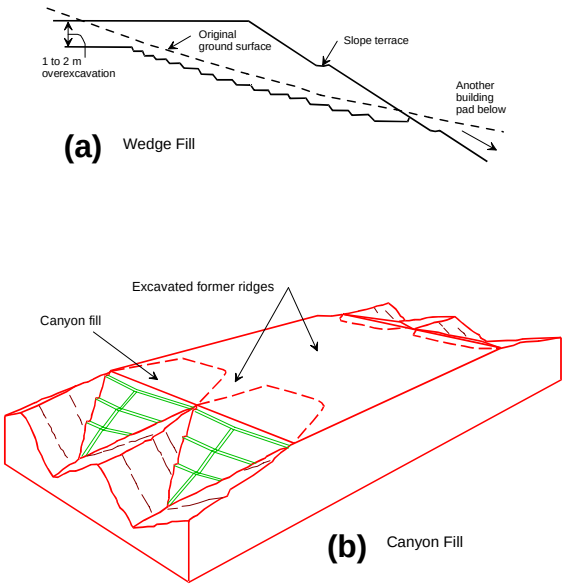

Fig. 1.1. Typical geometries of compacted fills.

1.2 OBSERVED BEHAVIOR OF STRUCTURAL FILLS DURING EARTHQUAKES

The performance of structural fills during earthquakes has been documented both in general field reconnaissance and in detailed studies of specific sites. The reconnaissance work involves observing the general characteristics of ground deformations across many sites. The detailed studies involve more intensive examination of the geotechnical and damage characteristics at a few specific sites.

The performance of structural fills during earthquakes has been documented following the 1906 San Francisco, 1971 San Fernando, and 1994 Northridge earthquakes. Lawson (1908) summarized observations of ground cracking in hillside areas from the 1906 San Francisco earthquake by noting "roadways and artificial embankments were particularly susceptible to … cracks." After the 1971 San Fernando earthquake, McClure (1973) noted the influence of fills on damage patterns, particularly when residences were constructed over cut/fills contacts. This study found that "…ground failure occurred on a higher percentage of sites that were on fill or

cut and fill than those sites which were on cut or natural grade" and "dwellings on cut and fill or fill had more relative damage than dwellings on cut or natural grade."

After the 1994 Northridge earthquake, Stewart et al. (2001) documented locations of about 250 sites where fill movements caused damage. As shown in Figure 1.2, concentrated damage occurred on the north flank of the Santa Monica Mountains, along the north rim of the San Fernando Valley, and in the Santa Clarita Valley area. Other affected areas include the south flank of the Santa Monica Mountains and portions of Simi Valley.

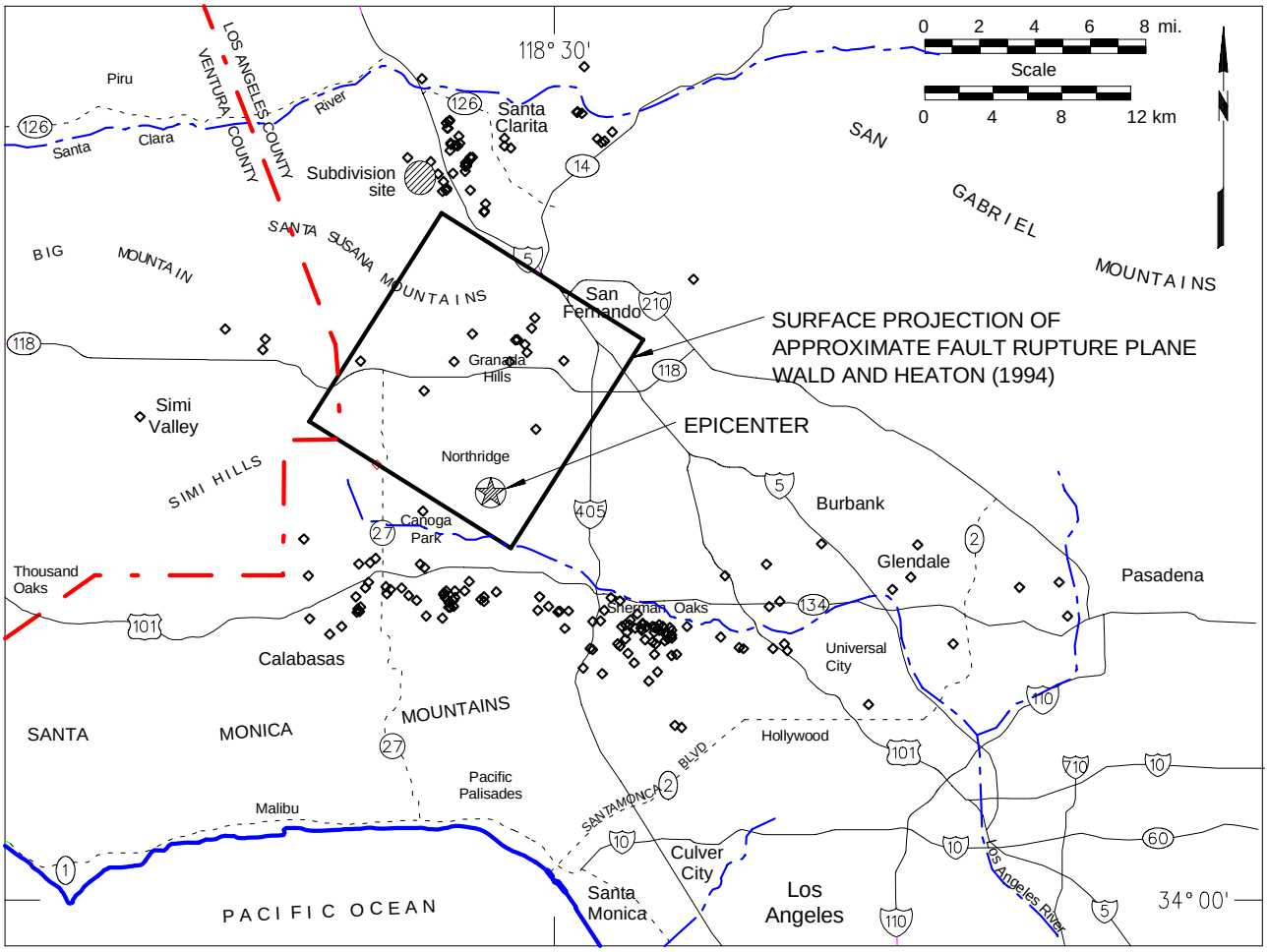

Fig. 1.2. Site locations where fill movements caused significant damage during Northridge earthquake (Stewart et al., 2001).

The data in Figure 1.2 can be used to roughly evaluate the levels of shaking that were required during the Northridge earthquake for seismic compression of fills to be a significant problem. Areas with significant damage such as Sherman Oaks, the northern San Fernando Valley, and Santa Clarita had peak accelerations in the range of 0.4 to 0.8 g (Chang et al., 1996), whereas outlying areas where incidents of seismic compression induced damage are relatively sparse (e.g., Calabasas, Universal City) had levels of shaking < 0.4 g. Based on analyses of typical fill geometries reported in Stewart et al. (2001), approximate levels of peak shear strain corresponding to those acceleration levels are generally on the order of > 0.1% in the areas with damage and < 0.1% in areas without significant damage. Those shear strain levels can be contrasted with volumetric threshold shear strains (i.e., the shear strains below which no volume change would be expected of $\gamma_{tv} \approx$ 0.01-0.02% for sands and $\gamma_{tv} \approx$ 0.04-0.09% for clays having PI ≈ 30 (Hsu and Vucetic, 2004).

As seen in Figure 1.3, typical damage patterns at the mapped fill deformation sites included:

- Cracks near cut/fill contacts: typically caused < 8 cm of lateral extension and 3 cm of localized differential settlement relative to cut
- Lateral extension in fill pad: observed in the form of tensile cracking parallel to the top of the slope, which typically caused 3-10 cm of horizontal or vertical offsets.
- Differential settlement on fill surfaces: observed as cracks with vertical offsets and tilted floors and swimming pools.
- Slope-face bulging: characterized by movement of surface drains running cross-slope (terrace drains) and down-slope (down drains).

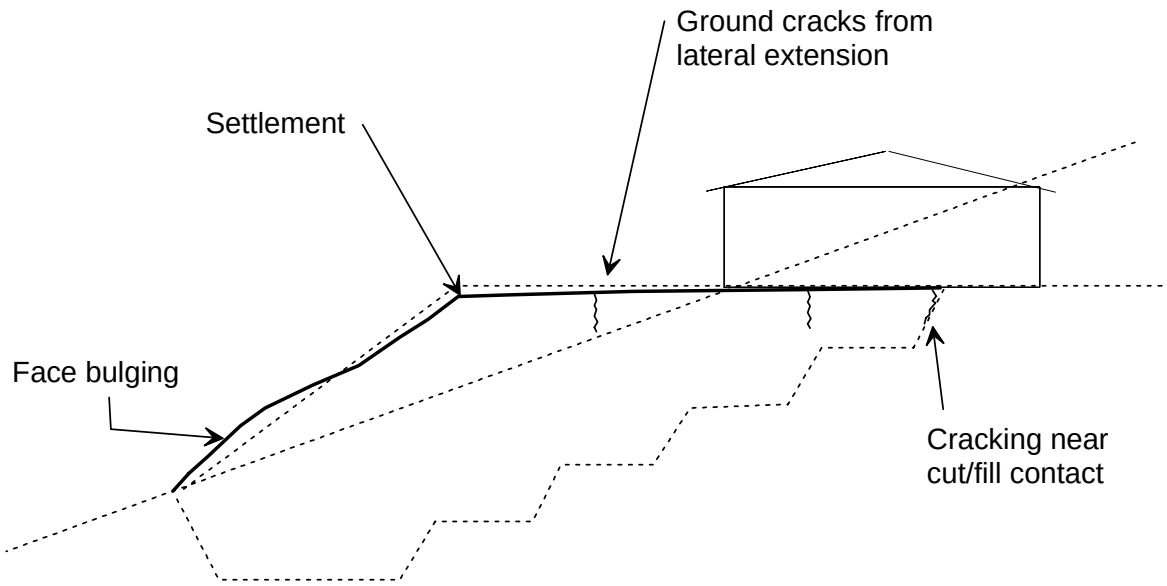

Fig. 1.3. Schematic showing typical damage to fill slope (Stewart et al., 2001).

In order to objectively evaluate the significance of fill site conditions on damage patterns, Stewart et al. (2001) compiled a complete inventory of damage within a subdivision with both fill and cut sites. By comparing damage patterns for the two site conditions, an objective assessment of the impact of fill materials on site performance can be made. A map of the subdivision is shown in Figure 1.4. As shown in the figure, all broken water pipes are on fill near the cut/fill contact area. Moreover, damage to structures is indicated with the red, yellow, green, and white colors in Figure 1.4 (red being the most severe damage, and white corresponding to no damage). The relative frequencies of the damage levels are summarized in Table 1.1, which shows much more severe damage on fill and cut/fill sites that on cut sites.

Table 1.1. Damage statistics for subdivisions as function of site condition. Indicated are numbers (and percentages in parentheses) of lots within each site category with different damage levels.

Site Condition	No Damage* (0)	Cosmetic Damage* (1)	Moderate Damage* (2)	Major Damage* (2)	Total
Cut	193 (77%)	49 (20%)	3 (1%)	5 (2%)	250
Cut/Fill	159 (66%)	60 (25%)	11 (4%)	12 (5%)	242
Fill	100 (65%)	39 (25%)	8 (5%)	7 (5%)	154
All lots	452 (70%)	148 (23%)	22 (3%)	24 (4%)	646

* 0. No damage. No observed distress, or no homeower request for inspection.

1. Cosmetic damage. Cracks in walls and ceilings that do not threaten structural integrity.
2. Moderate damage. Cosmetic damage + damaged roof, chimney, floors, windows, or plumbing suggesting some ground deformation or intense shaking.
3. Major damage. Moderate damage + cracked foundation and displacements observed in soil, suggesting significant ground deformatiion.

Fig. 1.4. Plan view of subdivision showing fill and cut zones and locations of damaged water pipes and structures (Stewart et al. 2001).

In addition to the above, there have been several detailed studies of specific sites subject to seismic compression. In each case, ground settlements caused by seismic compression were measured with pre- and post-earthquake surveys. The studies include a (1) 17 m thick fill that experienced 9-10 cm of settlement from seismic compression during the 1971 San Fernando earthquake (Pyke et al., 1975), (2) a fill up to 24 m thick that experienced up to 20 cm of settlement during the 1994 Northridge earthquake (Stewart et al., 2004), and (3) a fill up to 30.5 m thick that experienced up to 6 cm of settlement during the Northridge earthquake (Stewart et al., 2004).

1.3 MOTIVATION AND OBJECTIVES OF PRESENT STUDY

Largely because of the significant damage that occurred to structures as a result of seismic compression induced by the 1994 Northridge earthquake, there is increasing demand within the engineering profession for seismic compression analysis procedures. For example, in their report to the Governor of California following the 1994 Northridge earthquake, the California Seismic Safety Commission (SSC) recommended that "Seismically induced deformation caused by seismic compaction of fill and underlying alluvium (should) be considered in the design and construction of residential fills." More recently, the California Geological Survey (CGS) has required analysis of seismic compression as part of the design process for critical projects such as school and hospital structures (CGS, 2004).

The state-of-practice method for seismic compression analysis consists of a procedure by Tokimatsu and Seed (1987), which is intended for application to clean sands. The principal reason that the procedure is only applicable to clean sands is that a key component of the

procedure that relates shear strain demand and number of strain cycles to volumetric strains (herein termed a volumetric strain material model) is based solely on laboratory test data for clean sands by Silver and Seed (1971). The procedure has recently been extended to soil with large fines content and low plasticity by Stewart and Whang (2003), and both procedures are recommended for application by CGS (CGS, 2004). However, these two procedures remain extremely limited in their applicability, because they only apply for a few specific soil characteristics, and thus they are not broadly applicable. Accordingly, there is a major research need for laboratory testing to establish volumetric strain material models that cover a broad range of soil types and environmental conditions. The principal objectives of this research are to perform the necessary testing for a diverse array of soils and to develop from those results volumetric strain material models that can be used in practice.

The remainder of this report is organized into five chapters. Chapter 2 describes the capabilities of the UCLA-DCSS device, which has been developed as a state-of-the-art research tool. Chapters 3 – 5 describe the results of testing programs that investigated the seismic compression behavior of clean sands, sands with non-plastic fines, and high fines content/high plasticity materials, respectively. Chapter 6 summarizes our findings and presents recommendations for application and further research.

2 DIGITALLY CONTROLLED SIMPLE SHEAR APPARATUS FOR DYNAMIC SOIL TESTING

2.1 INTRODUCTION

Direct simple shear apparatuses have been utilized successfully for many years to characterize static and dynamic soil properties. This method of testing is often preferred when it is desirable for the specimen to experience a smooth and continuous rotation of the principal stress directions during shear. Initial stresses can be applied to simulate at-rest field conditions when wire-reinforced membranes are utilized that minimize lateral distortion of the sample (i.e., the NGI-type configuration, Bjerrum and Landva, 1966). Perhaps the most common application of simple shear testing has been for the simulation of vertical (or nearly vertical) shear wave propagation through a soil column. Advantages and limitations of simple shear tests relative to other types of laboratory tests have been described elsewhere and are not repeated here (e.g., Lucks et al., 1972; Shen et al., 1978; Saada et al., 1982; Vucetic and Lacasse, 1982; Budhu, 1985; Bhatia et al., 1985; Amer et al., 1987; Airey and Wood, 1987; Budhu and Britto, 1987; Boulanger et al., 1993).

Most simple shear apparatuses operate in a single horizontal direction and apply harmonic loading at frequencies which are typically slower than dynamic processes such as earthquake shaking (e.g., Tatsuoka and Silver, 1981; Doroudian and Vucetic, 1995; Lefebvre and Pfender, 1996; Riemer and Seed, 1997; Kusakabe, 1999; Hazirbaba and Rathje, 2004). While there are

always approximations involved in applying soil properties measured in the laboratory to field conditions, the inability of existing devices to provide rapid, multi-directional loading introduces further errors of unknown significance when laboratory-measured soil properties are used in engineering simulations.

A number of simple shear apparatuses have been developed to investigate soil response to multi-directional loading (e.g., Ishihara and Yamazaki, 1980; Boulanger et al., 1993; DeGroot et al., 1996). The University of California, Berkeley bi-directional cyclic simple shear (UCB-2D) device is noteworthy since it significantly reduced mechanical compliance issues that caused relative top/base cap rocking in earlier devices (e.g., Ishihara and Yamazaki, 1980; Ishihara and Nagase, 1988). Another significant feature of the UCB-2D device is chamber pressure control, which facilitates back-pressure saturation.

The principal limitation of the UCB-2D device, and earlier devices, is their inability to apply earthquake-like broadband loading at rapid displacement rates. This limitation also exists for most uni-directional simple shear devices. The reasons for this are twofold: (1) pneumatic loading systems use a compressible fluid (i.e., air) which introduces significant errors to the feedback loop at high frequencies; and (2) digitally-supervised analog controllers were employed which effectively limit the processing speed and sophistication of the control algorithms. Of course, shaking table and centrifuge experiments are capable of applying multi-directional earthquake-like loading to soil models (i.e., Pyke et al., 1975; Jafarzadeh and Yanagisawa, 1998; Kutter, 1995; Wilson et al., 2004). However, direct measurements of the soil element response (e.g., shear stress-shear strain relationships, volumetric strain and pore water pressure) in these types of experiments requires dense instrumentation arrays that can affect the response they are intended to measure, which in turn complicates data interpretation (e.g., Elgamal et al., 2005).

The capability of applying, with a reliable degree of control, multi-directional loading across a wide range of frequencies to soil elements in the laboratory is critical to advancing our fundamental understanding of dynamic soil properties. For example, broadband loading capabilities are needed to investigate rate effects on soil properties, which are known to be significant for clays (e.g., Lefebvre and Pfender, 1996; Sheahan et al., 1996). Moreover, the effect of shear rate and 2D loading on pore pressure generation and/or volume change behavior is less well understood and requires further investigation for some soil types. To meet these research needs, a digitally controlled simple shear device with capabilities for chamber pressure control and multi-directional excitation has been developed. This device, herein termed the Digitally Controlled Simple Shear (DC-SS) apparatus incorporates features such as servo-hydraulic actuation and true digital control to overcome the limitations of previous dynamic soil testing machines. The result is a truly unique simple shear apparatus with the capability to apply broadband (earthquake-like) displacement demands on soil specimens in two directions and with minimal cross-coupling between the horizontal motions. In this chapter, we describe this device and its capabilities for dynamic soil testing.

2.2 PHYSICAL DESCRIPTION OF DC-SS DEVICE

The mechanical design of the DC-SS device was developed using the UCB-2D device as a prototype (Boulanger et al., 1993). The DC-SS device was designed to retain the main features of the UCB-2D device such as inclusion of cell pressure for purposes of backpressure saturation, limited mechanical compliance with respect to simple shear boundary conditions (e.g. top and base platen "rocking") and bi-directional loading capability. In addition to these features, the DC-SS device incorporates several design improvements relative to the UCB-2D device including: (*i*) the use of a tri-post frame with high performance track bearings (which

accommodate vertical displacements of the top cap) to further reduce rocking; (*ii*) a servo-hydraulic control system to allow for high frequency loading; and (*iii*) a dual axis load cell to obtain post-friction shear load measurements.

Figure 2.1 shows the general assembly of the DC-SS apparatus. Photographs of the DC-SS device are shown in Figure 2.2. The DC-SS device was designed to test cylindrical soil specimens with a diameter of 10.2 cm or less. The specimen is located between relatively rigid bottom and top caps (Figure 2.1, Figure 2.2b) and is typically confined by a wire-reinforced membrane. As shown in Figure 2.2c, the horizontal (top and bottom) faces of the specimen are confined by the caps, which contain fine porous stones epoxied into a recess covering the entire face of the cap except for a retaining lip of aluminum around the edge. These caps provide a "frictional" surface while allowing for drainage into the porous stones if the stones are unsaturated (the stones can be saturated for undrained tests). The top cap/specimen/bottom cap stack is positioned between the top and bottom adaptor plates shown in Figure 2.1. The bottom cap fits into a recess within the bottom adapter plate. The top adapter plate is gently lowered such that a recess within the top adapter plate fits snugly over the top cap. The top and bottom caps are held tightly on their respective adaptor plates by three setscrews on each plate. Once the specimen is secured between the two adaptor plates, three LVDTs equally spaced around the specimen are mounted on the top adaptor plate and fixed to the plate by setscrews. The specimen is then consolidated by a vertical stress and is ready for shear loading.

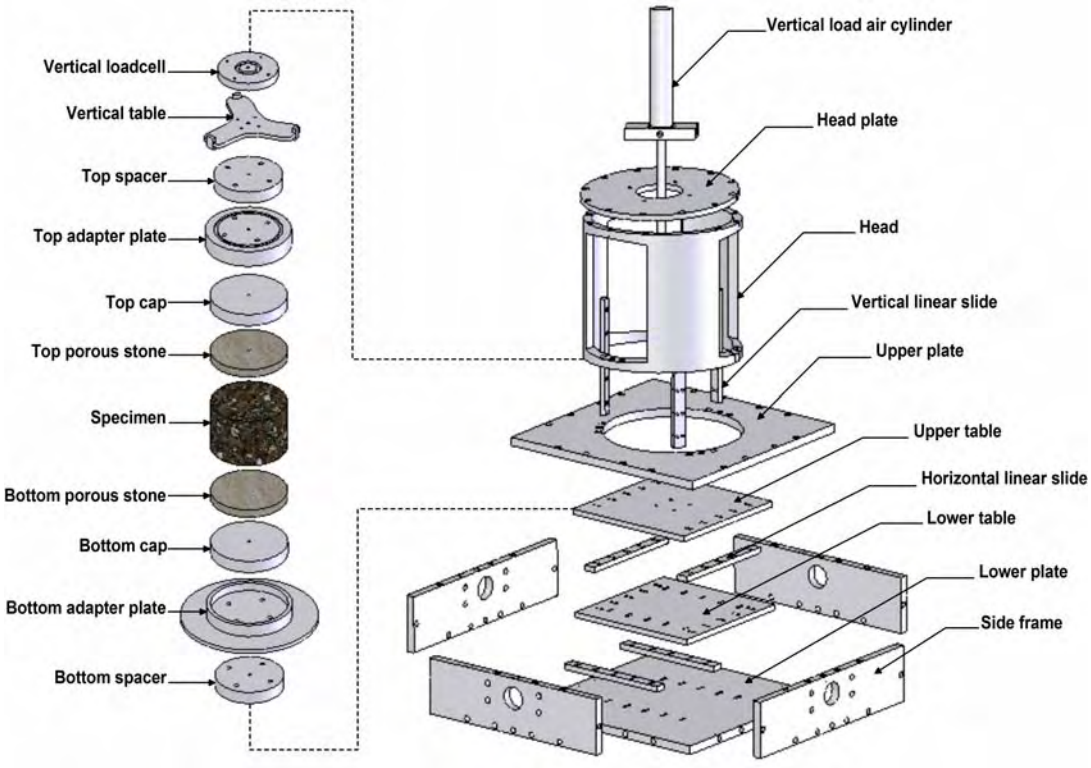

Figure 2.1. Schematic of the UCLA DC-SS Device.

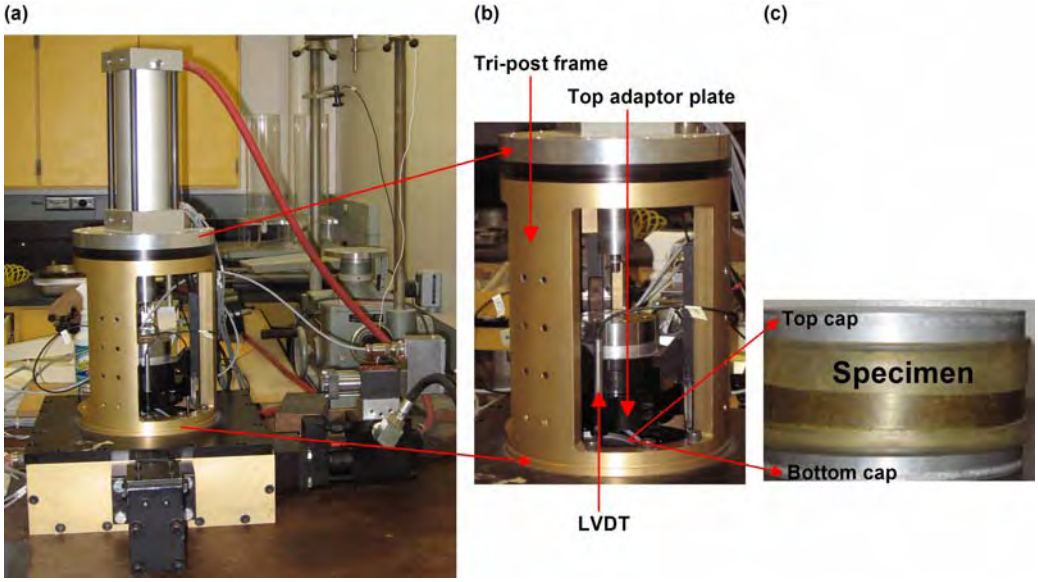

Figure 2.2. (a) Photograph of the UCLA DC-SS; (b) a close view of the tri-post frame, top adaptor plate, and LVDT to measure settlement (c) specimen confined by a wire-reinforced membrane covered at the top and bottom by caps which fit in the recess on the top and bottom adaptor plates.

Above the top adaptor plate is a vertical table, which in turn is attached to a vertical load cell (Figure 2.1). Vertical loads are transferred to the specimen through the vertical table, which is attached to three equally spaced linear slides. Each of the three linear slides is attached to a separate post, which effectively precludes lateral movements and rocking of the vertical table (and hence, practically speaking, the specimen as well). This tri-post frame is a significant improvement over the UCB-2D device, which employed a cantilever system (vertical table attached to a pair of track bearings along the same wall). Loads are applied to the vertical table by a pneumatic actuator mounted outside the main frame.

An important feature of the DC-SS device that was retained from the UCB-2D device is its bi-directional loading capability. Horizontal shear loads are applied at the base of the specimen through two independently controlled horizontal tables. The bottom horizontal table is mounted on linear slides attached to the main frame of the apparatus, and this table is free to move in only one horizontal direction. The upper horizontal table is also mounted on linear slides such that the movement of the upper table is exactly perpendicular to the lower table. The two horizontal tables can be controlled to produce net resultant movements of the bottom adapter plate in any horizontal direction. Loads are applied to the lower horizontal table by threaded rods that are attached to an actuator that can apply tension and compression. There is a tension-capable roller connection between the upper table and its actuator to accommodate perpendicular displacements of the lower table.

The loads applied to the tables are measured by loadcells mounted between the actuators and the tables. The loads measured by the loadcells are not identical to those imparted to the specimen due to friction in the linear slides. The magnitude of the frictional load within the system was characterized and observed to be quite small (approximately 2.2 N). The significance

of this frictional load is dependent on what type of testing is desired. This frictional load will produce inaccuracies of approximately 0.3 kPa (for a 10.2 cm diameter specimen), which represents a negligible percentage of the shear stress for most applications. However, if very low stress measurements are needed, post-friction shear stresses can be measured by using a dual-axis loadcell. The dual-axis loadcell fits in between the top adapter plate and the vertical table, a space which is otherwise occupied by a spacer block. The dual-axis loadcell is capable of measuring both the vertical and shear loads simultaneously with minimal cross talk between these channels. However, the presence of the dual-axis loadcell introduces system compliance (i.e., rocking and vertical deformations) that may be significant at medium to large strains. Therefore, most tests are performed without the dual axis loadcell in place.

Three LVDTs (linear variable differential transducers), mounted between the top and bottom adapter plates, are used to measure the vertical specimen deformations. These locations of LVDTs minimize errors due to mechanical compliance. The three LVDTs are used so that relative rocking of the specimen in either direction of loading can be measured. Data from the three LVDTs are averaged to define specimen height during a test. Horizontal deformations are measured by two LVDTs mounted to the horizontal tables in orthogonal directions.

The DC-SS device operates under "strain-control" conditions, meaning that table displacements are controlled and the actuator forces required to achieve those displacements are measured. The motions that can be imparted to the tables are limited by different aspects of the control system for different frequency bands. At low frequencies ($f \leq 0.24$ Hz), the limiting factor is the peak actuator displacement ($u_{max} = 51$ mm). At intermediate frequencies ($0.24 \text{ Hz} < f \leq 15$ Hz), the limiting factor is the flow rate capacity of the servo-valve ($Q_{max} = 158$ cm^3/sec). At frequencies $f > 15$ Hz, the limiting factor is the pressure capacity of the hydraulic pump ($p_{max} =$

21 MPa). For the case of harmonic control signals, these quantities can be related to the peak table motions as follows:

$$u(t) = D\sin(\omega t) \le u_{\max} \tag{2.1}$$

$$\dot{u}(t) = D\omega\cos(\omega t) \le Q_{\max}/A \tag{2.2}$$

$$\ddot{u}(t) = -D\omega^2\sin(\omega t) \le p_{\max}A/m \tag{2.3}$$

where *u(t)* and its derivatives describe the table displacement, velocity, and acceleration, *A* is the cross sectional area of the actuator (20.3 cm^2), *m* is the table mass (5.7 kg), and ω is the frequency of table motion (in radians/sec). The corresponding peak values of displacement, velocity, and acceleration are given in Figure 2.3. The control system is capable of producing any motion that lies below the limit lines in Figure 2.3.

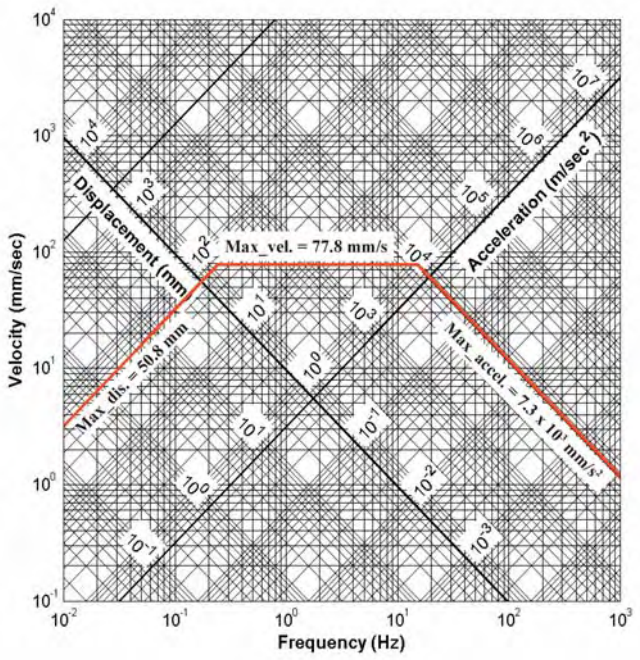

Figure 2.3. Tripartite plot demonstrating the theoretical limitations of the UCLA DC-SS device.

The theoretical oil column frequency of the actuator-table system is given by Conte and Trombetti (2000):

$$f_{oil} = \frac{A}{\pi}\sqrt{\left(\frac{\beta}{Vm}\right)} = 16.5Hz \tag{2.4}$$

where β is the bulk modulus of the hydraulic fluid ($1.7x10^6$ kPa) and V is the volume of oil in the actuator (463 cm^3). Physically, the oil column frequency represents the natural frequency of the SDOF hydraulic actuator system, which can be visualized as the table mass connected to a spring having a stiffness that is defined by the oil column in the actuator chamber. For command signals with frequencies near the oil column frequency, the performance of the actuator can be limited due to resonance behavior (e.g., Conte and Trombettti, 2000).

2.3 DC-SS CONTROL SYSTEM

As illustrated in Figure 2.4, the digital control system for the DC-SS device serves two purposes. The first is to provide control signals to direct drive servovalves that drive hydraulic actuators for each axis (direct drive servovalves have an onboard controller that correct tracking errors in the control signal before driving the hydraulic actuators). The second purpose is to acquire data from the LVDTs and loadcells. The physical device referred to here as DC-SS was originally developed with a *PC-based digitally-supervised analog control system*. This control system used a PID (Proportional-Integral-Derivative) control algorithm that ran within a Windows™ operating system. The principal problem with that control system was latency in the processing of feedback signals from instruments (such as an LVDT) and the generation of command signals. This limited the ability of the device to accurately replicate some command signals. These problems were especially acute for loading functions involving fast velocities and 2D shaking. The system was successfully used in previous testing (e.g., Whang et al., 2004; Whang et al., 2005), although those applications involved uni-directional shaking and a 1.0 Hz loading frequency, so control problems associated with the PC-based system were not

significant.

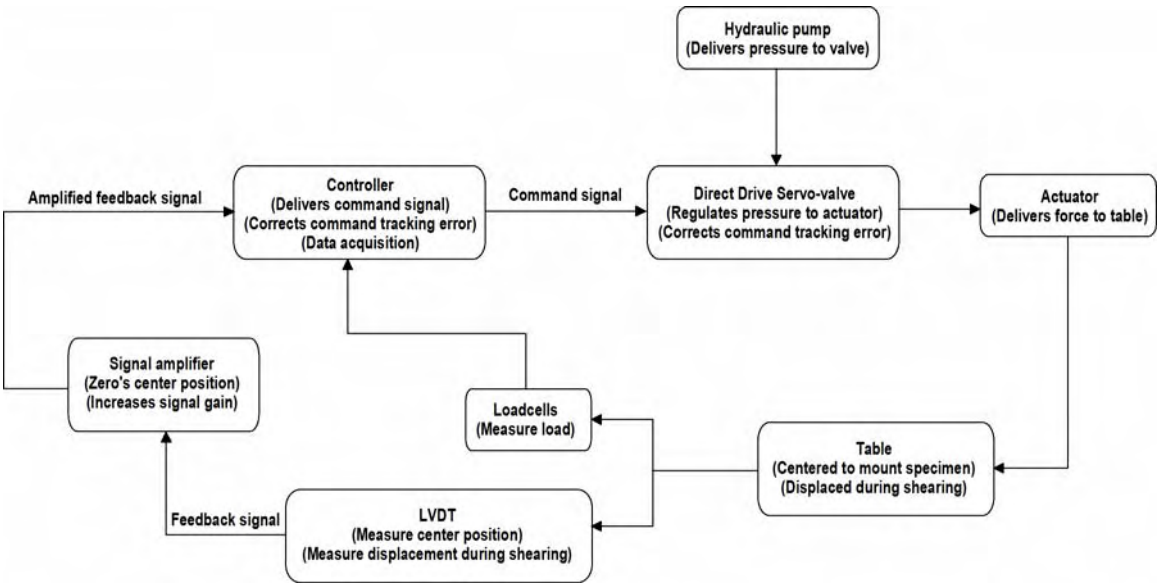

Figure 2.4. Layout of the different elements of the UCLA DC-SS device.

The control system for the present device uses a system referred to as *hard real-time digital control*. The principal difference from PC-based digital control is that the control functions are implemented on the controller board as opposed to a PC Operating System. This enables guaranteed sampling frequencies for the internal feedback loop of 5 kHz using displacement feedback from the horizontal LVDTs, whereas PC-based digitally-supervised analog control systems typically cannot reliably execute the computations required for complex control at feedback sampling frequencies higher than 200 Hz, depending on the processor clock-speed, control algorithm sophistication, number of background processes handled by the PC operating system, etc. The digital control system utilizes two dSPACE DS1104 controller boards. Each board contains a PowerPC 603e processor, four 16-bit 2 μs analog-to-digital (A/D) converters, four 12-bit 800 ns A/D converters and eight 16-bit 10 μs digital-to-analog (D/A) converters, in addition to other input/output ports. The two boards are mounted in PCI slots in a host PC but run their own real-time kernel (i.e., an operating system specifically tailored for control

functions) independent of the host PC's operating system.

A PID control algorithm was implemented for both PC-based and hard real time digital control. This is referred to subsequently as the "*PID controller*." Gains for the PID controller are tuned by trial-and-error for optimal performance using a step function command signal. The output of the PID controller is a digital voltage command that is sent to a Moog voltage amplifier via one of the D/A channels on the dSPACE board. The voltage amplifier, in turn, sends a voltage drive signal to the appropriate actuator servovalve. As illustrated in Figure 2.5a, PID control of the two axes are independent, and hence the control system as a whole is unable to compensate for cross-coupling effects (i.e., the influence of motion along one axis on the motion along the second axis).

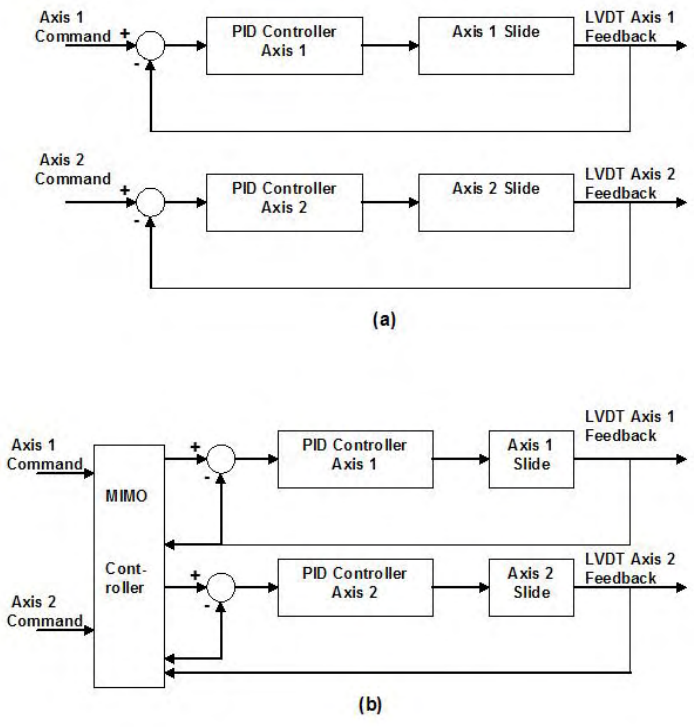

Figure 2.5. Controller architectures for (a) independent PID controller, and (b) MIMO-PID controller.

In order to minimize cross-coupling effects, the digital control system was enhanced by

introducing a multiple-input multiple-output (MIMO) control algorithm that interfaces with the PID controllers. As illustrated in Figure 2.5b, this controller uses LVDT feedback from both axes and generates a compensated command signal for each of the PID controllers, taking into account cross-coupling effects. The controller is designed and implemented as a discrete-time state space system using the LQG (Linear-Quadratic-Gaussian) optimal control method (Franklin et al, 1990). This method requires the estimation of four empirical quantities that reflect system properties. This is accomplished using the N4SID system identification algorithm (Van Overschee and De Moor, 1995). System identification algorithms operate on input-output data sequences; the data used for this purpose were two uncorrelated random inputs (generated by the PID controllers) and the corresponding LVDT output signals.

The combination of the MIMO control algorithm and the two PID controllers is referred to subsequently as the "*MIMO-PID controller*." The DC-SS device is configured so that the MIMO algorithm can be turned on or off. Hence, either PID or MIMO-PID digital control of experiments is possible. Data acquisition capabilities for either mode are summarized below:

Input motion time step: no practical lower limit

Number of input motion data points: no practical upper limit

Feedback sampling frequency (i.e., the internal frequency for the feedback loop): 5 kHz

Data logging frequency: upper bound is 5 kHz, can be down-sampled as needed.

2.4 DC-SS SYSTEM PERFORMANCE

To evaluate the performance of the DC-SS system (i.e., controller, pump, actuators, and servo-valves), both harmonic and broadband earthquake input motions were specified to the PID controller and the MIMO-PID controller and the resulting feedback signals were measured. Uni-directional tests were performed to evaluate the performance of each axis independently, and to

provide baseline results for evaluating interaction effects. Bi-directional loading was performed to evaluate cross-coupling between axes.

2.4.1 Sinusoidal Tracking

Figure 2.6 shows displacement histories and Fourier amplitude spectra of a displacement-controlled uni-directional harmonic command signal with amplitudes u = 0.20 mm and 0.012 mm (corresponding to shear strain values of 1.0% and 0.06% respectively for a typical 2 cm tall specimen) and f = 1 Hz along with the feedback signals obtained using the MIMO-PID controller. The LVDT feedback signals were recorded using a sampling frequency of 200 Hz. The tests shown in Figure 2.6 were performed in only one direction (zero command signal in the perpendicular direction).

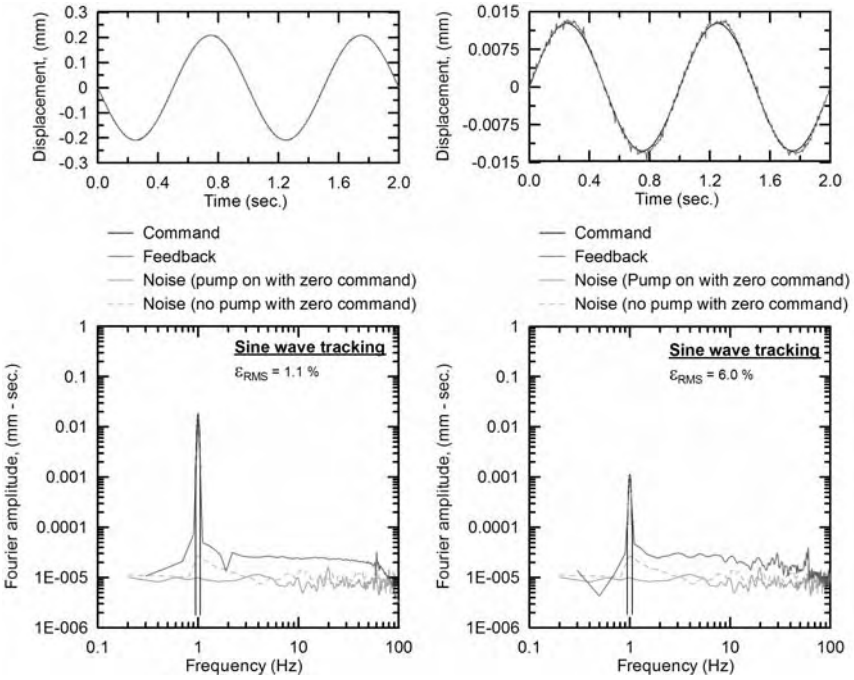

Figure 2.6. Sinusoid tracking of cyclic displacement amplitudes = 0.2 and 0.012 mm at f = 1 Hz for shearing along one axis at a time and noise level with pump on and off (MIMO controller).

The upper plots in Figure 2.6 show the feedback and command signals in the time domain. Visual inspection of the signals indicates better performance at larger amplitudes (u = 0.20 mm). There is a time lag between the command and feedback of about 0.005 to 0.010 sec (one to two times the time step of 0.005 sec), which is consistently observed regardless of the loading frequency. This lag has been removed in the plots shown in Figure 2.6 and subsequent plots. Following lag-removal, the normalized root mean square error of the feedback signal is calculated as:

$$\text{Normalized RMS tracking error, } \varepsilon_{RMS} = \frac{\sum_{i=1}^{N}\left(x_i^c - x_i^f\right)^2}{\sum_{i=1}^{N}\left(x_i^c\right)^2} \tag{2.5}$$

where x^c denotes the command signal, x^f denotes the feedback signal, and the summation occurs over time (N is the number of time steps in the displacement histories). Values of ε_{RMS} for 1 Hz shaking were computed to be 1.1% and 6.0% for u = 0.20 mm and 0.012 mm, respectively.

The lower plots in Figure 2.6 show the feedback and command signals in the frequency domain. Also shown for reference are noise spectra obtained with zero command signal and "pump on" and "pump off" conditions. The DC-SS device has one pump that operates the two valves (one on each horizontal axis). The no pump signal is electrical noise in the system and has a flat Fourier spectrum, which is consistent with white noise. System testing indicates that this noise is dominated by analog-to-digital (A/D) conversion of the feedback signal. This A/D noise is minimized by amplifying the feedback signal prior to the A/D conversion using the signal amplifier depicted in Figure 4. In Figure 6, the pump on spectrum essentially matches the no pump spectrum, indicating that there is no perceptible actuator movement due to leakage of hydraulic oil through the spool in the valve while the pump is running. Note that the Fourier amplitude of the feedback signal matches that of the command signal at frequencies where the

command signal is stronger than the noise spectrum, whereas outside of that relatively narrow frequency range, the spectra of the feedback signal is slightly stronger than the noise spectrum.

Figure 2.7 presents the variation of ε_{RMS} with harmonic loading frequency and displacement amplitude in uni-directional tests. As shown in Figure 2.7a, tracking errors for f = 1 Hz were observed to decrease with increasing displacement for u < 0.2 mm. This trend results from the increasing significance of system noise, illustrated in Figure 2.6, as displacement amplitude decreases. The above results were obtained for uni-directional tests performed along Axis 1; practically identical results were obtained for Axis 2 that are not shown here for brevity. Figure 2.7b shows the effect of frequency for two displacement amplitudes (u = 0.02 and 0.2 mm). In general, values of ε_{RMS} were observed to increase with increasing frequency.

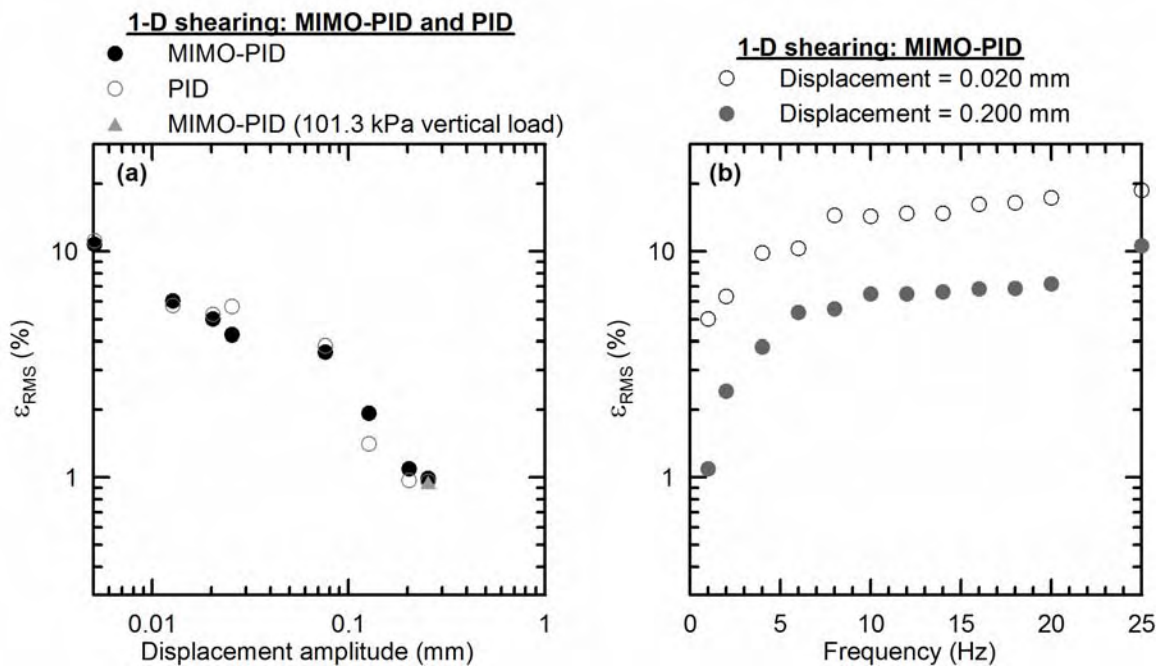

Figure 2.7. Variation of normalized root mean square of tracking errors for uni-directional shaking with (a) displacement amplitude and (b) loading frequency.

Also shown in Figure 2.7a are system errors for PID control relative to those for MIMO-PID control. As expected for uni-directional testing, error terms for both controllers are practically

identical. Most of the tests reported in Figure 2.7 were conducted with no sample and effectively zero normal stress acting on the sliding tables. To evaluate the effect of normal stress acting through a specimen, a separate test with the MIMO-PID controller was conducted with a specimen loaded to a normal stress of 101.3 kPa. The result, shown by the triangle in Figure 2.7a, indicates no noticeable effect on the ε_{RMS} values.

Interaction effects were investigated by providing simultaneous harmonic command signals in two horizontal directions. One axis is referred to as the baseline axis, and was consistently commanded a displacement amplitude of 0.20 mm at f = 1 Hz frequency. The second axis was commanded simultaneously with a sinusoidal amplitude of 0.20 mm at f = 2 to 25 Hz. Different frequencies were used for the second axis so that any cross-coupling effects could be readily identified (e.g., a significant feedback signal for the baseline axis at the excitation frequency for the second axis would indicate cross-coupling). The results are summarized in Figure 2.8 in the form of misfit of the baseline axis command/feedback signals as quantified by ε_{RMS}. In Figure 2.8, results for zero frequency indicate no commanded motion of the perpendicular axis. The results in Figure 2.8 illustrate two important points: (1) ε_{RMS} on the baseline axis increased by the presence of shaking on the perpendicular axis but is not significantly affected by the frequency of shaking on the perpendicular axis (observed by comparing results at zero frequency with finite frequencies); (2) ε_{RMS} is lower for MIMO-PID control than for PID control. Results similar to those in Figure 2.8 were obtained when the baseline axis is rotated 90 degrees (i.e., there is no significant difference in the ability of the device to control motions in the two horizontal directions). Although not shown for brevity, Fourier spectra of baseline-axis feedback signals with and without perpendicular excitation are indistinguishable (i.e., there is no permutation of the spectra at the excitation frequency for the perpendicular axis).

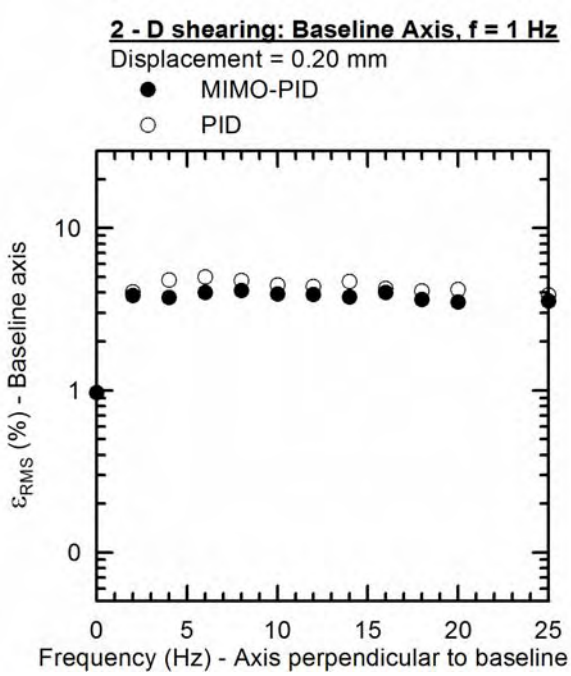

Figure 2.8. Normalized root mean square of tracking errors on baseline axis for varying frequencies of excitation on perpendicular axis (PID and MIMO-PID controllers).

2.4.2 Broadband Command Signal Tracking

The PID and MIMO-PID controllers have the ability to command realistic earthquake waveforms in two horizontal directions, which is a unique capability of the DC-SS device. An accelerogram from the M_w = 7.6 Chi Chi Taiwan earthquake is used to demonstrate this ability. The selected accelerogram was recorded in Wufeng Taiwan on firm soil (record TCU065, 90-degree component), and is digitized at a time step of 0.005 seconds (Nyquist frequency = 100 Hz). The acceleration history is applied to the laboratory specimen as a displacement history because (1) shear stress at a particular depth in a soil deposit is proportional to average accelerations of soil above that depth, and (2) shear strains (and hence shear displacements across an element) are roughly proportional to shear stress (for an equivalent-linear shear modulus). Hence, it follows that shear deformations of a soil element would have waveforms with similar phasing to an acceleration history.

Figure 2.9a shows the tracking of the Taiwan displacement history for uni-directional shaking under MIMO-PID control along a baseline axis with the input scaled to produce a peak displacement of 0.2 mm. Comparison of the Fourier spectra in Figure 2.9d indicates that the signal tracking is generally reasonable for frequencies less than approximately 35 Hz where the command signal is strong. At higher frequencies, the feedback signal becomes dominated by noise. During time windows with relatively large amplitude command signals (e.g. Figure 2.9c), tracking errors are small. Conversely, during time windows with effectively zero command signal (Figure 2.9b), the feedback signal consists of noise that is random with variable amplitude. We have investigated the amplitude of the noise feedback signal under conditions of zero command. As shown in Figure 2.10, the feedback signal was found to be normally distributed with a mean value that is effectively zero and standard deviation = 0.00027 mm. Because of these noise signals, large root mean square errors (ε_{RMS}) accumulate during time windows with low command amplitudes, such as that shown in Figure 2.9b.

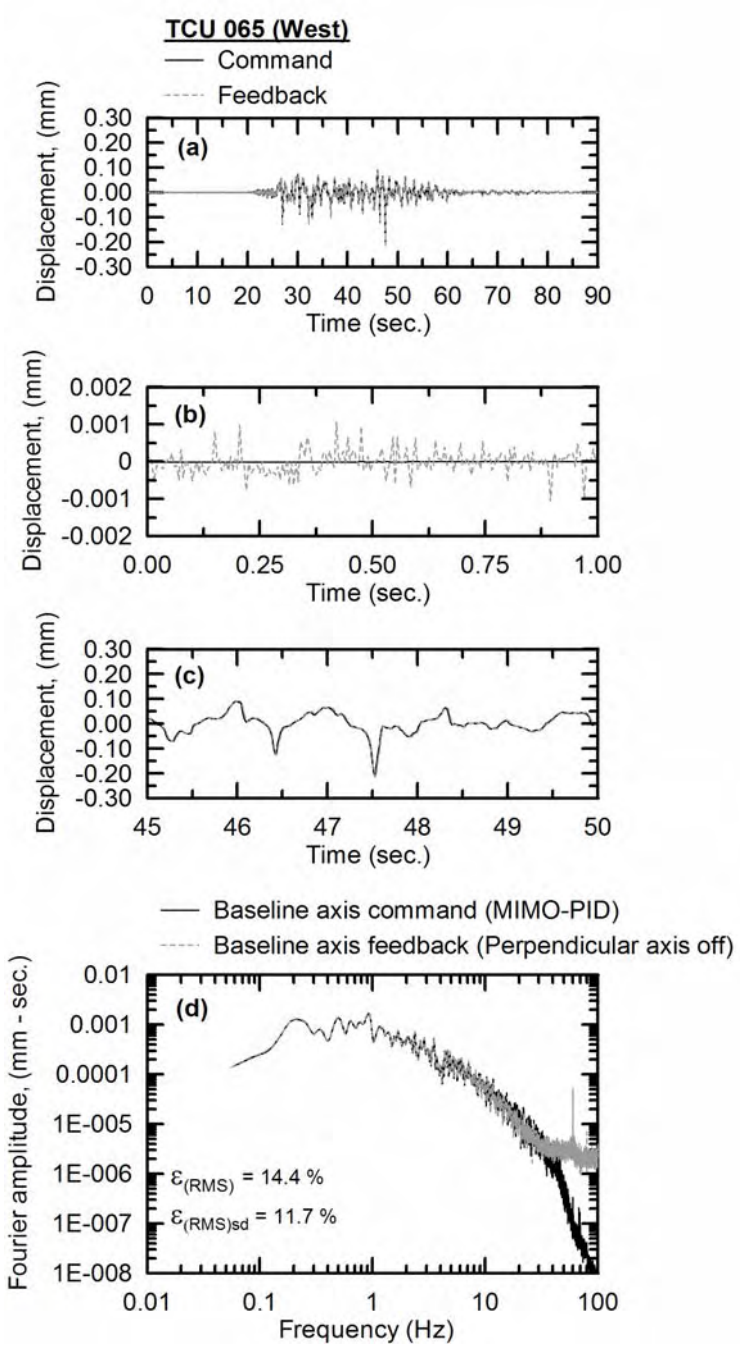

Figure 2.9. Reproduction of recorded history for shearing on one axis at a time (i.e., without interaction effects; MIMO-PID controller).

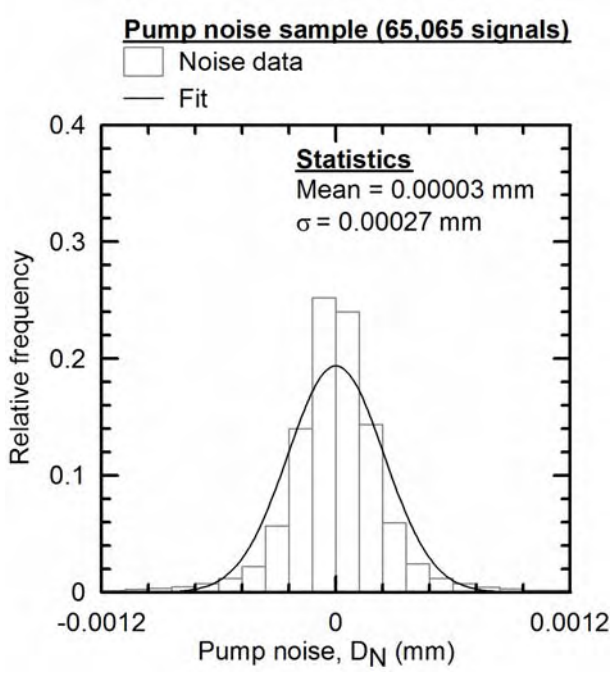

Figure 2.10. Distribution of values of noise feedback signal with pump on and zero command signal (D_N) along with normal probability distribution fit to the data.

Because earthquake recordings contain time windows with both weak and strong motions, the ε_{RMS} values tend to be much larger than those for sinusoidal command signals at a common peak amplitude. For example, at a peak amplitude of 0.2 mm, $\varepsilon_{RMS} \approx 14.4\%$ for the Taiwan broadband command whereas $\varepsilon_{RMS} \approx 1.1\%$ for harmonic command. These high ε_{RMS} values can be misleading, because it is generally the large-amplitude window of the broadband signal that is of the greatest engineering interest. Accordingly, to reduce contributions to ε_{RMS} from low-level shaking at the beginning and end of the acceleration record that may be of little engineering significance, error can be calculated using the time window during which the normalized Arias intensity increases from 5% to 95% (the length of this time window is typically referred to as the significant duration). Root mean square errors calculated within the window of significant duration are referred to as $(\varepsilon_{RMS})_{SD}$, and are reduced from $\varepsilon_{RMS} = 14.4\%$ to $(\varepsilon_{RMS})_{SD} = 11.7\%$ for the full record (see Figure 2.9d).

Figure 2.11 shows $(\varepsilon_{RMS})_{SD}$ values for the baseline axis as a function of peak displacement amplitude for cases of uni-directional shaking and multi-directional shaking (MIMO-PID and PID control). For the case of multi-directional shaking, identical command signals were applied in both horizontal directions. Several important trends are illustrated by the results as follows: (1) the tracking error decreases markedly with increasing peak displacement amplitude for both uni-directional and multi-directional shaking for u < ~0.2 mm, as was the case with harmonic loading (Figures 2.11a and 2.11b); (2) tracking errors along the baseline axis are not affected by whether the command is one-directional along that axis (e.g., MIMO-PID 1-D in Figure 2.11a) or whether bi-directional command is used (e.g., MIMO-PID 2-D in Figure 2.11a); (3) tracking errors for uni-directional shaking (Figure 2.11a) and multi-directional shaking (Figure 2.11b) are smaller for MIMO-PID control than for PID control. Although not shown for brevity, results are very similar to those in Figure 2.11 when the baseline axis is rotated 90 degrees.

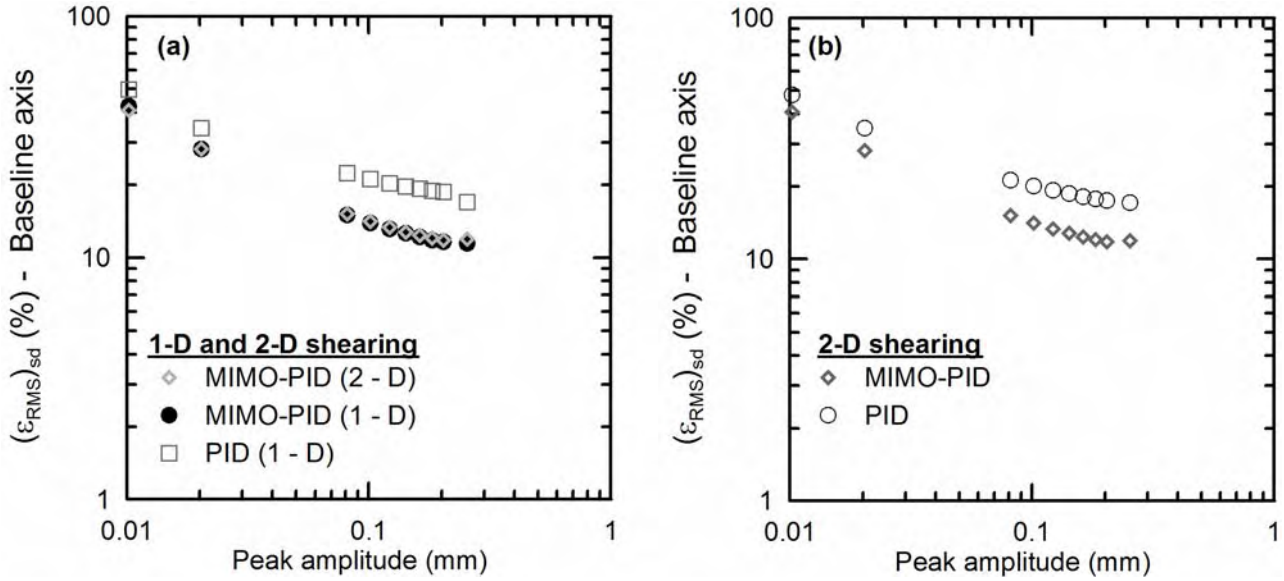

Figure 2.11. Normalized root mean square of tracking errors for uni-directional and multi-directional broadband command signals of different amplitude. Multi-directional command is with both PID and MIMO-PID control.

2.5 EXAMPLE TEST RESULT FOR DRY CLEAN SAND

To illustrate the capabilities of the device in actual tests of soil specimens, we tested specimens of clean uniform sand (Silica No. 2). The sand is relatively uniformly graded with D_{50}= 1.75 mm and has maximum and minimum void ratios of 1.02 and 0.69, respectively. The tested specimens were prepared to relative densities (D_R) of approximately 55%. The accumulations of vertical strains (ε_v) during two uni-directional tests and one bi-directional test (all on separate specimens) are presented in Figure 2.12. Each test was performed under a vertical stress of 101.3 kPa using a normally consolidated specimen. The Taiwan record used previously (TCU065) was applied at a peak shear strain amplitude of approximately 0.9%. For the 2-D test, the same record was used in both axes. The recorded feedback signals were virtually indistinguishable for all three tests, indicating repeatable controller performance. The difference between the two results for 1-D shaking results from slightly different initial relative densities. The strains accumulated during bi-directional shaking are less than twice the average value of 1-D shaking (i.e., average ε_v at end of 1-D was 0.6%; at end of 2-D, ε_v = 0.8%). Note that this result differs from the multiplier of two recommended by Pyke et al. (1975).

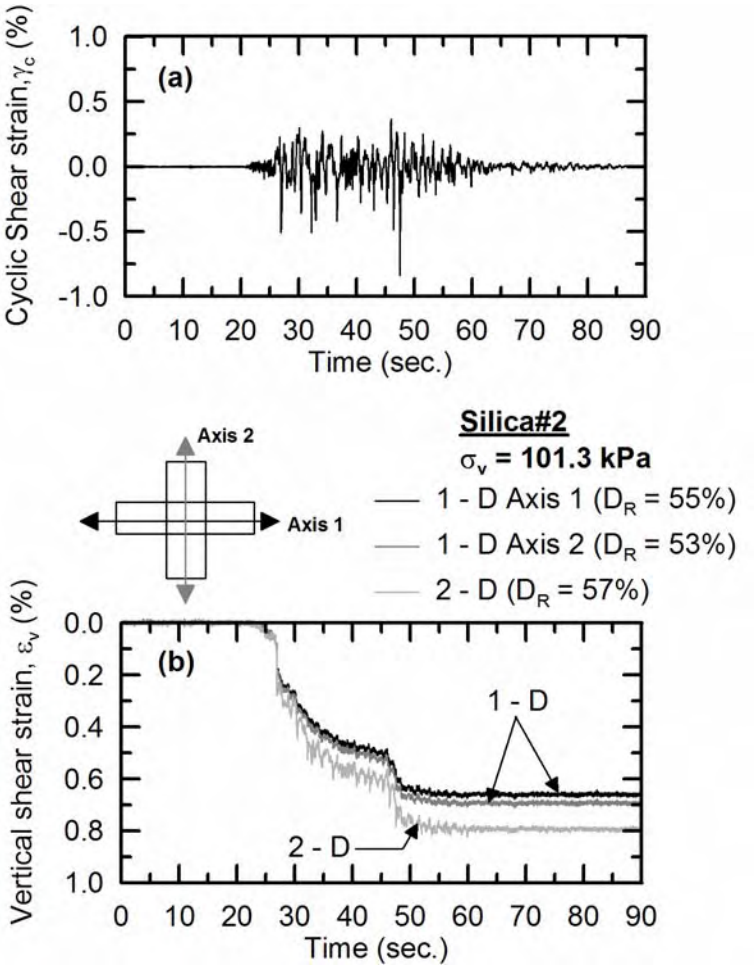

Figure 2.12. Comparison of vertical strains of a clean sand confined at 101.3 kPa to a comparable relative density. Soil was sheared uni-directionally and bi-directionally, respectively.

2.6 SUMMARY AND CONCLUSIONS

In this chapter we have described the mechanical components and control system of a state-of-the-art cyclic simple shear apparatus for soil testing. The mechanical features of this device include: (*i*) servo-hydraulic actuation to facilitate high frequency loading; (*ii*) a tri-post frame to minimize mechanical compliance effects due to rocking; (*iii*) bi-directional excitation; (*iv*) chamber pressure control for backpressure saturation; and (*v*) post-friction shear load measurement capabilities. The device incorporates true digital control to overcome the limitations of PC-based digitally-supervised analog controllers (i.e., latency in the feedback loop

and limited sophistication of control algorithms). The digital controller consists of two dSPACE DS1104 controller boards with PID and MIMO-PID control algorithms implemented at the board level. The MIMO-PID control algorithm was introduced to minimize cross-coupling effects using a LQG optimal control method and real-time system identification of feedback signals.

A series of tests were performed using harmonic command signals to characterize the performance of the device. The tracking error was quantified using normalized root mean square error (ε_{RMS}) per Eq. 2.5 for each test. When uni-directional sinusoidal command signals were applied to each axis, the feedback signal exhibited a strong dependence of error on displacement amplitude (u) for $u < 0.2$ mm with the smallest errors at large displacements being about 1%. Values of ε_{RMS} were observed to increase with frequency. Cross-coupling interaction effects were found to be negligible when the device was operated with the MIMO-PID controller. Cross-coupling effects lead to larger errors when bi-directional tests were performed with the more traditional PID controller.

Uni- and multi-directional excitation was performed using a command signal adapted from a recorded earthquake motion. The command and feedback displacement histories were nearly indistinguishable for time windows with relatively large command amplitudes. However, time windows with weak command amplitudes were not well reproduced, with the feedback signal instead being dominated by noise with zero mean and standard deviation = 0.00027 mm. Fourier spectra of the command and feedback signals compare favorably where the command amplitude is larger than the noise, which for the displacement history considered occurred at frequencies less than approximately 35 Hz.

3 VOLUMETRIC STRAINS OF CLEAN SANDS SUBJECT TO CYCLIC LOADS

3.1 INTRODUCTION

In this chapter, we present the results of an investigation for clean sand materials. The purpose of the investigation has been to expand the database of information on the behavior of clean sands under cyclic loading. The state-of-practice method for seismic compression analysis consists of a procedure by Tokimatsu and Seed (1987). A key component of the procedure, that relates volumetric strains to applied shear strains and number of strain cycles (herein termed a volumetric strain material model), is based solely on laboratory test data for a single clean quartz sand material (Crystal Silica No. 20) by Silver and Seed (1971). Additional data has been compiled since that time on other materials as summarized in Table 3.1, but the database remains inadequate to systematically investigate the effects of compositional and environmental factors on seismic compression susceptibility. In this chapter, we present the results of such an investigation for clean sand materials and synthesize the principal findings into an updated volumetric strain material model that can be applied in practice to clean sand materials with greater confidence than that of Silver and Seed (1971).

Table 3.1. Indices of soils tested in published and unpublished studies

Published tests Reference	Material	Fines Content (FC) (%)	LL	PI	D_{50} (mm)	C_u	$\gamma_{d,min}$ (kN/m^3)	$\gamma_{d,max}$ (kN/m^3)	$\gamma_{d,initial}$ (kN/m^3)	[1]D_R (%)	Saturation (%)
Hsu and Vucetic (2004)	Nevada sand	0	-	0	-	-	13.8	17.2	-	76 - 81	0 -100
	Fine soils	-	25-53	11 to 53	-	-	-	-	13 - 17.2	-	0 - 100
Stamatopoulous et al. (2004)	Sand	11	-	0	0.250	6	-	-	14 - 17.5	-	0
Tsukamato et al. (2004)	Ohgishima sand	22	-		0.213	5	-	14.9	14.2	90.0	50 - 100
Whang et al. (2004)	Newhall	44	27	2	0.100	150	-	20.6	-	[a]60-75	54 - 91
	Site A	54	33	15	0.060	110		21.2	-	[b]35-60	54 - 87
Shahnazari and Towhata (2002)	Toyoura sand	0	-	-	0.160	-	13.1	16.3	-	22 - 67	100
Chu and Vucetic (1992)	Clay	22	30	11	-	-	-	20.2	9.95 - 20.19	[c]75-100	59 - 98
Ohara and Matsuda (1988)	Kaolonite	100	53	25	-	-	-	-	11.5	-	100
Pyke et al. (1975)	Clay	-	-	-	-	-	-	20.6	18.9	[d]60	69
Youd (1972)	Ottawa sand	0	-	0	-	-	14.8	17.5	-	75 - 80	0
Silver and Seed (1971)	Crystal silica No. 20	0	-	0	0.650	2	13.2	15.9	-	45 - 80	0
Unpublished tests											
UCLA	Ursa	77	48	27	0.015	3	-	18.6	-	[b] 35-60	60 - 90
	Northshore A	31	28	np	-	-	-	18.2	-	[e] 40	70
	Northshore B1	65	42	17	-	-	-	17.8	-	[e] 40	90
	Northshore B2	74	64	33	-	-	-	17.2	-	[f] Loose-40	60 - 90
	Northshore C	75	58	26	-	-	-	16.8	-	[g] 10	

[1] Modified relative compaction (RC_{mod}) of clay soils is converted to equivalent relative density using $RC = 80 + 0.2*D_R$ (Lee and Singh, 1971)

[a] RC_{mod} = 92-95%

[b] RC_{mod} = 87-92%

[c] RC_{mod} = 95 - 100%

[d] RC_{mod} = 92%

[e] RC_{mod} = 88%

[f] RC_{mod} = 80 - 88%

[g] RC_{mod} = 10%

The compositional factor that has been identified as principally affecting the seismic compression potential of clean sands in past research is relative density (D_R), with volumetric strains found to decrease with increasing relative density (Silver and Seed, 1971; Youd, 1972). As shown in Figure 3.1, the results of those two early studies provide anecdotal evidence that at a given D_R sand-to-sand variability can be large. In the present work, we investigate a number of compositional factors that might be expected to affect seismic compression susceptibility, including sand mineralogy, fabric, gradation (as measured by mean grain size, D_{50}, and uniformity coefficient, c_u), and particle angularity. Previous studies of gradation effects have found liquefaction strength to not be affected by grain size or coefficient of uniformity (Kokusho et al., 2004), although the shear strength at critical state (which occurs at relatively large strains) was affected by gradation. A number of studies have found sand fabric to significantly affect liquefaction strength (e.g., Ladd, 1974; Mulilis et al., 1977; Vaid et al., 1999), although the

dependence on fabric seems to disappear when pore pressures are related to applied shear strains (NRC, 1985). The other compositional factors listed above have not been systematically investigated to our knowledge. None of these factors have been considered previously for application to the seismic compression problem.

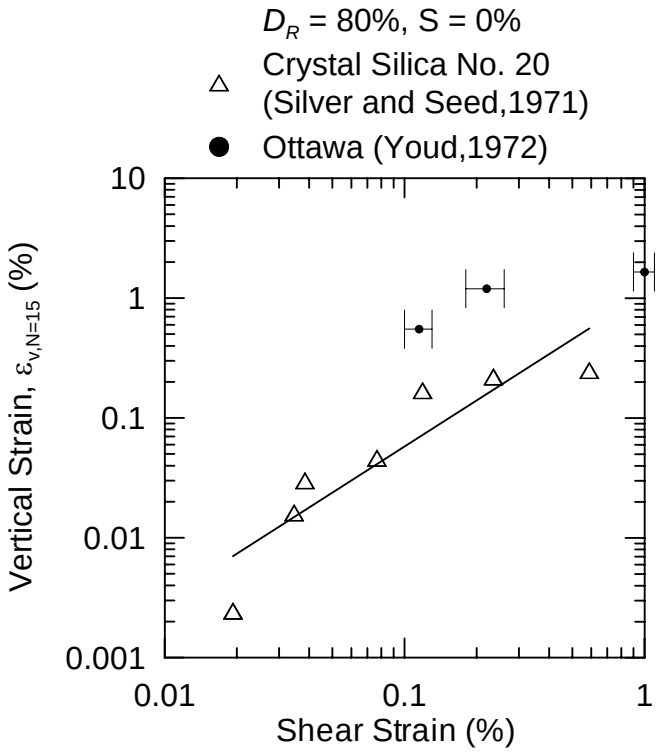

Figure 3.1. Comparison of Silver and Seed (1971) and Youd (1972) test results for clean sands tested under strain-controlled conditions.

Environmental factors potentially relevant to the seismic compression problem include degree of saturation, overburden stress, stress history, age (time under sustained load), and prior seismic loading. Youd (1972) found sands at saturation levels of 0 and 100% to have similar seismic compression potential, although this result is expected as matric suction is zero in both cases. The effect of intermediate saturation levels on seismic compression susceptibility is investigated here. Overburden effects were found to be negligible by Silver and Seed (1971) and Youd (1972) across the vertical stress ranges of σ_v = 0.25-2.0 atm and 0.05-2.0 atm, respectively.

Those findings are surprising given what has since been learned about the strong effect of confinement on liquefaction strength (e.g., Boulanger, 2003), and are re-examined in the present work. Stress history has not been investigated for seismic compression, but liquefaction strength has been shown to increase with over-consolidation ratio (OCR) beyond what would be expected from K_0 increase, although the significance of this effect has varied (Lee and Focht, 1975; Ishihara and Takatsu, 1979; Finn, 1981). We investigate stress history effects on seismic compression for several sands with different compositional characteristics. Time effects for clean sands were studied by Duku et al. (2006), and are discussed further in Chapter 5. Prior seismic loading has been investigated for both liquefaction and seismic compression (e.g., Martin et al., 1975; Seed et al., 1977), and is not investigated here.

3.2 SOILS TESTED

Fourteen (14) sand materials were utilized in this research so that a broad database could be generated to investigate compositional factors on seismic compression. The sands span a range of material gradation, particle size and particle shape. Table 3.2 presents a synthesis of compositional soil properties (additional information is available in Duku, 2007), while Figure 3.2 presents gradation curves for each of the tested sands. The maximum and minimum densities and void ratios reported in Table 3.2 were evaluated using the Modified Japanese method and dry tipping, respectively (comparable to ASTM D4253 and D4254, respectively). The sand mineralogy reported in Table 2 was evaluated by Geoff Martin (*personal communication*, 2006). Additional information on sand characteristics is available in Duku (2007).

Table 3.2. Soil indices for current study

Material	Fines Content (FC) (%)	D_{50}[a] (mm)	[a] C_u	[b] $\gamma_{d,min}$ (pcf)	[c] $\gamma_{d,max}$ (pcf)	Average shape factor (S_{avg}) Mean	Std.	Condition Virgin [V] or Resheared [R]
Flint No. 13	0	0.56	1.43	93.7	109.9	0.87	0.07	V
Flint No. 16	0	0.50	2.11	93.1	111.0	0.80	0.13	V
F-52	0	0.28	1.72	92.4	110.2	0.82	0.13	V
F-110	0	0.13	1.90	90.1	105.1	0.91	0.13	V
Silica No. 0	0	0.89	1.45	85.6	101.4	0.79	0.06	V
Silica No. 2	0	1.60	1.29	84.2	100.5	0.74	0.09	V
Post Office	0	0.29	5.00	99.5	117.1	0.82	0.11	V
Vulcan	0	0.51	2.90	92.3	113.1	0.77	0.11	V
Crystal silica No.	0	0.81	1.62	81.9	99.5	0.75	0.12	V
Nevada	0	0.19	1.30	89.0	109.3	0.94	0.11	V
Irwindale	0	1.00	4.67	97.1	114.3	0.70	0.15	V
Pacoima No. 1	0	0.38	3.07	88.4	108.5	0.87	0.11	V
Pacoima No. 3	0	0.55	3.18	90.2	110.6	0.80	0.11	V
Newhall	0	0.37	4.38	85.9	99.5	0.82	0.12	V

[a]ASTM D422
[b]Used the Japanese method which is equivalent to ASTM D4253
[c]Used the Dry tipping method which is equivalent to ASTM D4254

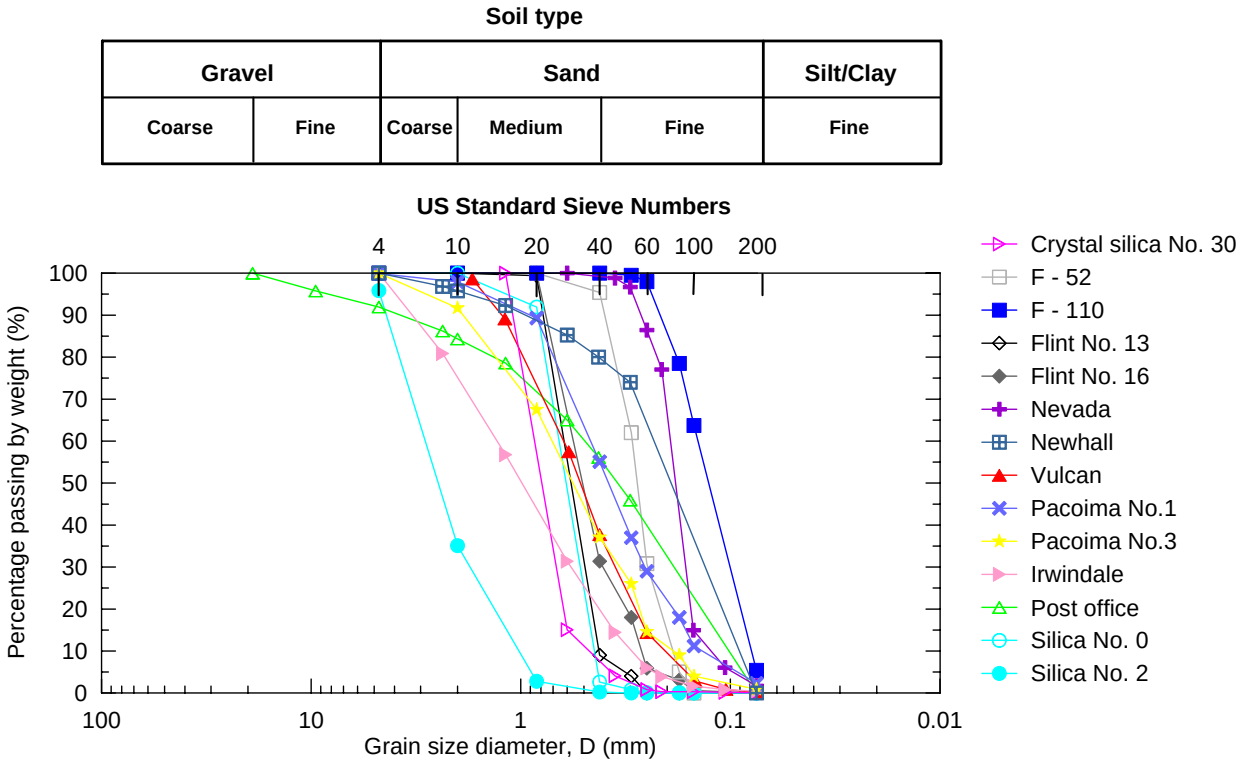

Figure 3.2. Gradation curves for the fourteen tested sands.

Particle shape was also characterized for each sand using image analysis techniques similar to those used by Zettler et al. (2000). The technique was applied to three equal weight fractions

by grain size: coarse, medium and fine. Particle shapes were characterized using a shape factor, defined by Zettler et al. (2000) as:

$$S_f = \frac{(4\pi \cdot area)}{(perimeter)^2} \tag{3.1}$$

Shape factor S_f is one for a circle and zero for a line. The shape factors and corresponding shape classifications are presented in Table 3.2.

3.3 LABORATORY EQUIPMENT AND TEST PROTOCOLS

The Digitally Controlled Simple Shear (UCLA-DCSS) apparatus at UCLA was utilized for the testing described here. More information is presented in Chapter 2.

All tested specimens were compacted in the laboratory to various target densities and saturation levels. Samples were prepared inside of a wire-reinforced Norwegian Geotechnical Institute (NGI) membrane with a diameter of 102 mm fitted inside of a mold. Following compaction, the samples were placed in the device and subjected to a vertical seating load, after which they were cyclically tested at a range of shear strain amplitudes (typically $0.1\% \leq \gamma_c \leq 1.0\%$) at a frequency of 1.0 Hz. Three issues associated with the sample preparation that are relevant to discussion presented subsequently in the article are: (1) lateral stress conditions in the specimens associated with the wire-reinforced membrane; (2) compaction methods used to achieve a range of soil fabrics; and (3) the manner by which different levels of saturation were achieved.

The lateral stress condition in soil specimens confined by NGI wire-reinforced membranes has been investigated in previous studies by instrumenting the membrane and relating the measured ring stresses to lateral soil stresses. Youd and Craven (1975) and Dyvik el al. (1981)

applied this technique to sand and clay specimens respectively, and found the lateral stresses to conform to at-rest (K_o) conditions as predicted by Jaky, 1944 ($K_0 = 1 - \sin\phi'$, where ϕ' = friction angle). However, Budhu (1985) performed similar tests using NGI wire-reinforced membranes on sand specimens and found lateral soil pressures considerably smaller than what would be expected for K_o conditions (nearly active pressures). Hence, the results of studies using instrumented membranes are contradictory. For soil specimens to have lateral soil pressures less than those for K_o conditions, tensile extension of the membrane wires is required, which in turn would cause an increase of the specimen's cross sectional area. Recognizing this, Dyvik et al. (1987) measured the strength of clay specimens under true undrained conditions (constant volume) and in a complementary suite of constant height tests (which would not be constant volume in the event of membrane relaxation). Results of the two suites of tests were similar, indicating that membrane relaxation was negligible. In consideration of the above, we assume for the purpose of subsequent discussion in the paper that membrane relaxation during testing is negligible, and that lateral pressures in soil specimens can be taken as:

$$K_0 = (1 - \sin\phi') \times OCR^h \tag{3.2}$$

where h is an empirical constant taken as 0.4 (Alpan, 1967).

Specimens were prepared using one of three methods: dry pluviation followed by vibratory compaction, tamping, and kneading. Dry pluviation involved pouring dry sand into the sample preparation mold (inside of which is the membrane) and then pulling a screen up through the specimen from its base. As needed, a 60 Hz vibrator was applied to the top cap to achieve a target density after application of the seating load. Similar dry pluviation procedures were applied by Silver and Seed (1971). The tamping method involved the use of a 38.1 mm diameter

tamper to two lifts of sand in the mold. Similar procedures have been applied in liquefaction studies by many investigators (e.g., Ladd, 1974; Mulilis et al., 1975; Zlatovic and Ishihara, 1997; Vaid et al., 1999; Polito and Martin, 2001; Yamamuro and Wood, 2004). The kneading compaction method utilized a Harvard miniature compactor with two lifts of soil in the mold, and is similar to the dry rodding method used by Mulilis et al. (1975) in liquefaction studies. All of the sample preparation methods were applied using a pre-weighed amount of sand prepared in the mold to a specified height to achieve the desired density following placement of the seating load and appropriate compaction effort.

All three sample preparation methods were used to prepare subsets of oven-dried specimens (S = 0%). Only the tamping and kneading methods were used to prepare partially saturated specimens. Partially saturated bulk sand specimens were created by adding a pre-determined amount of water to dry sand to achieve saturation levels of S = 30, 60 and 90%. Moistened bulk samples were cured for 24 hours in sealed buckets to ensure uniform mixing. Following curing, partially saturated specimens were prepared using the tamping and kneading methods described above.

3.4 TEST RESULTS

3.4.1 Form and Parameterization

The results of a typical strain-controlled cyclic simple shear test are shown in Figure 3.3 (Silica No. 2 Sand, γ_c = 0.66%, D_R = 60%). Essentially uniform cyclic shear strain amplitudes are achieved through a slight increase in the applied shear stress during the first few cycles until the soil's shear modulus has stabilized. The soil's equivalent shear modulus is effectively constant

after 10 cycles of loading. As shown in Figure 3.3(c), the majority of vertical strain accumulation occurs within the first few cycles of loading.

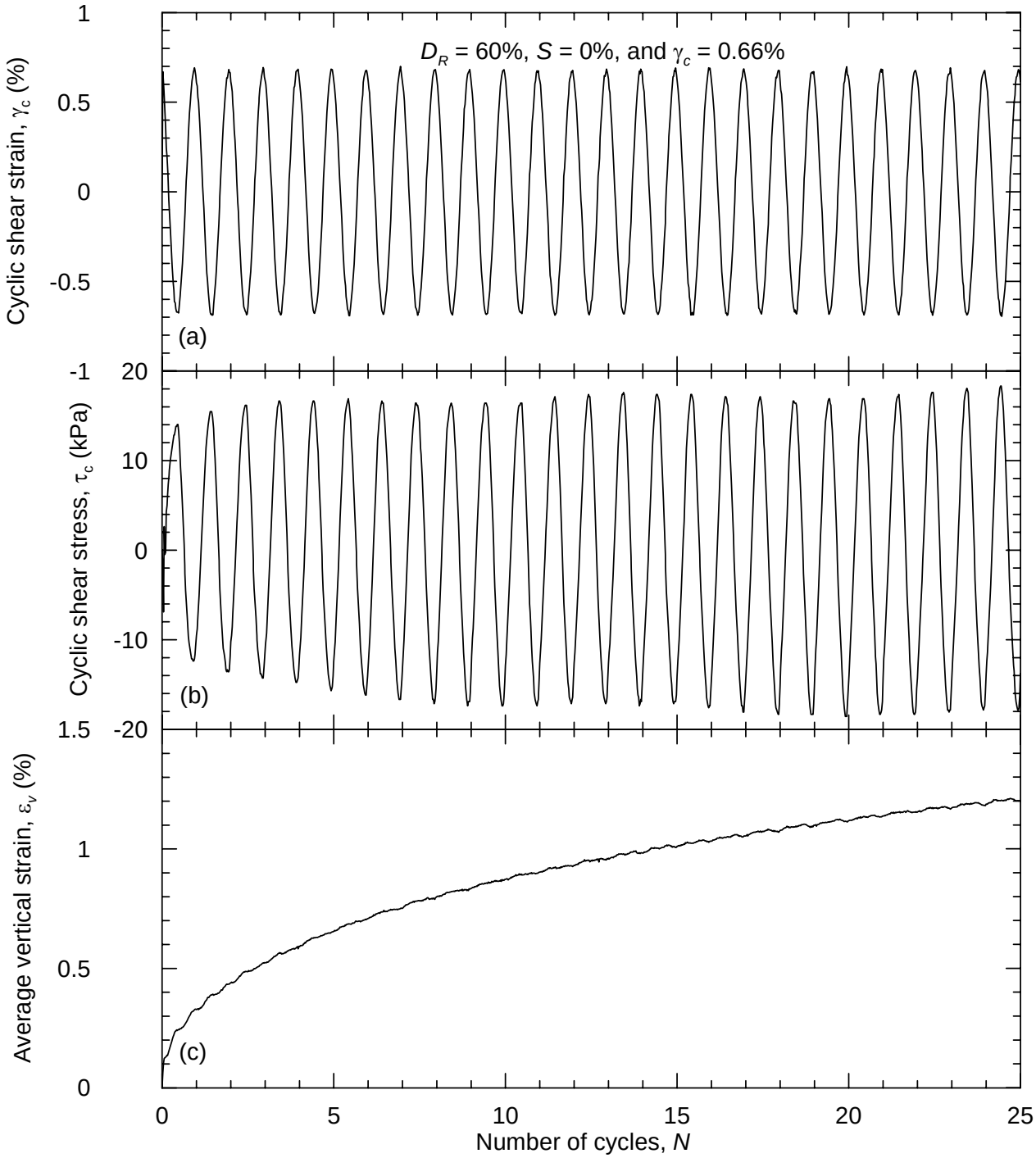

Figure 3.3. Typical cyclic simple shear test results (Silica No. 2 Sand, D_R = 60%, and S = 0%).

A cyclic simple shear test can be summarized by the relationship between (a) γ_c, the uniform cyclic shear strain amplitude and $(\varepsilon_v)_{N=15}$, the vertical strain associated with 15 cycles of loading and (b) C_N, the normalized vertical strain defined as $(\varepsilon_v)_N/(\varepsilon_v)_{N=15}$, versus N, the number of strain cycles. These two relationships comprise the volumetric strain material model which is used in simplified analysis procedures to estimate ground settlement from seismic compression (e.g., Tokimatsu and Seed, 1987).

For a specific sand, data are compiled from multiple simple shear tests at various cyclic shear strain amplitudes (γ_c), as shown for example in Figure 3.4(a). A γ_c-$(\varepsilon_v)_{N=15}$ relationship is defined using a power function curve-fit through the data as follows:

$$\left(\varepsilon_v\right)_{N=15} = a \cdot \left(\gamma_c - \gamma_{tv}\right)^b \tag{3.3}$$

where γ_{tv} = volumetric threshold strain, and a and b are material-specific constants. A typical range of γ_{tv} for sands is 0.01 - 0.03% (Hsu and Vucetic, 2004). As shown in Figure 3.4(b), the C_N-N relationship is nearly log-linear over the range of N of typical engineering interest and can be described by the following expression:

$$C_N = R\ln(N) + c \tag{3.4}$$

All sands must have $C_N = 1$ at $N = 15$, which implies that intercept parameter $c = 1/(\ln(15) \times R)$. Consequently, the C_N-N relationship for a given soil is fully described by slope parameter R. The log-linear fit is shown in Figure 3.4(b) by the line.

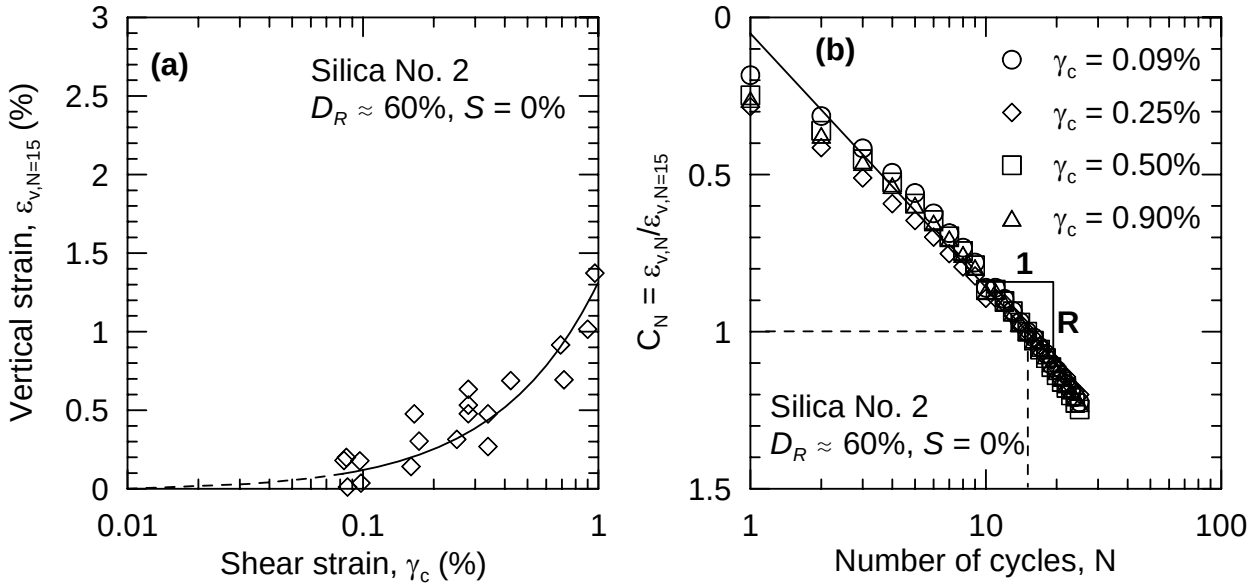

Figure 3.4. Volumetric strain material models summarizing test results, (a) $\varepsilon_{v,N=15}$ versus γ_c relationship and (b) $\varepsilon_v/\varepsilon_{v,N=15}$ versus N.

3.4.2 Effect of Relative Density

Multiple specimens of the fourteen subject sands were prepared at zero saturation to relative densities (D_R) near 60%. Specimens of two of these sands with significantly different gradation characteristics (Silica No. 2 and Vulcan) are prepared to $D_R \approx 45\%$ and 80%. All of these specimens are normally consolidated and loaded with a vertical stress of σ_v=101.7 kPa prior to cyclic loading. For a given sand material, multiple specimens were tested at different cyclic shear strain levels and regressions similar to those illustrated in Figure 3.4 were performed with the results given in Column A of Table 3.3 (regression parameters denoted a^* and b). Looking first at the slope parameter (b), we see in Table 3.3 and Figure 3.5 that the results generally fall between approximately 0.9 and 1.3, with an average value of b=1.1 and no apparent dependence on D_R. Given the consistency of the b values for the tested sands, we fix b at the average value of 1.1 (for the sake of developing a volumetric strain material model) and then re-regress the data for each sand/density combination to obtain new intercept values (a). Those values of a are listed in Column B of Table 3.3, and are not significantly different from a^*.

Table 3.3. Volumetric strain material model ($\varepsilon_{v,N=15}$) regression coefficients for all sands tested

		Column A		Column B
		Intercept parameter	Slope parameter	Intercept parameter
Material	D_R (%)	a*	b	[1]a
Vulcan	45	2.49 ± 0.05	1.45 ± 0.11	2.23 ± 0.13
	60	2.48 ± 0.03	1.26 ± 0.07	1.59 ± 0.07
	80	2.10 ± 0.08	1.31 ± 0.24	0.97 ± 0.09
Silica No. 2	45	1.88 ± 0.02	0.94 ± 0.07	1.97 ± 0.08
	60	1.50 ± 0.15	1.09 ± 0.20	1.38 ± 0.09
	80	1.09 ± 0.03	1.25 ± 0.06	0.97 ± 0.03
Crystal silica No. 30	60	1.17 ± 0.07	0.76 ± 0.11	1.52 ± 0.10
F-52	60	1.04 ± 0.03	1.09 ± 0.05	1.45 ± 0.05
F-110	60	1.71 ± 0.03	1.16 ± 0.05	1.65 ± 0.06
Fint No. 13	60	1.36 ± 0.04	1.07 ± 0.06	1.35 ± 0.04
Flint No. 16	60	1.80 ± 0.04	1.16 ± 0.08	1.71 ± 0.06
Nevada	60	1.40 ± 0.05	1.08 ± 0.10	1.41 ± 0.08
Newhall	60	1.53 ± 0.12	1.36 ± 0.22	1.14 ± 0.06
Pacoima No. 1	60	1.69 ± 0.02	1.04 ± 0.06	1.73 ± 0.06
Pacoima No. 3	60	1.47 ± 0.02	1.05 ± 0.04	1.50 ± 0.03
Irwindale	60	1.31 ± 0.06	1.03 ± 0.16	1.32 ± 0.10
Post Office	60	0.86 ± 0.03	1.02 ± 0.05	0.87 ± 0.04
Silica No. 0	60	1.88 ± 0.05	1.28 ± 0.07	1.55 ± 0.10

[1] Regression performed with slope parameter, b = 1.1

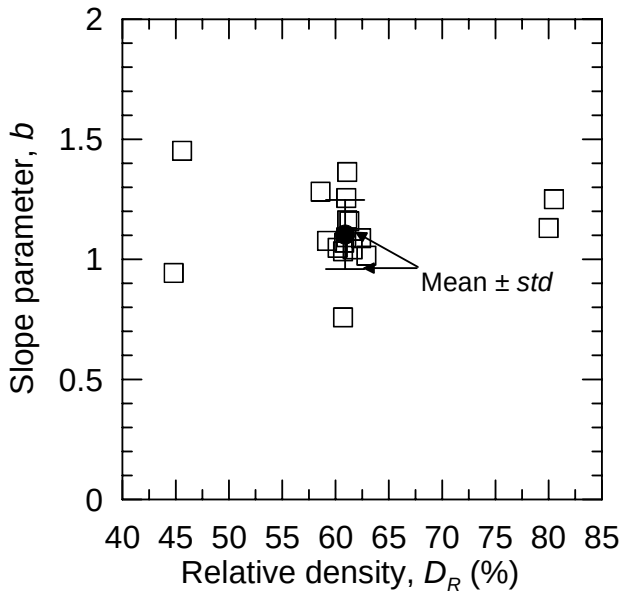

Figure 3.5. Relationship between slope parameter *b* and D_R, where *b* is from the simultaneous regression of slope and intercept parameters reported in column A of Table 3.3.

As shown in Figure 3.6, intercept parameter a decreases significantly as D_R increases. The trend is fit with a power law relationship, with the results of the regression indicated in Figure 3.6 and below:

$$a = 5.92 \cdot \exp\left(-0.023 \cdot D_R\right) \tag{3.5}$$

Recall that this relation for a applies with a fixed value of b = 1.1, and together these parameters along with γ_{tv} can be used with Eq. 3.3 to form that portion of the volumetric strain material model that describes $(\varepsilon_V)_{N=15}$. Model residuals are calculated as the difference between measured values of $(\varepsilon_V)_{N=15}$ and the model prediction for all of the individual test results for the 14 sands, with the results shown in Figure 3.7(a). The model is seen to be unbiased across the range of strains considered, and with a standard deviation that increases with increasing strain. Figure 3.7(b) is a histogram of normalized residuals (found to be normally distributed per the Chi-squared test at the 95% confidence level),which that indicates the coefficient of variation (COV) of the data to be 0.34.

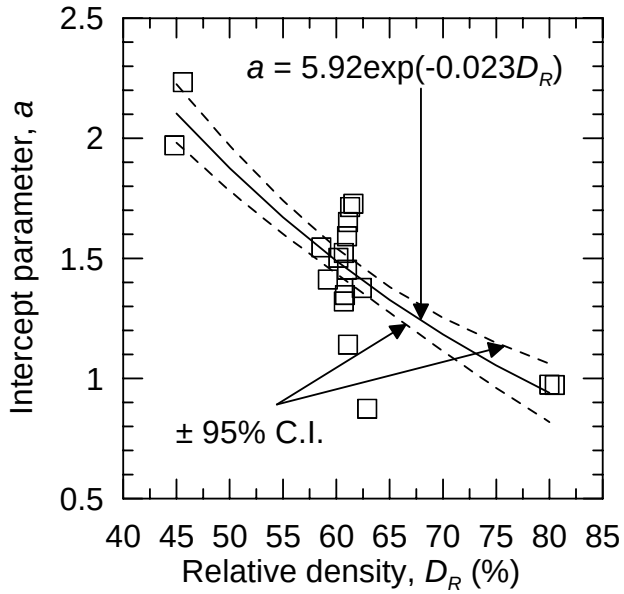

Figure 3.6. Relationship of intercept parameter a and D_R; where a is from regression with b = 1.1, column B of Table 3.3.

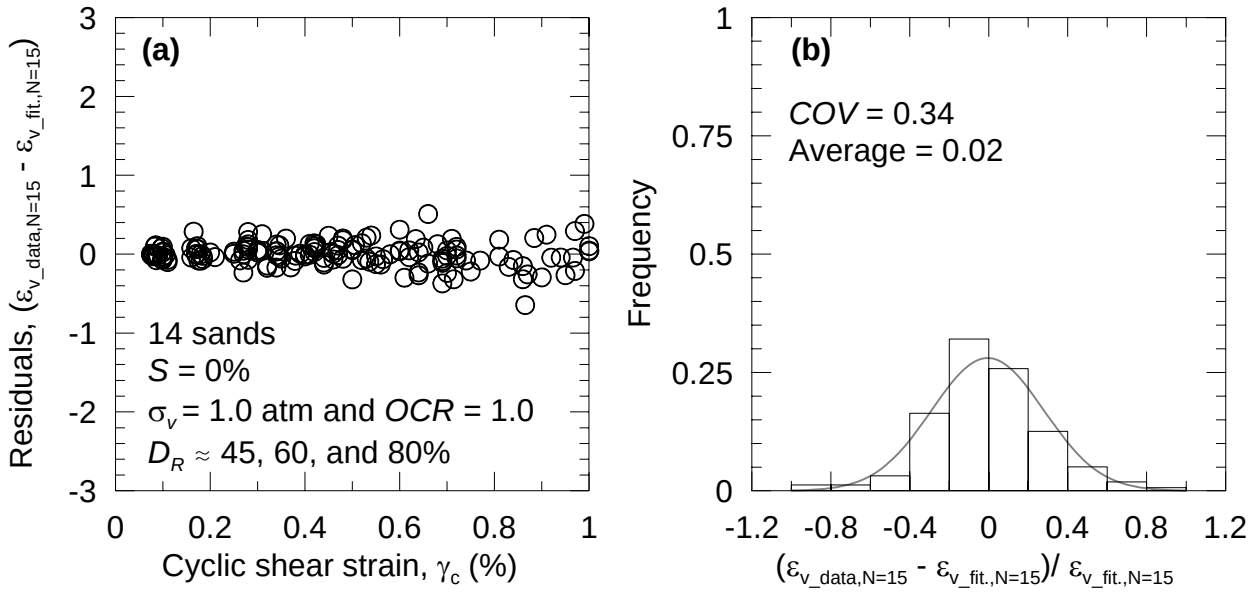

Figure 3.7. (a) Residuals of $\varepsilon_{v,N=15}$ versus γ_c, and (b) the distribution of the normalized residuals with *COV* = 0.34.

Figure 3.8(a) shows data points for all tested sands near D_R = 60% along with the model prediction. Figure 3.8(b) shows that the mean model predictions are slightly smaller than fit lines previously provided by Silver and Seed (1971) for Crystal Silica sand.

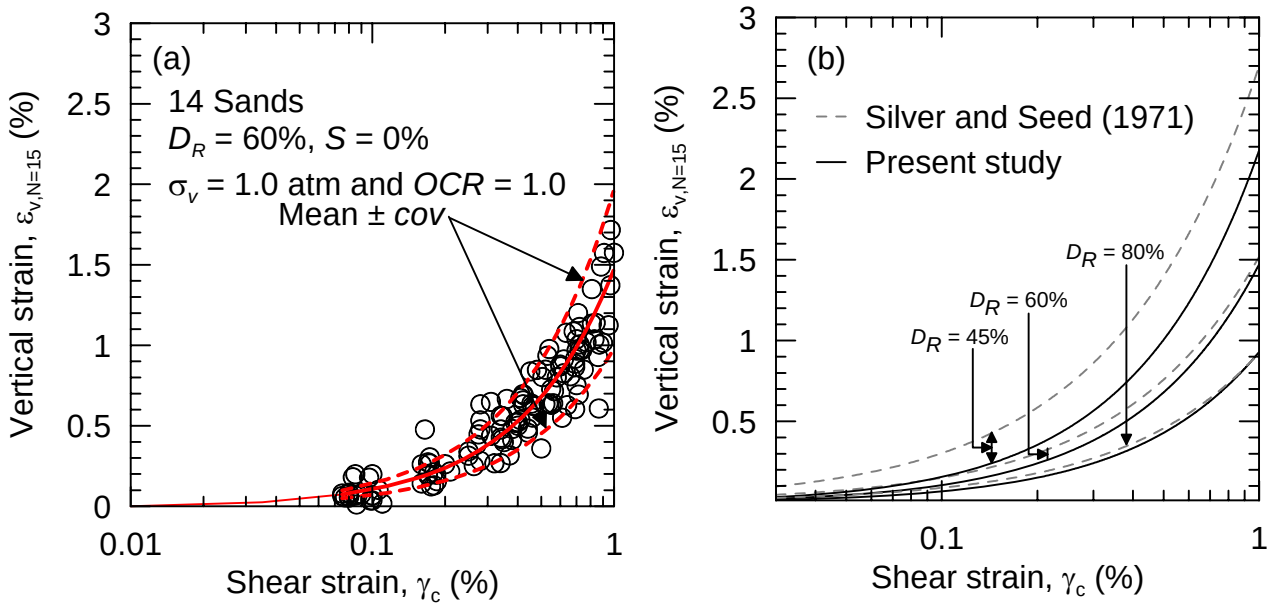

Figure 3.8. (a) Comparison of data to model for D_R = 60%. (b) Plot of mean model prediction compared to previous study of Silver and Seed (1971) at D_R = 45, 60, and 80%.

Test results showing the *R* parameter (used to parameterize the effect of number of cycles, Eq. 3.4) are given in Figure 3.9. Parameter *R* was not found to be dependent on strain level (e.g., Figure 3.4b), but is dependent on D_R as indicated in Figure 3.9 and by the regression equation below:

$$R = 0.386 \cdot \exp\left(-9.64 \times 10^{-7} D_R^3\right) \tag{3.6}$$

The data were found to be lognormally distributed with standard deviation $\sigma_{Ln} = 0.08$.

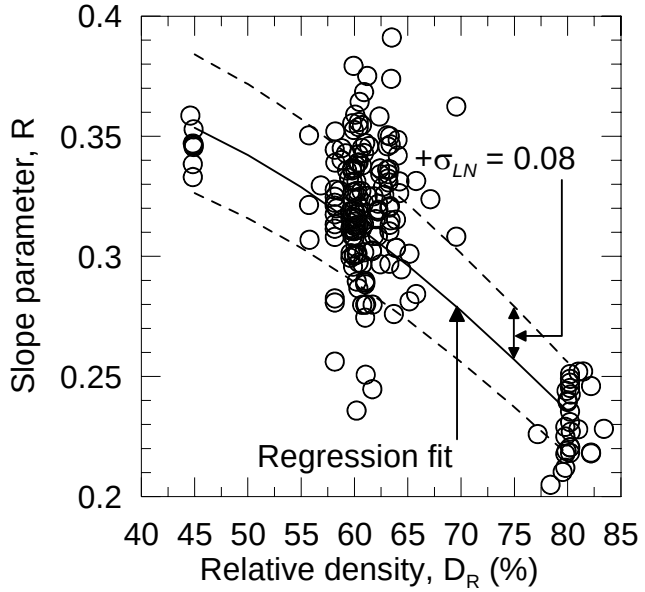

Figure 3.9. Trend of slope parameter (*R*) versus D_R.

3.4.3 Effect of Saturation, Loading Frequency, and Composition

The effect of saturation was investigated by preparing samples of Silica No. 2 and Vulcan sands to saturation levels of 0, 30, 60, and 90% at relative densities near 60%. The data in Figure 3.10(a) show no trend of $(\varepsilon_V)_{N=15}$ with saturation and all data fall within the expected scatter of the model fit from the previous section. From these results and similar results showing no effect of saturation on *R*, we conclude that saturation levels between zero and 90% do not affect the seismic compression behavior of clean sands. This finding is expected, as matric suction in partially saturated clean sands is minimal.

As shown in Figure 3.10(b), the effect of frequency was found to be negligible in suites of tests performed on dry specimens of Silica No. 2 sands. This result demonstrates the expected finding that cyclic volume change behavior of clean sands is not significantly rate-dependent.

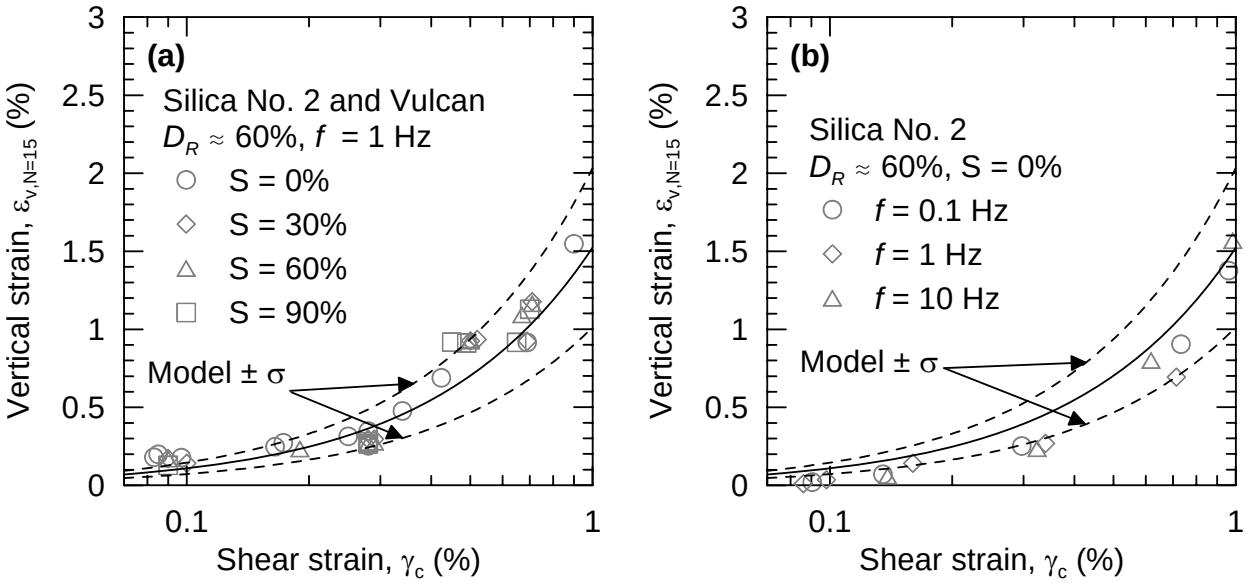

Figure 3.10. Results of testing that demonstrates the lack of effect of saturation and loading frequency on vertical strains from seismic compression.

The effects of soil composition were examined from multiple perspectives. First, we investigated the effect of soil fabric by testing specimens of Silica No. 2 sand prepared to 60% relative density with different specimen preparation techniques. The results in Figure 3.11(a) show the lack of effect of soil fabric in these tests, which is similar to trends identified from previous liquefaction strain-controlled tests (NRC, 1985). Next, we plot the *a* parameter from Table 3.3 as a function of gradation parameters (mean grain size D_{50}; uniformity coefficient, c_u) and particle angularity parameter S_f, and find no apparent trend as shown in Figures 3.11(b)-(d). The data in Figure 3.11(b)-(d) are plotted separately for quartz and volcanic minerologies, and show no significant differences overall for the two minerologies, and no recognizable differences between the two minerologies with respect to the trends with gradation/shape parameters. Finally, we plot the *a* parameter for both minerologies as a function of e-e_{min}, which was

motivated by previous research showing that e_{max}-e_{min} affects particle mobility and packing ability (Cho et al., 2006). As shown in Figure 3.11(e), we do not find that a correlates with e-e_{min} for quartz sands, although we cannot exclude the possibility that a increases with e-e_{min} for volcanic sands.

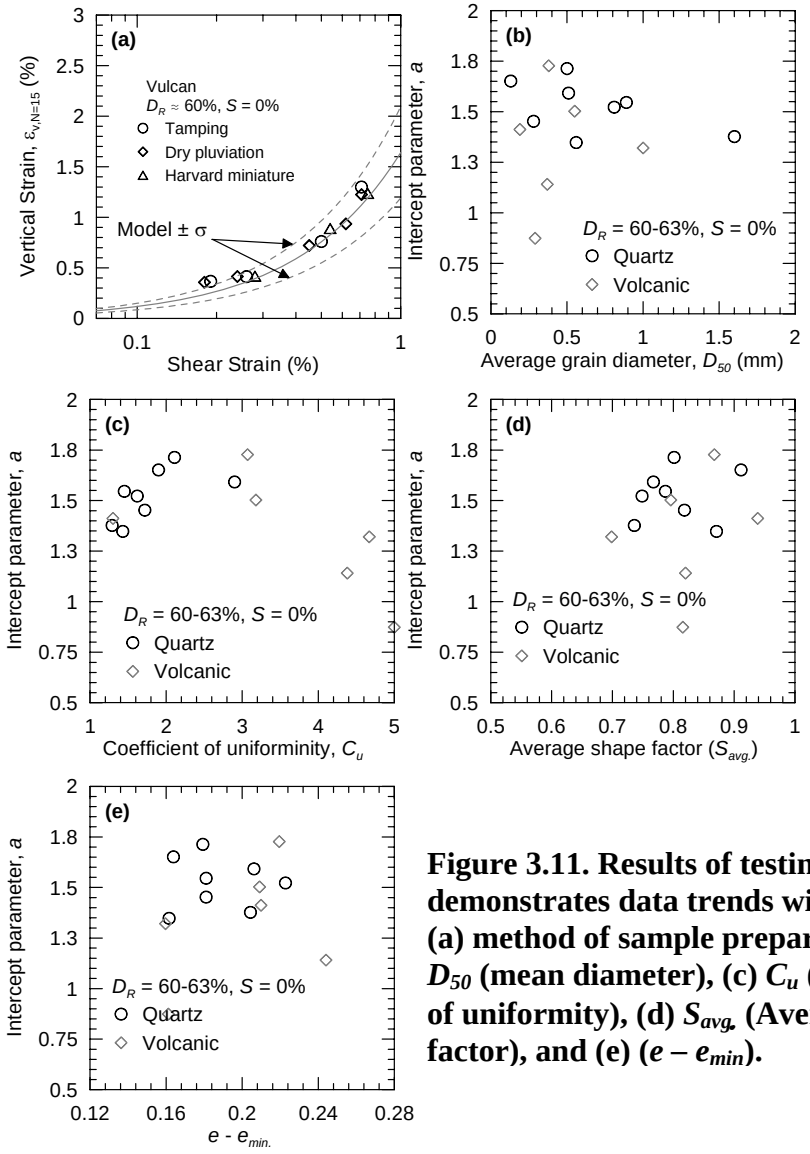

Figure 3.11. Results of testing that demonstrates data trends with respect to (a) method of sample preparation, (b) D_{50} (mean diameter), (c) C_u (coefficient of uniformity), (d) $S_{avg.}$ (Average shape factor), and (e) ($e - e_{min}$).

The results of the tests presented in this section show that saturation, frequency, and several compositional factors do not significantly affect the seismic compression behavior of clean sands. Accordingly, those parameters are not included in the volumetric strain material model.

The trend of vertical strains with e-e_{min} for volcanic sands is not considered to be sufficiently robust for e-e_{min} to be included as an additional parameter at this time.

3.4.4 Effect of Overburden Pressure

The effect of overburden pressure was investigated by placing dry, normally consolidated specimens of Silica No. 2 and Vulcan sands under vertical stresses of σ_v = 0.5, 1, 2 and 4 atm prior to cyclic loading. Example results are given in Figure 3.12(a), which shows that $(\varepsilon_V)_{N=15}$ decreases significantly as overburden pressure increases. This trend contradicts previous findings of Silver and Seed (1971) Youd (1972), who found no dependence of vertical strains on overburden stress. Nonetheless, we consider the effect to be robust, as similar trends were observed for different relative densities and for both tested sands. The complete set of tests used to evaluate overburden effects is summarized in Table 3.4.

Table 3.4. Parameters used for evaluating overburden effects

Material	D_R (%)	σ_V (atm)	a_σ	b_σ	a_σ (b_σ = 1.1)
Silica No. 2	60	0.5	1.81	0.88	1.90
		1.0	1.50	1.08	1.38
		2.0	1.11	1.08	1.12
		4.0	0.86	1.23	0.84
	80	0.5	1.26	0.88	1.32
		1.0	1.09	1.25	0.97
		2.0	0.83	1.08	0.84
		4.0	0.79	1.28	0.76
Vulcan	60	0.5	2.93	1.17	2.19
		1.0	2.48	1.26	1.59
		2.0	2.10	1.26	1.40
		4.0	1.86	1.28	1.18
	80	0.5	2.32	1.22	1.92
		1.0	2.10	1.31	0.97
		2.0	1.66	1.44	0.85
		4.0	1.12	1.30	0.77

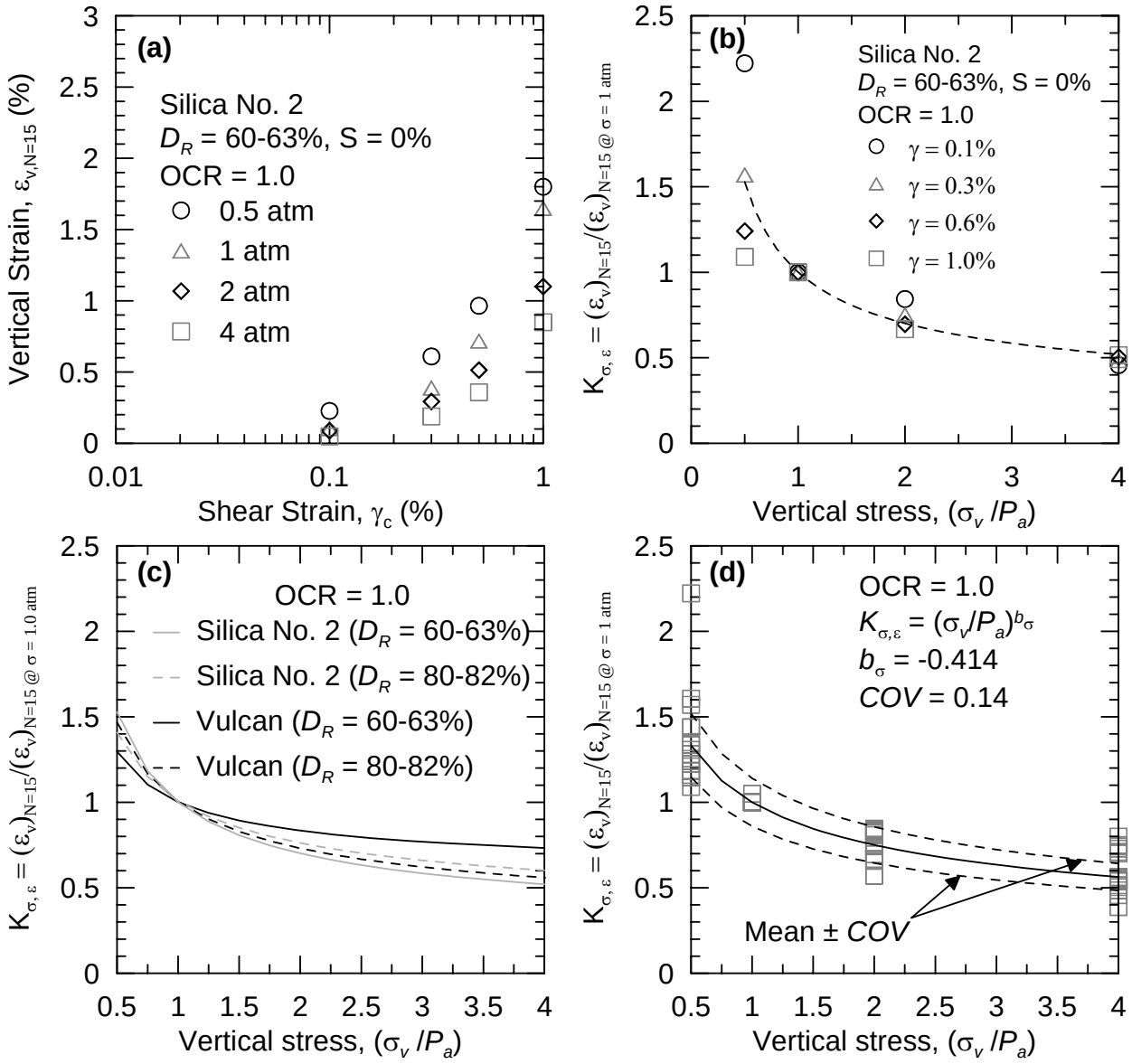

Figure 3.12. (a) Effect of overburden pressure on vertical strains from seismic compression of Silica No. 2 sand at D_R = 60-63%; (b) Overburden correction factor $K_{\sigma,a}$ derived using the data from (a); (c) mean power law fits for two sands at two D_R levels; and (d) recommended overburden correction factor derived from combined data with error term.

The average value of *b* from the results in Table 3.4 is 1.2, which can be compared to the average value of 1.1 obtained for normally consolidated sands (Figure 3.5). This difference is not considered to be significant, so the value of *b*=1.1 is retained and the data are re-regressed using this value to obtain the *a* values shown in Table 3.4. Parameter *a* decreases significantly with

increasing σ_v. In order for overburden effects to be accounted for in volumetric strain material models, overburden correction factor $K_{\sigma,\varepsilon}$ is proposed:

$$K_{\sigma,\varepsilon} = \frac{a_\sigma}{a_{\sigma=1.0atm}} \tag{3.7}$$

As indicated in Eq. 3.7, the coefficient $K_{\sigma,\varepsilon}$ is calculated for a given level of overburden pressure (σ_v) by normalizing the fitted a value from Table 3.4 (denoted a_σ) by the model prediction for σ_v=1.0 atm (i.e., as obtained using Eqs. 3.3 and 3.5). Example results are shown in Figure 3.12(b) for Silica No. 2 sand at D_R = 60%, where each symbol represents the fit results for a suite of tests across a range of shear strains. The trend of the $K_{\sigma,\varepsilon}$ values in Figure 3.12(b) can be represented with a power law, which is shown by a line in the figure. The apparent bias at low vertical stresses in Figure 3.12(b) is not systematic for other sands and density levels as shown subsequently. Power law fits for all tested sands and density levels are given in Figure 3.12(c), from which we note no systematic variations between fit lines for different materials and D_R levels. Accordingly, we combine all data to develop the recommended power law relationship as follows:

$$K_{\sigma,\varepsilon} = \left(\frac{\sigma_v}{P_a}\right)^{-0.243} \tag{3.8}$$

This relationship is shown in Figure 3.12(d) along with the coefficient of variation of the data. Note that this relationship does not show the aforementioned bias at small stress levels.

In order to compare these results to overburden correction factors previously identified for liquefaction problems (e.g., Boulanger, 2003), we convert our strain-based overburden correction factor ($K_{\sigma\varepsilon}$) to the stress-based factor (K_σ) as follows: (*i*) as shown in Figure 3.3, cyclic shear stresses (τ_c.) in a given test vary with time, but the stresses are bounded by selecting τ_c at N = 1

and 15 cycles [$(\tau_c)_1$ and $(\tau_c)_{15}$]; (*ii*) those values of τ_c are normalized by σ_v to give cyclic stress ratio [$CSR_1=(\tau_c)_1/\sigma_v$ and $CSR_{15}=(\tau_c)_{15}/\sigma_v$] – example plots are shown in Figure 3.13(a); (*iii*) effective K_σ values are derived as $K_{\sigma,1}=CSR_1(\sigma_v)/CSR_1(\sigma_v=1)$ and $K_{\sigma,15}=CSR_{15}(\sigma_v)/CSR_{15}(\sigma_v=1)$. Example values of K_σ for N = 1 and 15 are shown in Figure 3.13(b), from which we see that the K_σ implied by our test results does not vary significantly with N. Finally, in Figure 3.13(c) the K_σ range implied by our data is seen to follow similar trends as curves recommended in previous studies. A perfect match is not expected, as the stress paths in drained versus undrained tests are obviously very different.

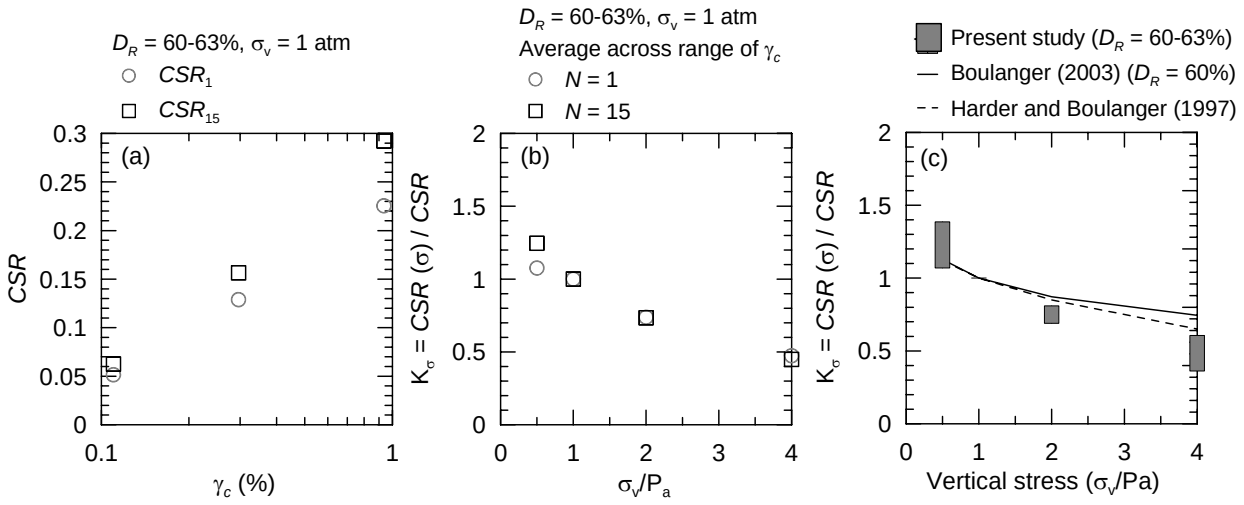

Figure 3.13. (a) Equivalent values of *CSR* for different shear strain levels in strain-controlled tests; (b) effective K_σ values at N = 1 and 15; (c) comparison of results to previous studies.

The interpretation of the trend in traditional K_σ -σ_v plots is well known – critical state soil mechanics implies more contractive soil behavior as σ_v increases, thus decreasing the liquefaction strength. The trend in $K_{\sigma\varepsilon}$ (Figure 3.12d) seems to suggest the opposite – less contractive behavior, as manifest by lower vertical strains, as σ_v increases. However, the data in Figure 3.13 shows this apparent contradiction to be a by-product of attempting to explain

material behavior in terms of stresses in one case and strains in the other, which is complicated by the strong effect of shear (and bulk) modulus on σ_v. In short, increasing σ_v causes the soil to be more contractive (in terms of stresses), but this is more than compensated by the increased bulk modulus at high σ_v, reducing the volume change.

3.4.5 Effect of Stress History

To investigate stress history effects, we compare measured vertical strains in normally consolidated and overconsolidated sand specimens that are otherwise similar (same material, $_v$, and D_R). These tests are performed on Silica No. 2 and Nevada sands prepared to relative densities of approximately 60 and 80%, σ_v=0.5 and 1.0 atm, and OCR values of 1.0, 1.5, 2.0, and 4.0. The full matrix of test parameters used to investigate OCR effects is given in Table 3.5 along with the test results (expressed using a^* and b parameters from regression of the data using Eq. 3.3).

Table 3.5. Parameters used for evaluating stress history effects

Material	D_R (%)	σ_v (atm)	*OCR*	a_{OCR}^*	b_{OCR}	a_{OCR} *(b = 1.1)*
Silica No. 2	60	1.0	1.0	1.50	1.08	1.38
		1.5	1.5	1.39	1.21	1.30
		2.0	2.0	0.92	1.22	0.69
		4.0	4.0	0.78	1.27	0.60
	80	1.0	1.0	1.09	1.25	0.97
		1.5	1.5	0.98	1.23	0.95
		2.0	2.0	0.95	1.27	0.67
		4.0	4.0	0.72	1.28	0.57
Nevada	60	1.0	1.0	1.40	1.08	1.41
		1.5	1.5	1.23	1.23	1.17
		2.0	2.0	0.85	1.21	0.69
		4.0	4.0	0.76	1.26	0.58

Representative results of these tests are shown in Figure 3.14. Figure 3.14(a)-(b) show test results at σ_v = 1.0 atm and D_R = 60-63% and 80-82%. The data show a decrease of vertical stain with increasing OCR, which is consistent with results of previous liquefaction testing (Lee and

Focht; Ishihara and Takatsu, 1979; Finn, 1981). The amount of strain decrease observed in overconsolidated specimens is greater that what would be expected from the overburden increase that results from over-consolidation (details in Duku, 2007). Interestingly, the OCR effect is insignificant at σ_v = 0.5 atm, as shown in Figure 3.14(c). The results at low overburden pressure (Figure 3.14c) are of the greatest practical significance, because compacted fills tend to be overconsolidated due to compaction-induced stresses near the surface (upper 3-6 m) but normally consolidated at larger depths (Duncan et al., 1991). Because stress history effects appear to be negligible at the low overburden pressures in that depth range, it appears that such effects can be neglected for the analysis of seismic compression in clean sand fills.

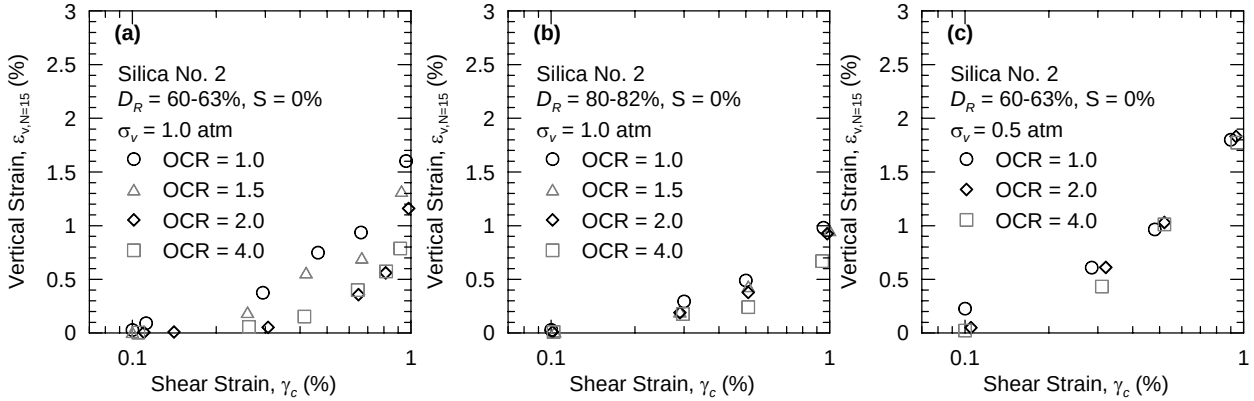

Figure 3.14. *OCR* effect for Silica No. 2 with baseline σ_v = 1.0 atm (a) at D_R = 60-63%, (b) at D_R = 80-82%, and (c) *OCR* effect for Silica No. 2 at D_R = 60-63% and σ_v = 0.5 atm.

3.5 DISCUSSIONS AND CONCLUSIONS

In this article, we present a comprehensive investigation of the seismic compression susceptibility of clean sand materials. We investigate the effects of a number of compositional and environmental factors on the vertical strain at 15 uniform shear strain cycles, $(\varepsilon_v)_{N=15}$, and on a parameter representing the cycle-to-cycle variation of vertical strain, $C_N=(\varepsilon_v)_N/(\varepsilon_v)_{N=15}$. These effects are investigated using strain-controlled cyclic simple shear laboratory testing of 14 different clean sand materials.

The compositional factor found to principally affect seismic compression susceptibility is relative density (D_R), which is consistent with previous research. Additional composition factors that were found to not significantly affect seismic compression susceptibility include gradation parameters (mean grain size, uniformity coefficient), particle angularity, soil fabric, mineralogy, and void ratio "breadth" e-e_{min}. The environmental factor found to principally affect seismic compression susceptibility is confining stress, with volumetric strains decreasing with increasing stress. Environmental factors found to not significantly affect seismic compression susceptibility for clean sands include saturation (this study) and age (Duku et al., 2006). Stress history can decrease vertical strains from seismic compression for certain conditions, but we find such effects to not be significant for the levels of overburden stress where compacted fills are typically overconsolidated.

An empirical model is developed to capture the trends in the test data with respect to D_R. In this model, $(\varepsilon_v)_{N=15}$ is calculated using Eq. 3.3 with b=1.1, γ_{tv}=0.01-0.03%, and a evaluated from Eq. 3.5. Parameter C_N is calculated using Eq. 3.4 with R evaluated from Eq. 3.6. The important effect of overburden stress can be captured by a multiplicative correction to the a parameter, $K_{\sigma\varepsilon}$, represented by Eq. 3.8. This model can be readily extended for use with penetration resistance data obtained in the field by estimating relative density with the following empirical relationships (Idriss and Boulanger, 2003):

$$D_R = \sqrt{\frac{(N_1)_{60}}{45}}$$
$$D_R = 0.478(q_{c1N})^{0.264} - 1.063 \qquad (3.9)$$

where $(N_1)_{60}$ is an overburden-corrected standard penetration test blow count and q_{c1N} is an overburden corrected tip resistance from a CPT sounding.

4 SEISMIC COMPRESSION BEHAVIOR OF NON-PLASTIC SILTY SAND

4.1 INTRODUCTION

Available laboratory test data for soils with fines from which volumetric strain material models can be derived have been presented by Pyke et al. (1975) and Whang et al. (2004). Pyke et al. (1975) performed a limited number of cyclic simple shear tests on a well-graded clayey sand (SC) at two densities (modified Proctor relative compaction, RC = 84.4 and 92%) and one water content (w = 10%). The results indicated that volumetric strains in the clayey sand at RC = 92% were less than approximately one-third of the expected settlement in a clean sand prepared to a comparable relative density (D_R = 60%). Whang et al. (2004) performed cyclic simple shear laboratory testing on four fill soils containing significant fines with varying levels of fines plasticity. The result of this research is discussed further in Chapter 5.

Additional studies on soils with fines were performed by Chu and Vucetic (1992), Hsu and Vucetic (2004) and Tsukamoto et al. (2004), and provide valuable insights into seismic compression behavior with regards to the volumetric threshold strain and other effects. However, the data produced from these studies do not easily lend themselves to the development of volumetric strain material models**.**

This chapter presents data that begins to fill the knowledge gap regarding the effect of plasticity and the transitional behavior from sands-dominated behavior to fines-dominated

behavior as *FC* increases, with a focus on the effect of non-plastic fines on seismic compression. In particular, we document the results of a laboratory simple shear testing program that provides insight into the effects of density, saturation, and fines content on volumetric strains from seismic compression.

4.2 SOILS TESTED

The soil materials tested in this study were artificial mixtures of sand and silt. Two sand materials and one silt material were used. Sand No. 1 is termed "Vulcan sand," which is commercially available from Vulcan Materials Company in Irwindale, California. Vulcan sand is well-graded with a mean grain size, D_{50}, of 0.51 mm and particle shapes that range from subangular to subrounded. Sand No. 2 is termed "Silica No. 2," which is commercially available from US Silica Company. Silica No. 2 is poorly graded with a mean grain size, D_{50}, of 1.6 mm and subrounded particles. The silt used in this study was Sil-Co-Sil No. 52 obtained from US Silica Company. The silt material is non-plastic, being comprised of Quartz particles of very small size (i.e., rock flour). It is very difficult to estimate liquid limit using ASTM procedures for these materials, but LL is known to be $< \sim 17$ based on tests performed.

For each sand material, four different sand-silt mixtures were created with silt contents varying from 10 to 50%. In addition, tests were performed on the host sands without adding silt materials. Index testing performed on these materials include gradation, modified Proctor compaction, minimum/maximum void ratio, and matric suction. The maximum and minimum dry densities and void ratios of each sand-silt combination were determined using the Modified Japanese method and dry tipping, respectively (these techniques are comparable to those in ASTM D4253 and D4254). The matric suction tests were performed using the filter paper

method (ASTM D5298-03) in which soil materials are compacted on dry filter paper, which then absorbs water from the soil. We used Whatman No. 42 filter paper for those tests. The paper absorbs relatively little water if the matric suction is large (soil effectively holds the water in its grains), and more water if matric suction is small. Results of the matric suction tests are summarized in Table 4.1.

Table 4.1. Soils tested

Material	Fines Content FC (%)	Void ratio		Matric suction, Ψ (kPa)[1]	
		e_{min}	e_{max}	S = 30%	S = 60%
Vulcan sand	0	0.412	0.904	< 15.7	< 15.7
Vulcan 90-10 mix	10	N/A	0.352	N/A	N/A
Vulcan 80-20 mix	20	N/A	0.289	N/A	N/A
Vulcan 65-35 mix	35	N/A	0.297	N/A	N/A
Vulcan 50-50 mix	50	0.174	0.474	30.2	N/A
Silica No. 2 sand	0	0.662	1.006	< 15.7	< 15.7
Silica No. 2 80-20 mix	20	0.405	0.860	N/A	N/A
Silica No. 2 70-30 mix	30	0.298	0.819	N/A	N/A
Silica No. 2 60-40 mix	40	0.398	1.177	N/A	N/A
Silica No. 2 50-50 mix	50	0.457	1.442	525.4	50.0

N/A = not measured
1 Matric suction head - all tests performed for RC ~ 87%

4.3 LABORATORY TESTING EQUIPMENT AND PROTOCOLS

Laboratory testing was performed using the DCSS (Digitally Controlled Simple Shear) device described previously in Chapter 2. Cyclic simple shear (CSS) tests were performed under partially drained conditions to evaluate vertical strain accumulation when uniform-amplitude cycles of shear strain are applied to the soil specimen. For each sand-silt combination, cyclic simple shear tests were performed at varying levels of modified Proctor relative compaction (*RC* = 87, 92, and 95%) and as-compacted saturation (*S* = 0, 30, and 60%). Commercially available wire-reinforced membranes were used to laterally confine the 102 mm diameter specimens, which were prepared by kneading compaction. All tests were performed under the same vertical

stress of 1.0 atm = 101.3 kPa. A sinusoidal loading frequency of 1.0 Hz and shear strain amplitudes varying from γ_c = 0.1 to 1% were used in the tests.

4.4 RESULTS OF CYCLIC SIMPLE SHEAR TESTS

4.4.1 Form and Parameterization of Results

The results of a strain-controlled CSS test can be summarized by the relationships between (a) γ_c and $(\varepsilon_v)_{N=15}$, where γ_c = uniform cyclic shear strain amplitude and $(\varepsilon_v)_{N=15}$ = vertical strain associated with 15 cycles of loading; and (b) C_N and N, where $C_N = (\varepsilon_v)_N/(\varepsilon_v)_{N=15}$ and N = number of strain cycles. These two relationships comprise what is referred to herein as the "volumetric strain material model" for the soil.

For a specific soil, multiple CSS tests were performed at various cyclic shear strain amplitudes (γ_c), and these results can be used to construct the γ_c-$(\varepsilon_v)_{N=15}$ relationship, an example of which is shown in Figure 4.1(a). Each individual data point in Figure 4.1(a) represents a single CSS test at the indicated γ_c value on a "virgin" soil specimen (i.e., no shearing prior to the application of γ_c). The ensemble of the data shows the expected increase of $(\varepsilon_v)_{N=15}$ with γ_c. Scatter in the data is due to unavoidable specimen-to-specimen deviations in density, water content, and other factors. A curve was fit through the γ_c-$(\varepsilon_v)_{N=15}$ data having the following equation:

$$\left(\varepsilon_v\right)_{N=15} = a \cdot \left(\gamma_c - \gamma_{tv}\right)^b \tag{4.1a}$$

where γ_{tv} = volumetric threshold strain and a and b are fit parameters.

The fit obtained using Eq. 4.1(a) is shown by the line in Figure 4.1(a). The scatter of the data around the fit is quantified from the coefficient of variation (COV), which typically ranges from 0.01 to 0.23.

An example of C_N-N data for an individual CSS test is shown in Figure 4.1(b). The data is nearly log-linear over the range of N of typical engineering interest, and hence can be described by the expression:

$$C_N = R \ln(N) + b \tag{1b}$$

All soils must have C_N = 1 at N=15, which implies that intercept parameter b = 1-ln(15)×R. Consequently, the C_N-N model represented by Eq. 4.1(b) is fully described for a given soil by slope parameter R. The log-linear fit is shown in Figure 4.1(b) by the line. For a suite of tests on a given material, R can be compiled as a function of γ_c as shown in Figure 4.1(c).

The test results in Figure 4.1 apply for a specific material type, target density, and target water content. Many such CSS test suites were performed to cover a range of material types, fines contents, and compaction conditions. In the following sections, we describe key trends observed from those data regarding the effects of density, degree of saturation, and fines content on the γ_c-$(\varepsilon_v)_{N=15}$ and C_N-N relationships.

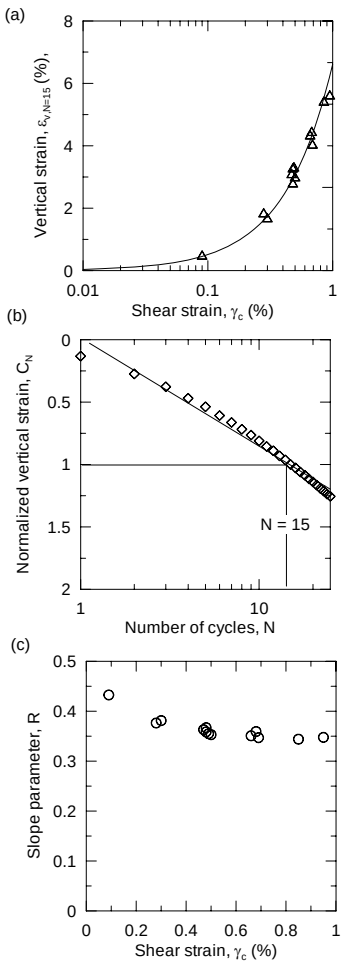

Figure 4.1. Volumetric strain model (Vulcan 50-50 mix).

4.4.2 Effect of Density

Figure 4.2 shows data and fit curves for CSS test suites performed on Vulcan 50-50 mix (50% Vulcan sand – 50% silt mixture) at different relative compaction levels. As expected, the results show that vertical strains decrease with increasing *RC*, although the difference between 87% and 92% *RC* is much greater than that between 92% and 95% *RC*. This trend with *RC* was observed at each saturation level investigated for all of the tested materials independent of host sand and fines content. Similar findings to those described above have been previously presented for dry sands by Silver and Seed (1971), Youd (1972), and Pyke et al. (1975), and for soils with high fines content by Chu and Vucetic (1992) and Whang et al. (2004).

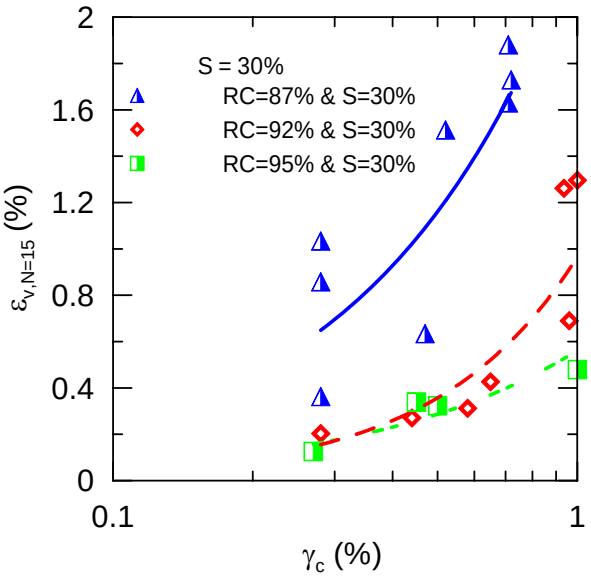

Fig. 4.2. Effect of density on Vulcan 50-50 mix at S = 30%.

4.4.3 Effect of Saturation

Figure 4.3 shows data and fit curves for CSS test suites performed on Vulcan 50-50 mix at different saturation levels. For each soil, specimens with densities of *RC* = 87% and 92% prepared to *S* = 0, 30, and 60% were tested. The results generally show the highest level of $(\varepsilon_v)_{N=15}$ for *S* = 0% and the lowest strains for *S* = 30%, with *S* = 60% providing either intermediate strain levels or levels comparable to those at *S* = 0%. Similar results were obtained for materials at lower silt contents.

The trend described above has not been observed previously. Previous studies that have investigated saturation effects on seismic compression include Youd (1971), Whang et al. (2004), and Tsukamoto et al. (2004). The Youd work performed cyclic simple shear testing on fully saturated and dry sands (*S* = 100% and 0, respectively) under drained conditions, and found that vertical strains from seismic compression were essentially identical at these two saturation levels. Whang et al. investigated the seismic compression behavior of a very low plasticity silty sand (*PI* = 2, *FC* = 44%) under drained conditions, and found no effect of saturation for *S* = 54 to

91%. Tsukamoto et al. performed undrained cyclic triaxial tests on a non-plastic silty sand (*FC* = 22%) prepared to three different saturation levels (*S* = 50, 75 and 100%), and monitored the volume change both during and after the conclusion of shaking. As expected, vertical strains during shaking were found to be small for high saturations and large for low saturations, with the converse being true for post shaking strains. Interestingly, Tsukamoto et al. found no effect of saturation on the total vertical strain across the tested saturations.

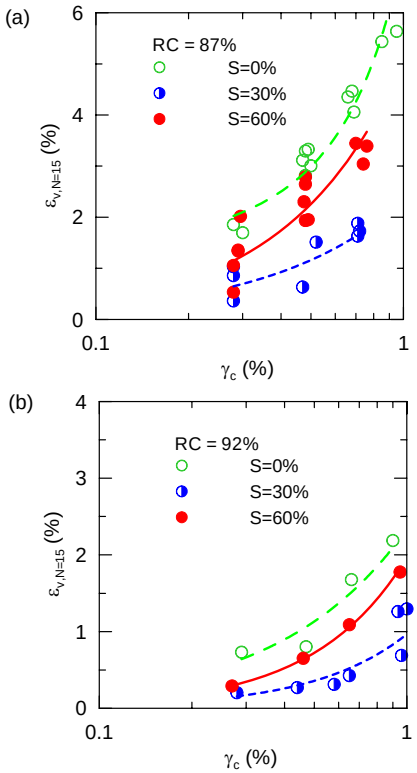

Fig. 4.3. Effect of saturation on Vulcan 50-50 mix at (a) *RC* = 87% and (b) *RC* = 92%.

To enable a comparison of our results to those of previous studies in a consistent format, we present in Figure 4.4 the vertical strain normalized by the vertical strain at high saturations (i.e., $S \geq 60\%$) for the present data as well as the data from Whang et al. (2004) and Youd (1972). The present results indicate a decrease in $(\varepsilon_v)_{N=15}$ with increasing saturation up to $S \sim 30\%$, and a subsequent increase in $(\varepsilon_v)_{N=15}$ with increasing saturation up to $S \sim 60\%$. As shown in the figure,

the Whang et al. (2004) tests were all performed at relatively high saturation levels (≥ 50%), where the effects of saturation were found to be negligible. Values of $(\varepsilon_v)_{N=15}$ at S = 0 and $S \geq$ 60%, are reasonably similar, which is consistent with the Youd (1972) results. When interpreted in this manner, we find the present test data to be consistent with previously identified trends, but also to provide new insights into saturation effects at intermediate to low saturation levels.

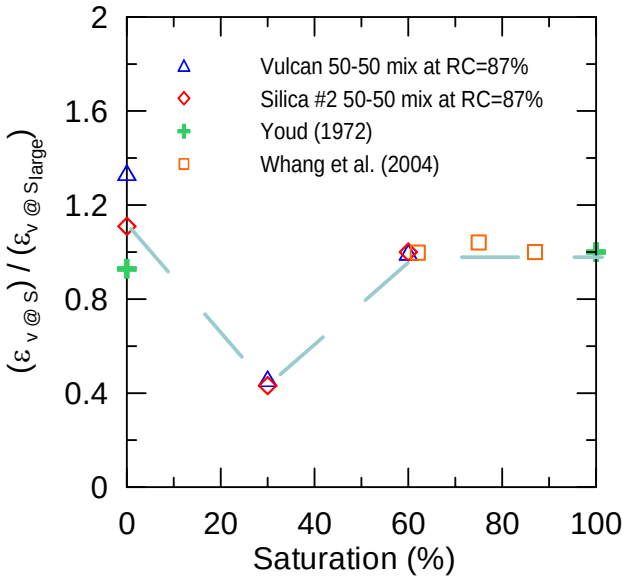

Fig. 4.4. Variation of normalized seismic compression with saturation.

A factor that may be responsible for the saturation effect on $(\varepsilon_v)_{N=15}$ is matric suction in the soil, which is maximized at low saturation levels (S = 30%), and decreases as S decreases towards zero or increases towards 60% (Table 4.1). Figure 4.5 shows for RC = 87% the variation of matric suction and $(\varepsilon_v)_{N=15}$ at γ_c = 0.3% with saturation. At S = 30%, where $(\varepsilon_v)_{N=15}$ is minimized, matric suction is maximized. The matric suction increases the effective stress in the sample, which in turn increases soil moduli (as also shown in Figure 4.5). Accordingly, it is postulated that saturation levels that give rise to high matric suction increase the moduli of the specimen, and that these increases in moduli in turn reduce the susceptibility to volume change upon the application of cyclic loading across the strain range considered.

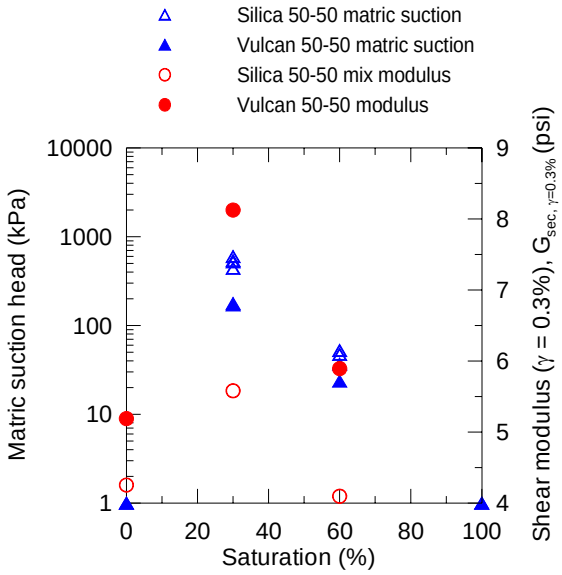

Fig. 4.5. Variation of matric suction and shear modulus with saturation.

4.4.4 Effect of Fines Content

4.4.4.1 *Overview and Concept of Limiting Fines Content*

Testing was performed in an attempt to isolate the effect of fines content from other effects associated with the degree of saturation and the soil density.

Previous studies of the effect of fines content on soil behavior have typically used constant relative density, constant global void ratio or constant sand skeleton void ratio as the basis of comparison. In the present study, constant relative compaction (essentially constant relative density) across a range of fines contents was used as a basis of comparison. The minimum and maximum void ratios for the two soil mixtures are plotted as a function of fines content (*FC*) in Figure 4.6. The dip in these void ratio quantities at mid-level *FC* is typical of non-plastic sand-silt mixtures, which has been explained by Polito and Martin (2001) utilizing the concept of limiting silt content (FC_L). Parameter FC_L is defined as the maximum amount of silt that can be contained in the void space between sand particles while maintaining a contiguous sand skeleton. For $FC < FC_L$, the addition of silt merely fills in inter-grain void space, thus decreasing void

ratio. For $FC > FC_L$, sand grains float within a silt matrix, and increasing FC increases the overall void ratio because intra-fines void ratios are relatively high. Hence, FC_L can be identified as the FC corresponding to lowest possible minimum void ratio. Using Figure 4.6, values of FC_L are identified as approximately 20% and 30% for the Vulcan-silt and Silica-silt mixtures, respectively. These are typical values for FC_L based on data compiled by Polito (1999).

The FC_L quantity forms the basis of a useful concept for visualizing the behavior of silty sands (Thevanayagam, 1998). Thevanayagam postulated that a soil mixture is a delicate matrix comprised of two submatrices, a coarser-grain matrix and finer-grain matrix. For $FC < FC_L$, the finer-grain matrix does not actively participate in the transfer of contact frictional forces, or their contribution is secondary. It follows that the coarser-grain matrix at $FC < FC_L$ can be described by the intergranular void ratio, e_s (Thevanayagam, 1998):

$$e_s = \frac{e + FC}{1 - FC} \tag{4.2}$$

where FC is expressed as a decimal. At $FC > FC_L$, the soil force chain is governed primarily by the contacts within the finer matrix and the coarser grains float in the finer-grain matrix. Consequently, the finer-grain matrix at $FC > FC_L$ can be described by the interfine void ratio, e_f, as follows (Thevanayagam, 1998):

$$e_f = \frac{e}{FC} \tag{4.3}$$

Using the above definitions, void ratio terms e_s and e_f are shown in Figure 4.6. Void ratios corresponding to relative densities intermediate between 0 and 100% (corresponding to e_{max} and e_{min}, respectively) have similar variations with FC. For example, shown in Figure 4.6 is a curve corresponding to a modified Proctor relative compaction of RC = 87%, which corresponds for

this material to D_R = 70%. The use of *RC* is motivated by its routine use as a density parameter for fill soils. Similar results for a higher density of *RC* = 92% (corresponding to D_R = 80%) were obtained but are not shown.

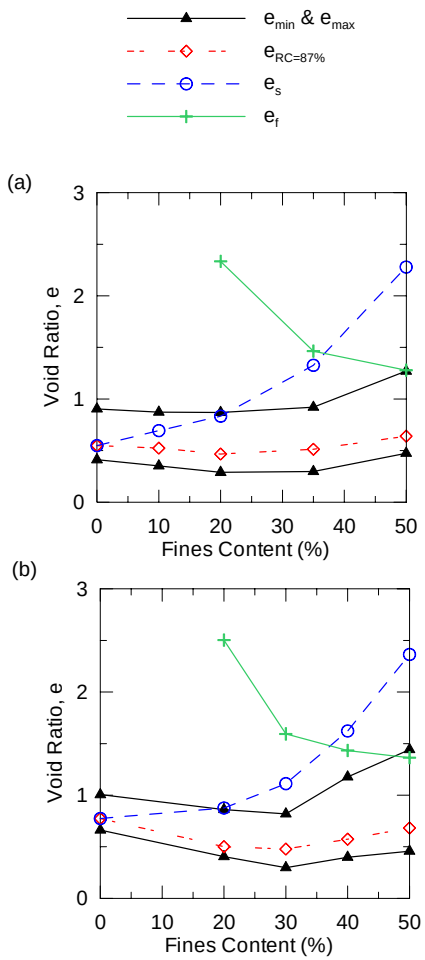

Fig. 4.6. Index void ratios at RC = 87% for (a) Vulcan and (b) Silica No. 2 host sands.

4.4.4.2 *Seismic Compression Test Results and Interpretation*

Figure 4.7 shows the effect of *FC* on seismic compression susceptibility for varying levels of *RC* and *S* for the Vulcan sand-silt mixtures. For each of these graphs, the seismic compression susceptibility is summarized by $(\varepsilon_v)_{N=15}$ at γ_c = 0.45%. In general, increasing *FC* increases the seismic compression susceptibility when using constant *RC* as a basis of comparison. However, the extent to which *FC* influences seismic compression appears to be dependent on $(\varepsilon_v)_{N=15}$.

Conditions which yielded lower $(\varepsilon_v)_{N=15}$ values such as S = 30% or RC = 92% experienced a less pronounced effect of FC than conditions producing higher $(\varepsilon_v)_{N=15}$ values such as S = 0% or RC = 87%. Similar results were found for Silica No. 2 sand-silt mixtures.

The observed increase in seismic compression with increasing FC below FC_L can be explained using the conceptual framework of Thevanayagam (1998) presented above. In particular, for $FC < FC_L$. the increase of intergranular void ratio (e_s) with FC (i.e, Figure 4.6) explains the observed increase in $(\varepsilon_v)_{N=15}$ values, because e_s is the void ratio that controls the soil behavior for this range of FC.

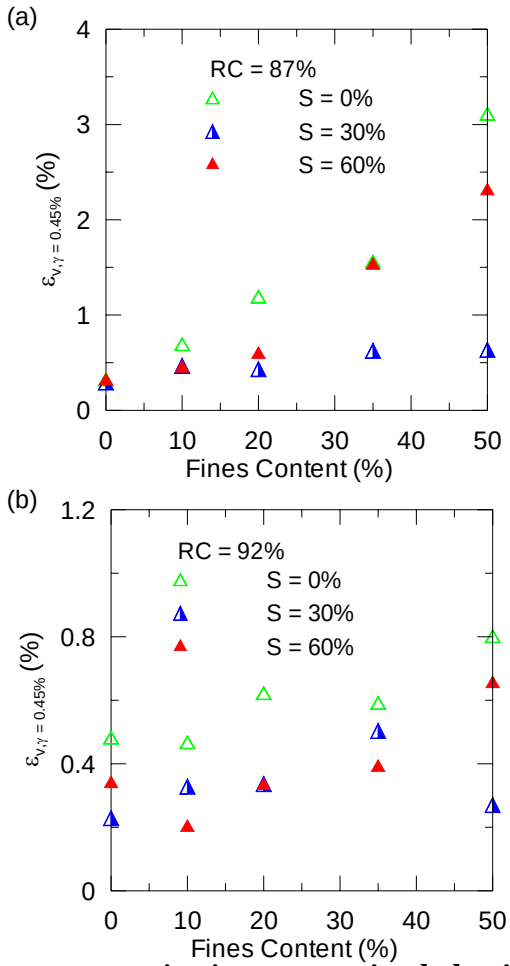

Fig. 4.7. Effect of silt content on seismic compression behavior of Vulcan host sand.

For $FC > FC_L$, the interfine void ratio, e_f, decreases with increasing FC (Figure 4.6) which would suggest a reduction in $(\varepsilon_v)_{N=15}$ values with increasing FC above FC_L. However, the opposite occurs, that is, $(\varepsilon_v)_{N=15}$ increases with FC. We attribute this to the highly compressible nature of the fine-grained matrix. To investigate this hypothesis, air-dried Sil-Co-Sil No. 52 pure silt specimens were tested at a D_R = 77%. The pure silt specimens were found to be much more contractive (in some cases by a factor of 10) than sand specimens prepared to a similar relative density. Consequently, for $FC > FC_L$, as FC increases, the effect of decreasing e_f appears to be counterbalanced by the increasing volume of highly compressible fines, thereby giving rise to the observed increase in seismic compression with FC.

4.4.4.3 *Comparison to Previous Studies*

Whang et al. (2004) evaluated the seismic compression behavior of silty sands and found that for the same Modified Proctor relative compaction (RC), soils with fines experience less seismic compression than clean sands for a common RC. Conversely, the present study found seismic compression to increase with FC. These seemingly contradictory effects of FC on seismic compression can be explained by considering the plasticity of the soils' fines fraction. The present study used truly non-plastic silt (LL < ~ 17; PL unmeasurable), whereas the Whang et al. soil contained small to moderate levels of plasticity (LL ~ 28 and 32; PI ~ 2 and 15). While those differences in plasticity would appear to be small, the literature contains compelling evidence to suggest that they may nonetheless be significant. For example:

- Undrained testing of nonplastic silty sands by Polito and Martin (2001) found that the liquefaction resistance for a fixed relative density is less for $FC > FC_L$ than for

$FC < FC_L$. This result is consistent with the present study, in the sense that the soils are more contractive at high *FC*.

- Undrained testing of sands with plastic fines by several investigators (Lee and Fitton, 1968; Ishihara and Koeski, 1989; Yasuda et al., 1994; and Bray et al., 2004) found that the liquefaction resistance for a fixed relative density increases with *FC*.

The above studies suggest that adding fines to a clean sand, while maintaining a constant relative density (or relative compaction), makes the material more contractive if the fines are non-plastic and less contractive if the fines have plasticity. Viewed in this context, the results of the present study are not contradictory with those of Whang et al. (2004).

There is a practical need to distinguish materials exhibiting the above two types of behavior (i.e., plastic versus non-plastic fines). This can be accomplished using results of soil plasticity tests, in particular LL, which can be estimated even for "non-plastic soils" (i.e, soils with unmeasurable PL). While the available data is not sufficient to definitively evaluate the boundary segregating the two classes of material behavior, it is noted that soil with LL as low as about 30 exhibited one type of behavior (seismic compression decreasing with increasing *FC*, Whang et al., 2004) while soil with LL < 17 exhibited different behavior (seismic compression increasing with increasing *FC*, present study). Hence the boundary LL is estimated to lie within the approximate range of LL = 15-30. Further testing will be needed to narrow this range.

4.4.5 Effect of Number of Cycles

As previously described and illustrated in Figure 4.1, the variation of normalized volumetric strain parameter $C_N = (\varepsilon_v)_N/(\varepsilon_v)_{N=15}$ with number of cycles *N* is approximately log-linear, and can

be completely described by slope parameter R. The cyclic simple shear test results were compiled to evaluate R as a function of various soil and test parameters.

The data suggest that slope parameter R does not have any significant dependence on the test parameters considered. There are also no significant variations between soil types. Accordingly, the data can be assembled together to estimate a mean and standard deviation, which were found to be 0.36 and 0.04, respectively, for non-plastic silty sands.

4.5 CONCLUSIONS

Cyclic simple shear laboratory testing was performed to investigate the seismic compression behavior of non-plastic silty sands. A series of 8 different silty sand materials that span a range of fines contents ($10 \leq FC \leq 50\%$), relative compaction levels and degree-of-saturations were tested. The silt materials added to the sands consisted predominantly of quartz minerals that are truly non-plastic (i.e., unmeasureable plastic limit), with a liquid limit estimated as < ~17.

The following conclusions regarding the seismic compression behavior of non-plastic silty sands were drawn from this study:

1. As expected, the seismic compression susceptibility of non-plastic silty sands was observed to decrease with increasing relative compaction independent of saturation and host sand material.

2. The effect of intermediate $S \approx 30\%$ was found to decrease vertical strains relative to values for dry ($S = 0\%$) and high saturation ($S \geq 60\%$) conditions, which produce similar amounts of vertical strains. The observed variation with saturation is likely related to matric suction in the soil, which is maximized at low saturation levels ($S = 30\%$), and decreases as S decreases towards zero or increases towards 60%.

3. The effect of increasing *FC* was observed to monotonically increase the seismic compression susceptibility when using constant *RC* as a basis for comparison. This result occurs in part because of the highly contractive nature of the non-plastic fines. Other studies have found the opposite trend for soils with plastic fines; hence, fines plasticity plays a major role in determining seismic compression susceptibility of high fines content soils.

4. The dependence of vertical strain accumulation on the number of cycles was found to be insensitive to loading and soil parameters.

5 SEISMIC COMPRESSION OF PLASTIC SOILS

5.1 INTRODUCTION

The amount of information on seismic compression of fine-grained soils with plasticity is much more limited than the available data for clean sands (Chapter 3) and non-plastic silty sands (Chapter 4). Nonetheless, a number of important insights have been gained from testing these materials in past research and from the research conducted during this investigation. In Section 5.2, we review the results of previous research. In Sections 5.3 – 5.4 we discuss the results of additional testing of fine-grained soils conducted as part of the present investigation. In Section 5.5 we synthesize the available information to develop recommendations for seismic compression analysis for fine-grained, plastic soils (although such recommendations carry limitations due to the scarcity of available test data at present).

5.2 LITERATURE REVIEW

Pyke et al. (1975) performed a limited number of cyclic simple shear tests on a well-graded clayey sand (SC) for back-analysis of settlements that occurred at the Jensen Filtration Plant during the 1971 San Fernando earthquake. Tests were performed on an NGI-type apparatus at one water content (w = 10%) and two Modified Proctor (ASTM D1557) densities (RC = 84.4 and 92%) under cyclic strain-controlled loading (γ_c = 0.1 to 0.4%). The simple shear apparatus used for this testing was the same as that used by Silver and Seed (1971). Figure 5.1 shows the

vertical strains obtained by Pyke et al. at 10 cycles of loading along with the Silver and Seed results for sands at D_R = 60% (a reasonable estimate of D_R given the *RC* range of the fine-grained fill soil). These test results indicate that vertical strains for the clayey sand were < 1/3 of the vertical strains in sand at a comparable density. Another important finding from Pyke et al. is the lack of sensitivity of seismic compression to variations in confining stress. As shown in Figure 2.6, Pyke et al. tested the Jensen fill under two vertical stresses (σ_v = 95 and 191 kPa) and found no detectable variation in vertical strain. It should be noted that these results contrast significantly with results presented in previous chapters for other materials: (1) in Chapter 3 we showed a strong effect of overburden pressure for clean sands, whereas the results in Figure 6.1 show no effect and (2) in Chapter 4 we showed a increase of vertical strain with non-plastic fines content, whereas the results in Figure 6.1 show reduced vertical strain for the soil with fines.

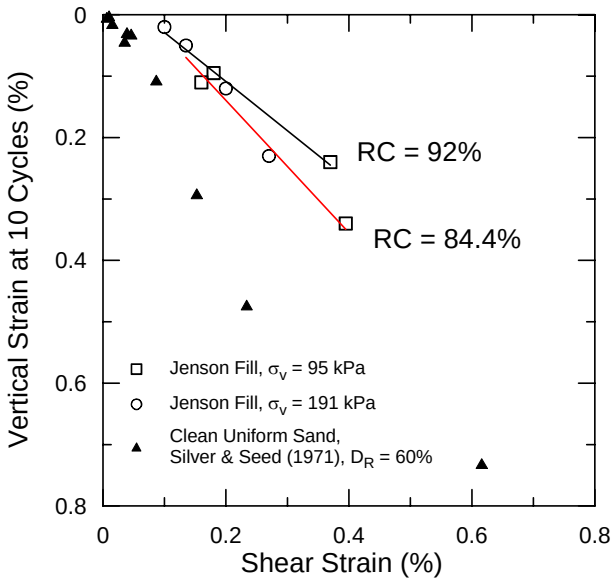

Fig. 5.1. Relationship between shear strain and vertical strain at *N* = 10 cycles for fill material at Jensen Filtration Plant (after Pyke et al., 1975).

Chu and Vucetic (1992) investigated seismic compression of a low-plasticity (PI = 10.5) clay using an NGI-type simple shear device. The testing was performed at three water contents at very high relative compaction levels (Modified Proctor *RC* between 95 and 100%). Figure 5.2 shows the variation of vertical strain (ε_v) with γ_c for N = 3, 10 and 40 cycles of loading. From these test results, Chu and Vucetic concluded that (1) for γ_c > 0.1%, ε_v for compacted clay significantly increases with γ_c and N, (2) ε_v for this particular compacted clay does not depend significantly on w for small γ_c, and (3) the volumetric threshold strain, γ_{tv}, of this compacted clay, i.e., the shear strain below which the settlement is negligible, is around 0.1%.

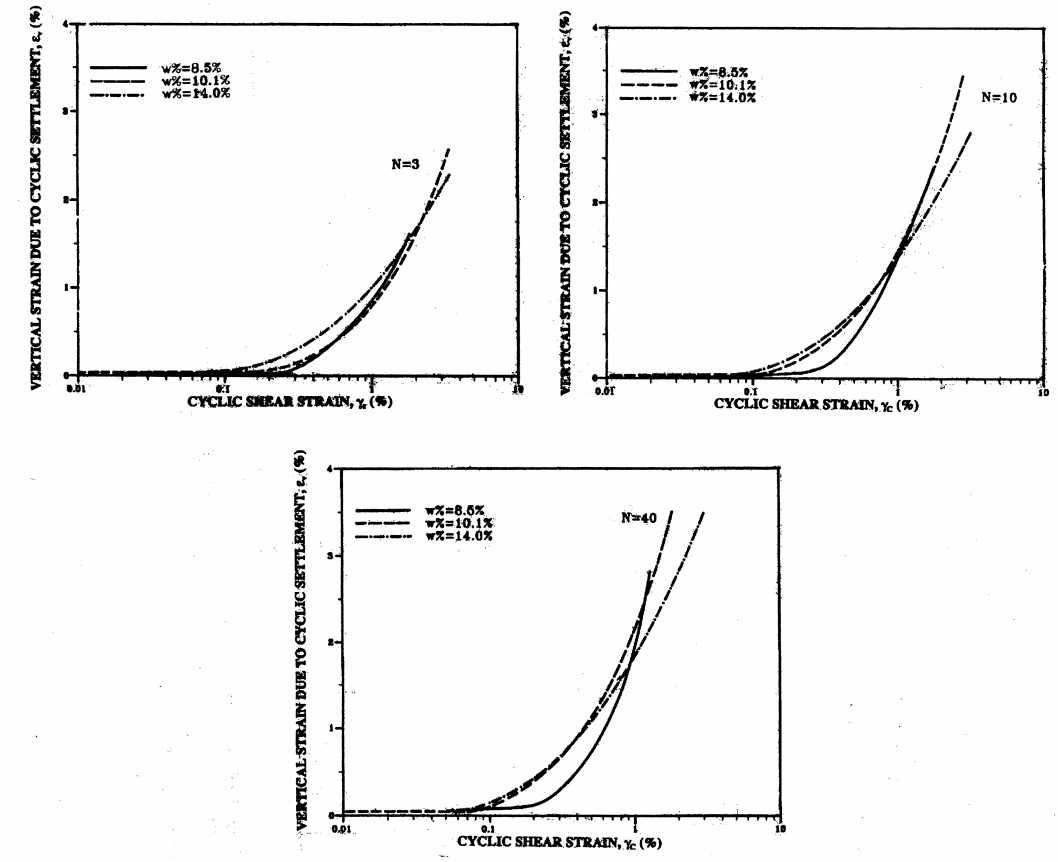

Fig. 5.2. The effect of *w* on settlements of a low-plasticity clay for *N* = 3, 10, and 40 cycles (Chu and Vucetic, 1992).

With respect to the second conclusion, it should be noted that specimens at different *w* in this testing program also had different preconsolidation Modified Proctor *RC,* which ranged from 95% to 100%. Hence, the effect of *w* was not truly isolated from the effect of *RC* in these tests. Moreover, the large compaction effort needed to produce the high *RC* in the tested samples would be expected to break down macro-structural features such as clods that might have been present at lower densities. Accordingly, the apparent lack of dependence of ε_v on *w* in this testing may not be applicable to the lower *RC* levels.

Hsu and Vucetic (2004) performed a similar set of tests to those reported above for Chu and Vucetic (1992). In the more recent testing program, seven different sands and clays were prepared to different saturations and tested in simple shear to evaluate the volumetric threshold shear strain, γ_{tv}. The threshold strains were found to be $\gamma_{tv} \approx 0.01$-0.02% for sands and $\gamma_{tv} \approx 0.04$-0.09% for clays having PI ≈ 30.

Hsu and Vucetic (2004) interpret their findings for a range of saturations in a manner similar to that of Tsukamoto et al. (2004) – namely, vertical strains occurring during cyclic shear are distinguished from those occurring following shear. Hsu and Vucetic (2004) found that the strains during shear are significantly impeded if the degree of saturation of the specimen is ≥ 90%. The density of the specimens tested by Hsu and Vucetic was not maintained at consistent values from specimen-to-specimen, and are not reported relative to a common standard such as relative compaction. Accordingly, the results cannot be compared to those from other studies discussed in this document.

Whang et al. (2004) performed a laboratory testing program on fill soils containing significant fines with varying levels of fines plasticity. Testing was performed on four specimens with nearly 50% fines contents and PI ranging from 2 to 15. The seismic compression

susceptibility of each specimen was evaluated using strain-controlled cyclic simple shear laboratory testing with the UCLA digitally-controlled simple shear (UCLA-DCSS) apparatus. Each soil material was compacted to a range of formation dry densities and degrees-of-saturation.

The results for a low plasticity soil (PI = 2) are summarized in Figure 5.3. Figure 5.3a shows a small effect of Modified Proctor relative compaction (*RC*) between *RC* ≈ 92 and 94%, and negligible effects of as-compacted degree of saturation. Figure 5.3b compares the test results for this low plasticity soil with fines to results for an equivalent clean sand prepared to a compatible relative density. The results indicate that the soil with low plasticity fines experiences less seismic compression than clean sands. While consistent with the aforementioned results of Pyke et al. (1975), this findings of reduced seismic compression as fines content increases contradicts the trend found in Chapter 4 for non-plastic fine-grained soils.

The results for a medium-plasticity soil (PI = 15) are summarized in Figure 5.4. Figure 5.4a shows that the seismic compression decreases not only with increasing *RC*, but also for moderate *RC*s decreases with increasing as-compacted degree-of-saturation (*S*). As shown in Figure 5.4b, at low *S*, volumetric strains from seismic compression are comparable to those for sand (at a common *RC*), whereas at high *S* the strains are approximately one-quarter of those for sand.

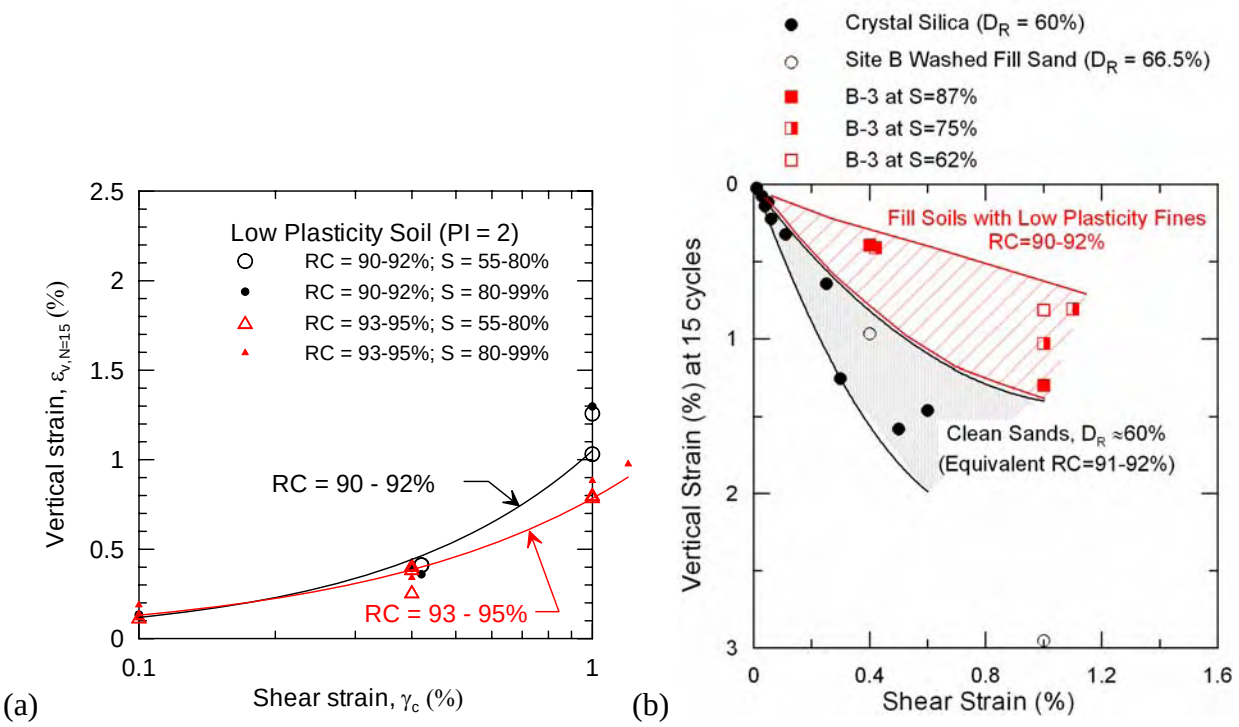

Fig. 5.3. Seismic compression test results for low-plasticity silty sand (Whang et al., 2004).

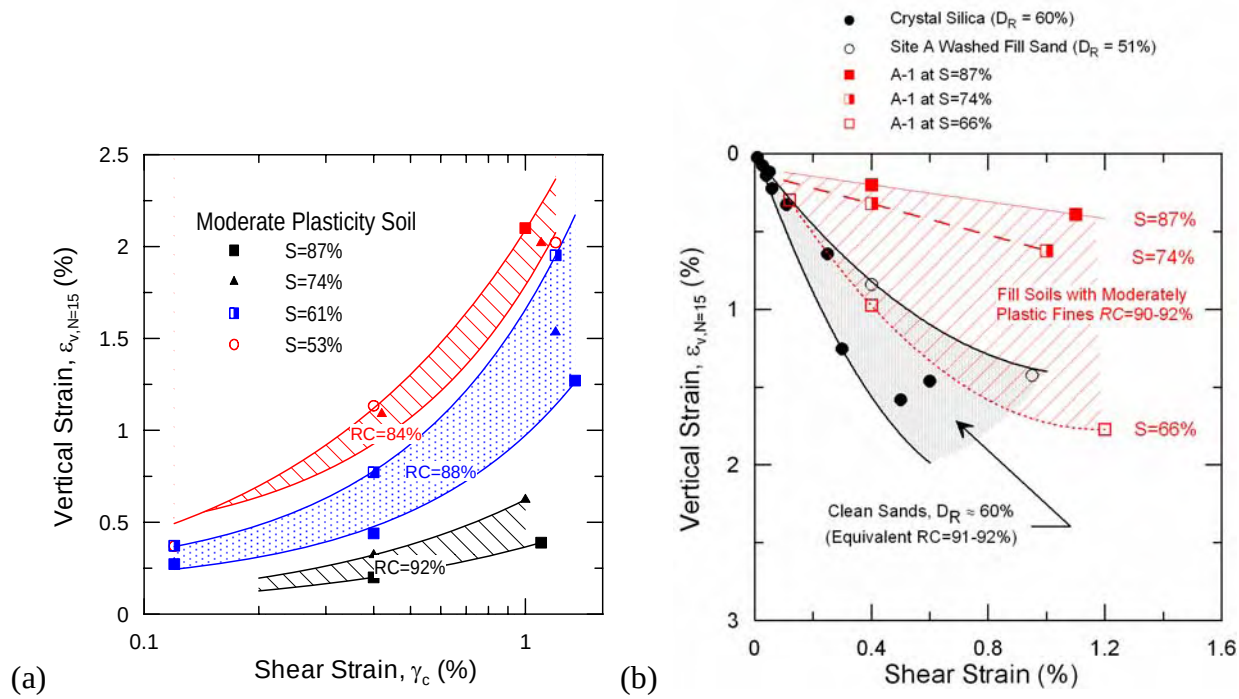

Fig. 5.4. Seismic compression test results for medium-plasticity clayey sand (Whang et al., 2004).

5.3 TESTING PERFORMED IN PRESENT RESEARCH

The testing performed as part of the present research had two principal objectives. The first was to test materials with a wide range of plasticities. In particular, we tested several materials with much higher plasticity than the maximum value of PI=15 in prior tests. Second, we investigate the effect of ageing (time under sustained load) for several fine-grained soils.

5.3.1 Testing Protocols

Laboratory testing was performed using the DCSS (Digitally Controlled Simple Shear) device at UCLA (Duku et al., 2007). Soil specimens were prepared to target values of saturation (*S*) and modified Proctor relative compaction (*RC*) using kneading compaction with a Harvard miniature compactor. Commercially available wire reinforced membranes were used to confine the 10 cm specimens Porous stones were placed above and below the specimens, and an O-ring sealed the wire reinforced membrane to the stones. After preparation, the specimen-stone-membrane assemblage was placed in the DCSS device and a specified overburden pressure (σ_c) was applied for a specified time (t_c). The density and corresponding relative compaction due to compression of the specimen under the seating load were noted. The specimens were subjected to cyclic loading with amplitude=γ_c and frequency=1 Hz. Vertical displacements were continuously monitored during compression under the seating load, shearing, and following cyclic shearing.

5.3.2 Soils Tested

The materials used in this investigation are summarized in Table 5.1. The first soil material listed in the table is a natural soil retrieved as a bulk sample from a site in southern California. The material was provided by Nirun Tungkongphanit of URS Consultants. The gradation curve for

the soil, as obtained from wet sieving and hydrometer tests (ASTM D2487 and D4221), is shown in Figure 5.5. The material has a fines content of 77% and a clay content (based on fraction smaller than 2 μm) of 2-3%. The mean grain size, D_{50} = 0.02 mm. Atterberg limits tests were performed according to ASTM D4318, with the results shown in Figure 5.6. Based on the gradation and Atterberg limits tests, the soil would classify as a low plasticity clay (CL) by the Unified Soil Classification System. Finally, a modified Proctor compaction curve (ASTM D1557) was developed for the soil, with the results shown in Figure 5.7.

Table 5.1. Soil indices and test conditions

Material	Confining stress (kPa)	[a] Fines Content (%)	[a] Liquid Limit	[a] Plastic Limit	[a] Plasticity Index	Max. Dry Density (kN/m^3)	Optimum water content (%)	In-situ Rel. Comp., RC (%)	In-situ Water Content (%)	Sat. at In-situ wc (%)
URS-A	101.1	77	48	21	27	18.6	14	87	13.3 - 19.9	60 - 90
								92	11.7 - 17.6	60 - 90
WL-A	25.5	31	28	0	np	18.2	14	88	15.0	70
WL-B1	50.5	65	42	25	17	17.8	13	88	22.5	90
WL-B2	50.5	74	64	31	33	17.2	17	82	22.5	60
								88	27.3	90
WL-C	25.5	75	58	32	26	16.8	19	82	25.0	70

[a] Atterberg limits performed according to ASTM D4318

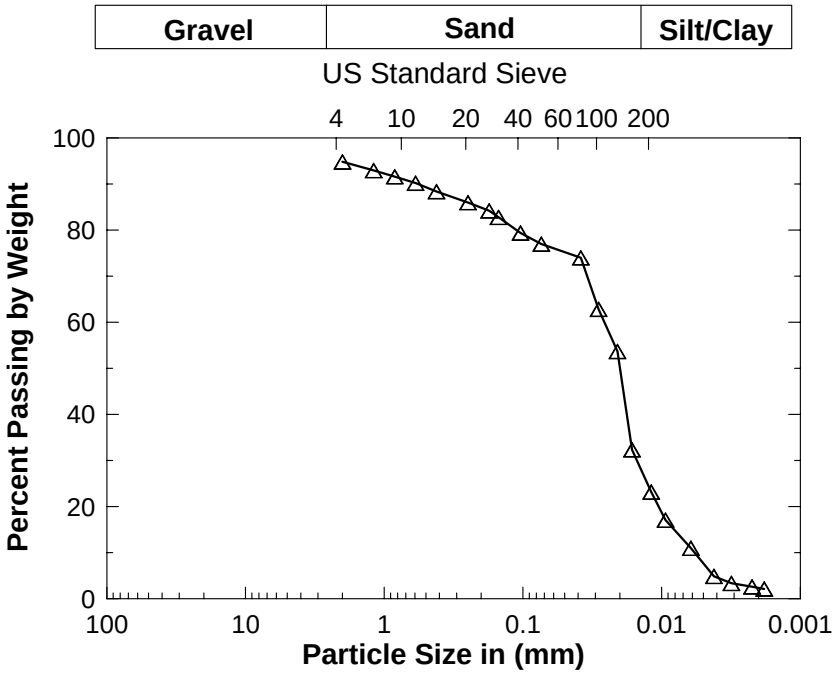

Fig. 5.5. Grain size distribution curve for the tested plastic clay soil.

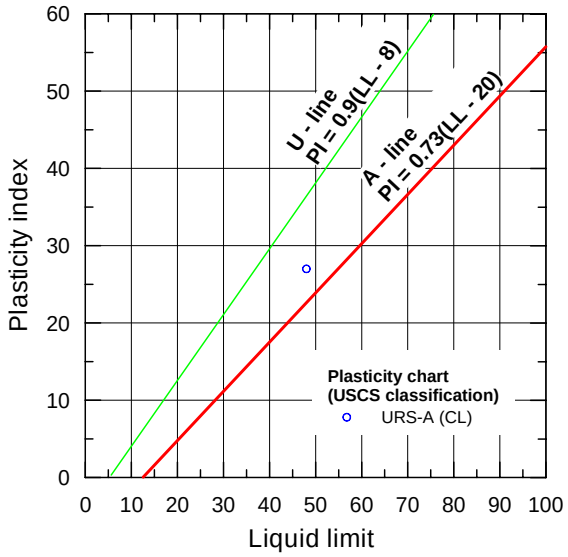

Fig. 5.6. Results of Atterberg limits tests for clayey soil.

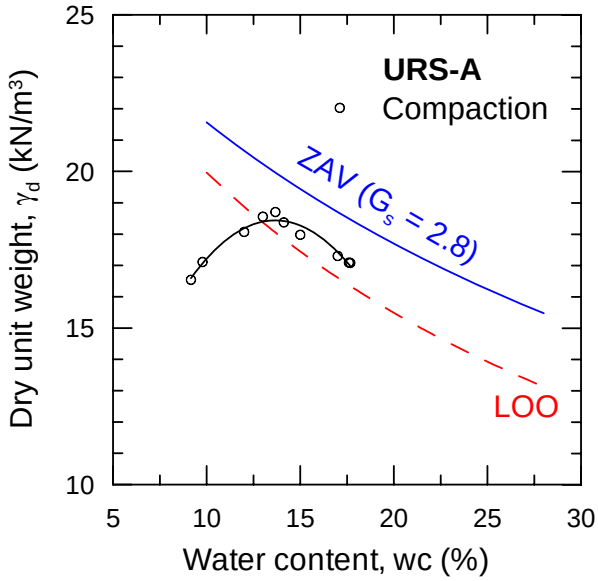

Fig. 5.7. Modified Proctor compaction curve for clayey soil.

The other four materials tested in this research were recovered from different portions of a single site in Westlake Village, California. The results of gradation and plasticity tests on these materials are summarized in Figures 5.8 and 5.9. The results of modified Proctor compaction tests on these materials are synthesized in Figure 5.10. Plasticity indices of the Westlake materials range from zero to 33, but three of the materials have high-plasticity (PI=25, 31, and 33). Based on the Unified Soil Classification System, these inorganic soils are classified as

shown in Figure 5.9. Also shown in Table 5.1 are in situ dry densities (expressed as a relative compaction with respect to modified Proctor standard), water content, and saturation conditions. The laboratory testing was directed toward reproducing those in situ conditions. Note that five of the specimens were tested on the dry side of optimum (S < 80%) and four on the wet side of optimum (S > 80%). Except for the URS-A material, the rest of the materials were confined at stresses < 101.3 kPa to match field conditions.

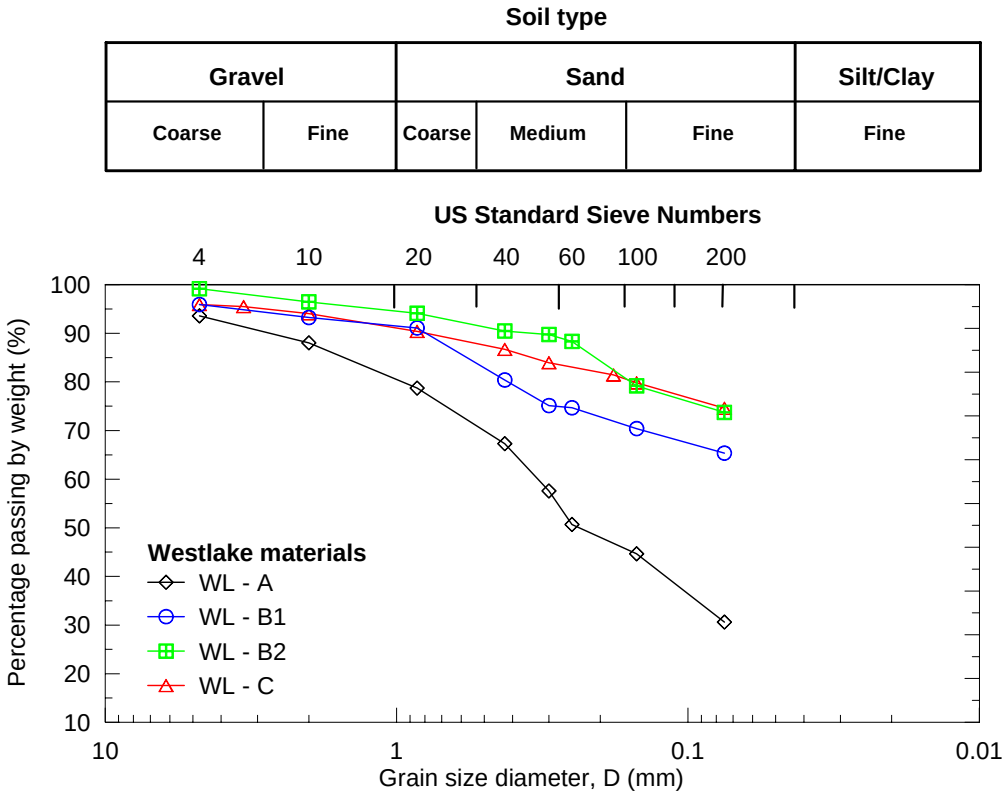

Figure 5.8. Grain size distribution for Westlake materials tested.

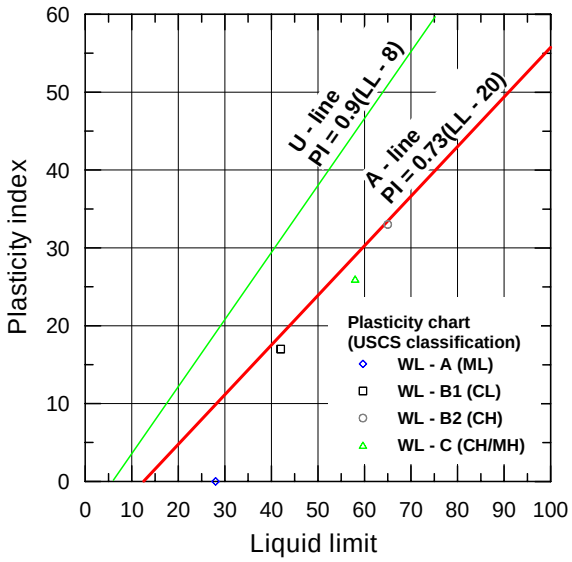

Figure 5.9. Atterberg test for Westlake materials with USCS classification shown in parenthesis.

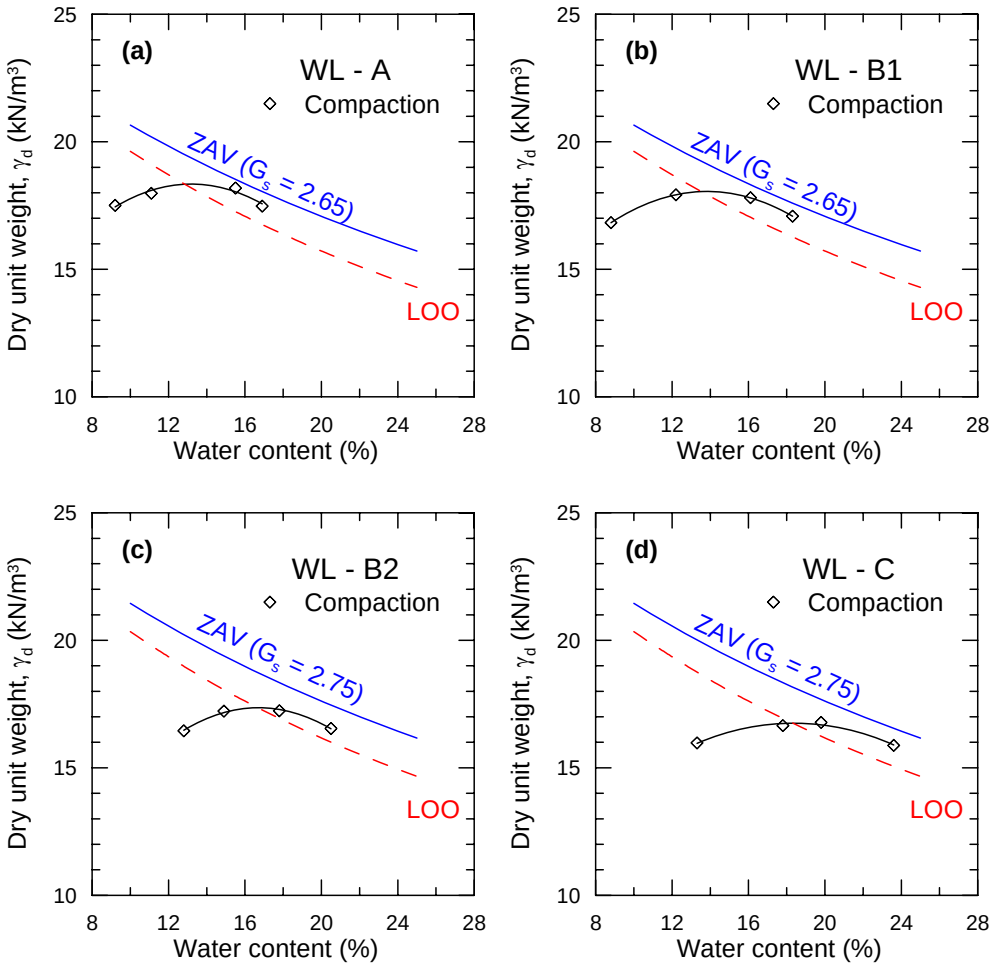

Figure 5.10. Compaction curves for Westlake materials tested shown together with ZAV (Zero Air Voids) curve and LOO (Line Of Optimum).

5.4 TEST RESULTS

The results in this section are segregated in terms of stress history. One group of specimens were tested under essentially normally consolidated (NC) conditions. A second group was placed on a sustained load for a an extended time period prior to dynamic loading. Volume change can occur under sustained load, which produces a pseudo-overconsolidated (OC) condition. All five materials listed in Table 5.1 were tested under NC conditions. Materials WL – A, WL – B1, WL – B2, and WL – C were also tested under OC conditions. This section is organized to present test data for NC materials in Section 5.3.1 and for OC materials in Section 5.3.2.

5.4.1 Test Results for Fine-Grained Plastic Soils

(a) Soil URS – A

The URS-A material consists of a high plasticity clay that was confined at 1.0 atm and tested across a range of relative compaction levels and saturation levels in a manner similar to the prior research of Whang et al. (2004) described in Section 5.2. The test results are synthesized in Figure 5.11. Figure 5.11(a) shows that vertical strains for the high-PI URS soil are much smaller than those for PI=15 materials by Whang et al. (2004). All of the test results in Figure 5.11(a) apply for a low RC level (87-88) and saturation levels dry of the line of optimums. Figure 5.11(b) shows that this high PI material demonstrates only a modest decrease of vertical strain with increasing RC. Figure 5.11(c) shows that for a given RC level, vertical strains are smaller for specimens prepared on the wet side of the line of optimum, which is consistent with previous findings for other materials (Whang et al., 2004). This phenomena is attributed to soil structure – namely, material on the dry side of the line of optimums has a clod structure that is susceptible to seismic compression, whereas material prepared on the wet side has a relatively continuum-like structure with lower seismic compression susceptibility.

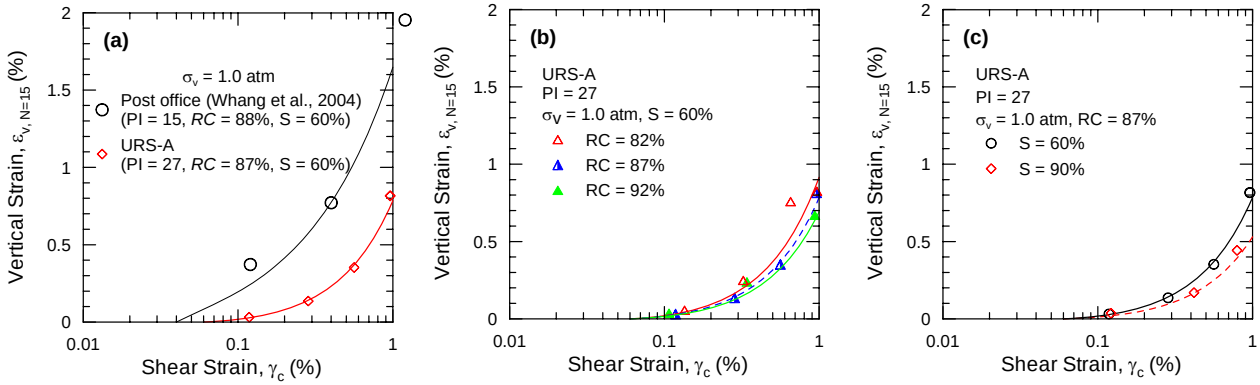

Figure 5.11(a) Effect of plasticity index on seismic compression, (b) saturation dependence for PI = 15 soil, and (c) saturation dependence for PI = 27 soil.

(b) Soil Westlake (WL) – A

Material WL - A consists of a relatively non-plastic, silty sand that was confined at 0.25 atm and compacted to RC = 88% at S = 65%. It was not practical to measure the plastic limit of this material and hence the PI is taken as zero. The relationship between vertical strain and shear strain for this material under the above conditions are shown in Figure 5.12.

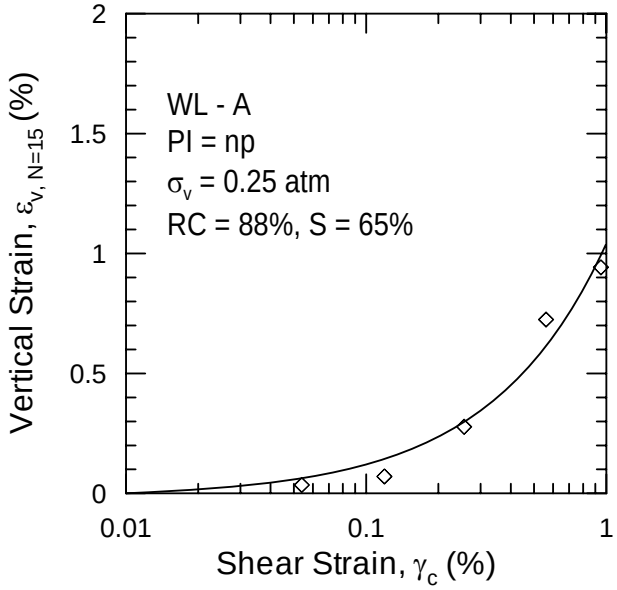

Figure 5.12 Seismic compression of Westlake A confined at 0.25 atm compacted to RC = 88% at S = 65%.

(c) Soil Westlake (WL) – B1

Material WL – B1 consists of a low plasticity clay that was tested at 0.5 atm overburden pressure. The material was compacted to *RC* = 88% at *S* = 89%. The relationship between vertical strain and shear strain for this material under the above conditions is shown in Figure 5.13.

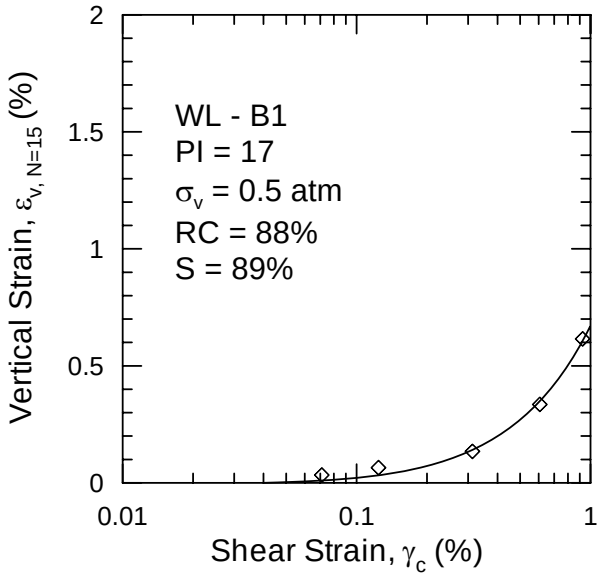

Figure 5.13. Seismic compression of Westlake B1 confined at 0.5 atm compacted to RC = 88% at S = 89%.

(d) Soil Westlake (WL) – B2

Material WL – B2 consists of a high plasticity clay that was tested at 0.5 atm overburden pressure. The material was compacted to *RC* = 80 and 88% at saturations of 61% and 89%, respectively. The relationship between vertical strain and shear strain for this material under the above conditions is shown in Figure 5.14. The results for the two different compaction conditions are similar.

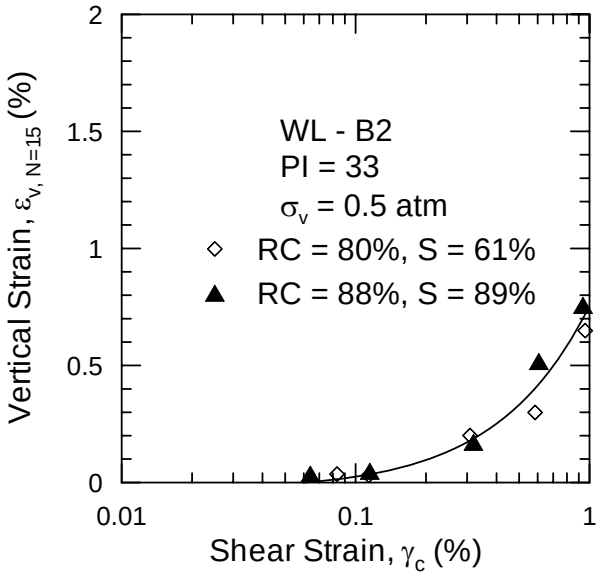

Figure 5.14. Seismic compression of Westlake B2 confined at 0.5 atm compacted to different RC at different S.

(e) Soil Westlake (WL) – C

Material WL – C consists of a high plasticity clay that was tested at 0.25 atm overburden pressure. The material was compacted to *RC* = 82% at *S* = 75%. The relationship between vertical strain and shear strain for this material under the above conditions is shown in Figure 5.15.

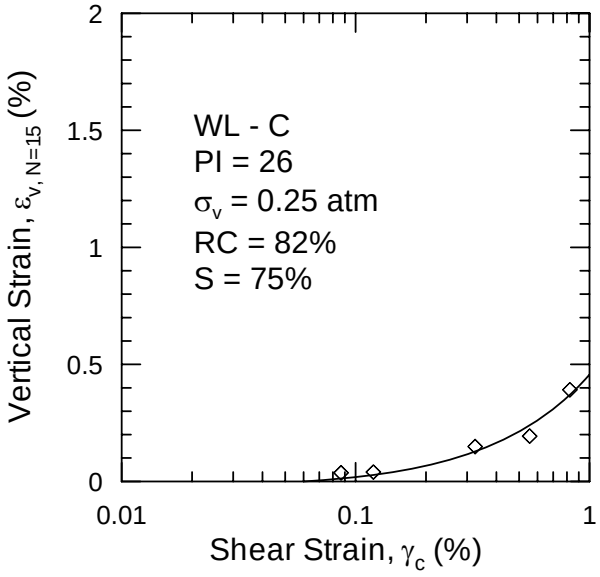

Figure 5.15. Seismic compression of Westlake C confined at 0.25 atm compacted to RC = 82% at S = 75%.

5.4.2 Seismic Compression of Pseudo-Overconsolidated (Aged) Soils

Ageing effects were investigated by testing multiple specimens of the same material (i.e., mineralogy and as-compacted density and water content) that have different times under sustained vertical load, t_c. Tests were performed on a non-plastic soil and multiple plastic soils, as described below. The results given here were originally presented by Duku et al. (2006).

(a) Non-plastic soil (Material WL-A)

Typical test results for Material WL-A are shown in Figure 5.16. Static compression histories for two specimens with t_c = 2 min. and 2 hr are shown in Figure 5.16(a); note that there is little secondary compression after the initial compression phase for this material. Vertical strains during 25 shear strain cycles and for 8 min following cyclic shearing are shown in Figure 5.16(b). Vertical cyclic strains are comparable for both specimens, and there is no significant post-cyclic shearing consolidation.

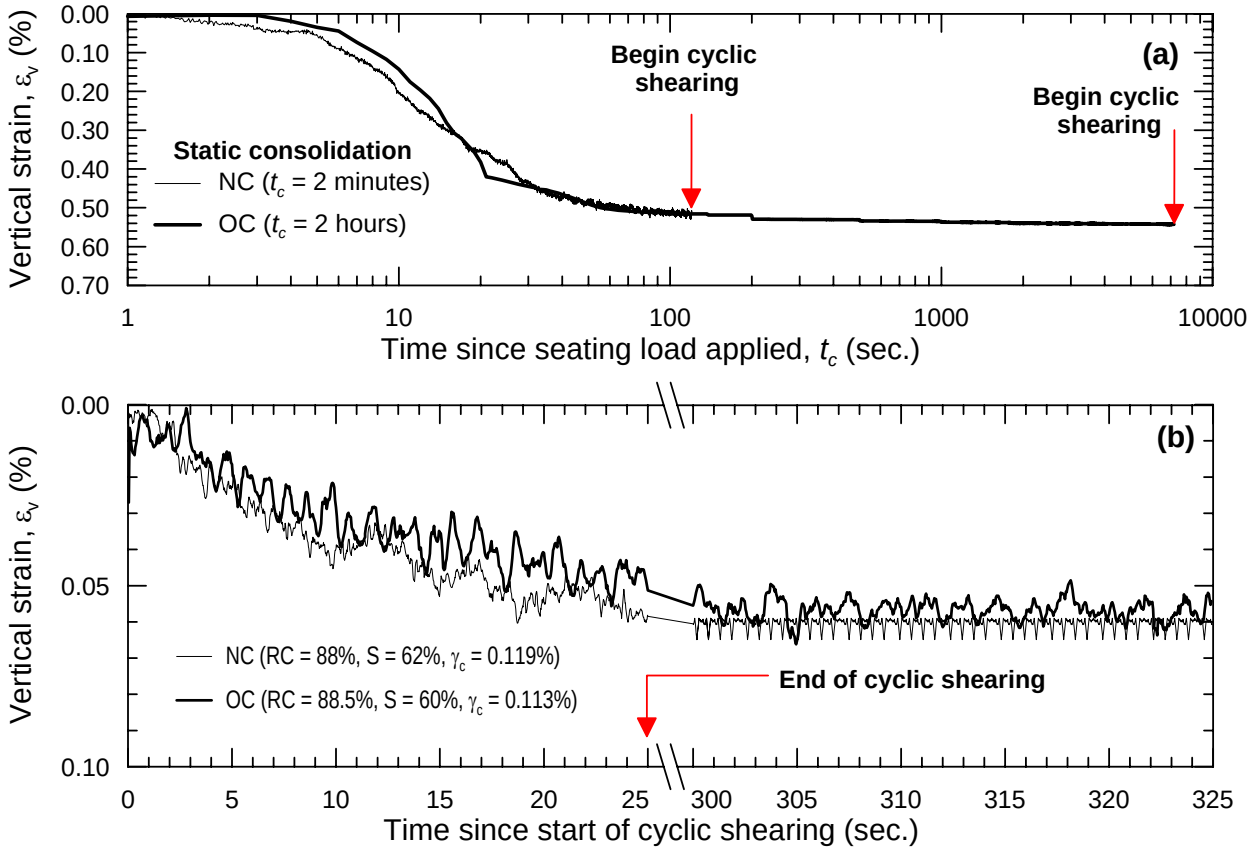

Figure 5.16. Material A (a) static consolidation and (b) seismic compression test results.

(b) Plastic soil (Materials WL-B1, WL-B2, WL-C)

Test results for Material WL-B2 are shown in Figure 5.17. Figure 5.17(a) shows static compression histories at 2 min (taken as NC conditinos) and 2 hrs (producing OC conditions). There is significant secondary compression following the initial consolidation for this material and cyclic shear in each case occurred during the secondary compression phase. Vertical strains during and following cyclic shearing at γ_c=0.95% are shown in Figure 5.17(b). Vertical cyclic strains are larger for the NC specimen than for the OC specimen. It is also notable that compression occurs following cyclic shearing for each of the specimens, although this compression is larger for the NC specimen. Similar trends were obtained for the other plastic soil specimens (WL-B1 and WL-C). A summary of test results for all the tested specimens is

provided in Table 5.2. The general features of the results described above occurred both for samples compacted to the wet and the dry side of the line of optimums.

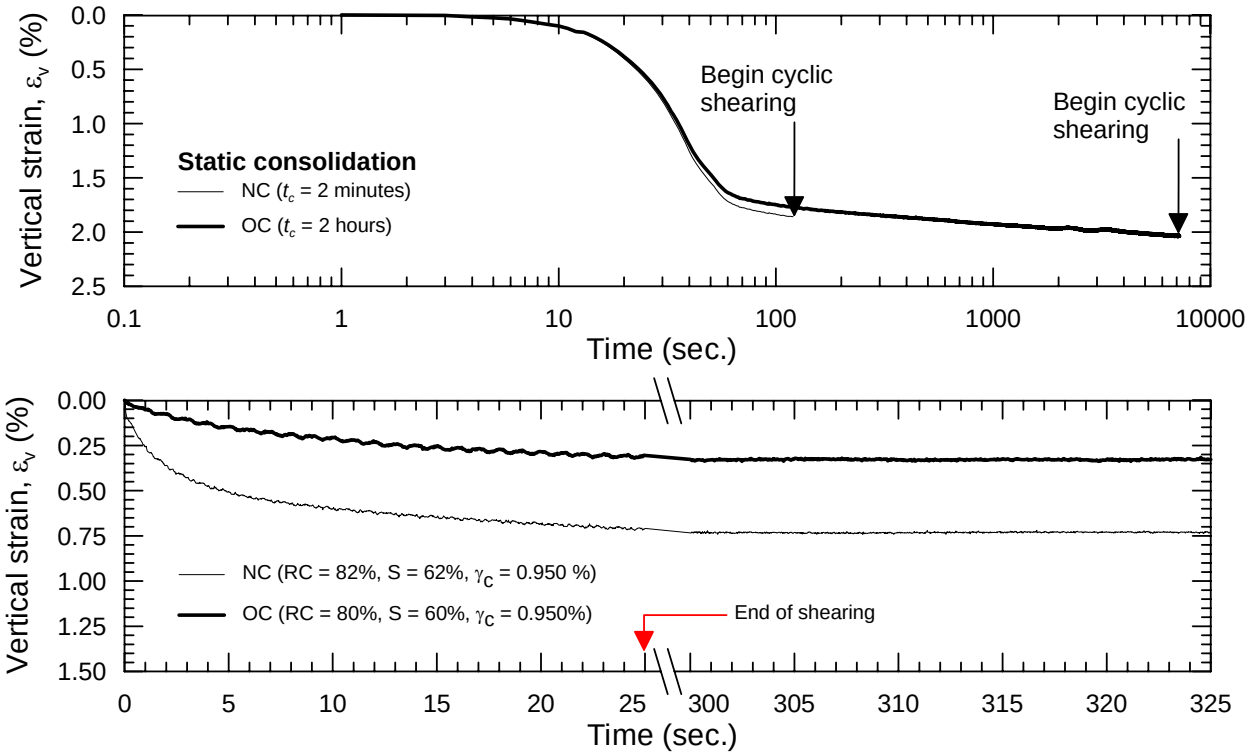

Figure 5.17. Material B2 (a) static consolidation and (b) seismic compression test results.

Relationships between vertical strains and shear strains for NC and OC specimens are shown in Figure 5.18 for materials WL-B1, WL-B2, and WL-C. The results show that ageing increases the volumetric threshold shear strain (γ_{tv}) to values between approximately 0.3 and 0.4% for these materials. Those values of γ_{tv} are much higher than previously observed values of 0.04% to 0.09% for NC soils (Hsu and Vucetic, 2004).

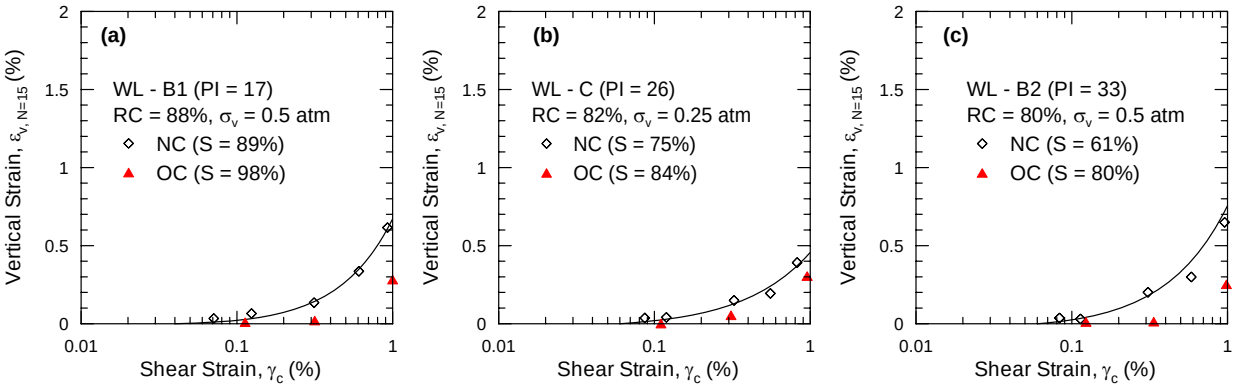

Figure 5.18. (a) – (c) Effects of ageing on seismic compression of plastic soils.

Table 5.2. Test results for materials tested to investigate the effects of ageing

Material	γ_c (%)	Rel. Comp., RC (%)[1]	p_c (kPa)	Sat. (%)[1]	t_{50} (sec)[2]	c_v (mm^2/s)[3]	t_c (sec)	$c_{\alpha\varepsilon}$ (%)[4]	$(\varepsilon_v)_{N=15}$ (%)	$(\varepsilon_v)_{N=25}$ (%)	ε_v after cyclic shear (%)[5]
A	0.119	88.0	26.2	62.9	12	2.65	120	0.015	0.036	0.055	0.000021
	0.281	87.6	26.2	60.4	14	2.27	120	0.01	0.035	0.056	0.000032
	0.583	86.0	26.2	61.3	15	2.12	120	0.01	0.283	0.337	0.000088
	0.964	86.6	26.2	62.3	12	2.65	120	0.01	0.739	0.867	0.000024
A	0.054	86.5	26.2	64.2	15	2.12	7200	0.02	0.035	0.054	0.000020
	0.113	87.3	31.0	63.7	16	2.05	7200	0.02	0.035	0.054	0.000034
	0.256	86.7	26.2	62.6	16	1.99	7200	0.02	0.277	0.327	0.000090
	0.561	88.4	26.2	65.9	18	1.77	7200	0.02	0.725	0.842	0.000021
	0.949	88.6	26.2	65.2	14	2.27	7200	0.02	0.942	1.064	0.000016
B1	0.124	86.0	48.3	90.3	20	1.59	120	0.40	0.065	0.094	0.036000
	0.313	86.4	51.7	90.3	20	1.59	120	0.45	0.134	0.176	0.093750
	0.607	85.5	51.7	89.0	25	1.27	120	0.40	0.336	0.395	0.040599
	0.925	86.1	51.7	87.9	22	1.44	120	0.43	0.615	0.694	0.022130
B1	0.113	86.2	51.7	97.0	60	0.53	7200	0.30	0.009	0.012	0.000240
	0.316	86.1	48.3	96.0	55	0.58	7200	0.33	0.021	0.025	0.000625
	1.000	86.8	51.7	95.0	65	0.49	7200	0.34	0.282	0.321	0.007066
B2	0.114	82.8	51.7	63.6	35	0.91	120	0.38	0.031	0.034	0.055418
	0.308	82.1	51.7	61.2	30	1.06	120	0.42	0.201	0.229	0.056713
	0.585	82.4	51.7	62.2	32	0.99	120	0.40	0.300	0.344	0.051441
	0.958	82.1	51.7	62.1	30	1.06	120	0.44	0.649	0.709	0.033461
B2	0.123	79.8	48.3	61.2	70	0.45	7200	0.20	0.011	0.037	0.000660
	0.336	78.4	48.3	58.6	75	0.42	7200	0.24	0.012	0.015	0.001050
	0.983	77.5	48.3	57.3	68	0.47	7200	0.19	0.252	0.305	0.025600
C	0.110	84.7	26.2	83.0	100	0.32	7200	0.20	0.001	0.011	0.000226
	0.310	84.1	26.2	80.6	105	0.30	7200	0.22	0.054	0.069	0.001392
	0.955	83.2	26.2	79.2	102	0.31	7200	0.18	0.305	0.374	0.008500

[1] Actual values following initial consolidation - may differ from target values in Table 1
[2] Time to 50% consolidation (e.g., see Holtz and Kovacs, 1981)
[3] Coefficient of consolidation
[4] Secondary compression coefficient (vertical strain per log cycle of time)
[5] Post cyclic vertical strain (over 1.5 log cycle of time)

It is apparent that the seismic compression potential of plastic soils decreases with time as secondary compression occurs (although the level of reduction cannot yet be quantified for general engineering application because a limited number of materials have been tested and the effects of initial density have not been investigated). We refer to this as an ageing effect. Plastic soils that experience ageing also appear to experience compression following cyclic shearing. Ageing and post-cyclic compression were not observed for a non-plastic soil. Our interpretation of these results is that secondary compression and ageing effects on seismic compression are linked. As secondary compression occurs, it appears that volumetric strain potential is reduced, resulting in less seismic compression susceptibility. This effect of secondary compression on seismic compression is not related to density increase – the increase in relative compaction from the volume change associated with secondary compression varies from nearly zero to about 0.3%, which should not significantly affect subsequent seismic compression.

5.5 SUMMARY AND RECOMMENDATIONS

As described in Section 5.2, prior to the present study, the database available for the development of volumetric strain material models for fine-grained soils essentially consisted of suites of tests for two materials tested by Whang et al. (2004). Those materials consisted of a low plasticity (PI = 2) silty sand and a medium plasticity (PI = 15) clayey sand.

In the present study, we have tested five additional plastic soils (characteristics listed in Table 5.1), which significantly expands the seismic compression database for fine-grained soils with measurable plasticity. In this section, we synthesize all of the available test data to develop preliminary recommendations regarding the seismic compression potential of plastic soils under normally consolidated conditions. We note that a large effect of ageing seems to be present for

some of these materials, but unfortunately the available information at this time is not sufficient to develop correction factors to apply to volumetric strains estimated for NC conditions.

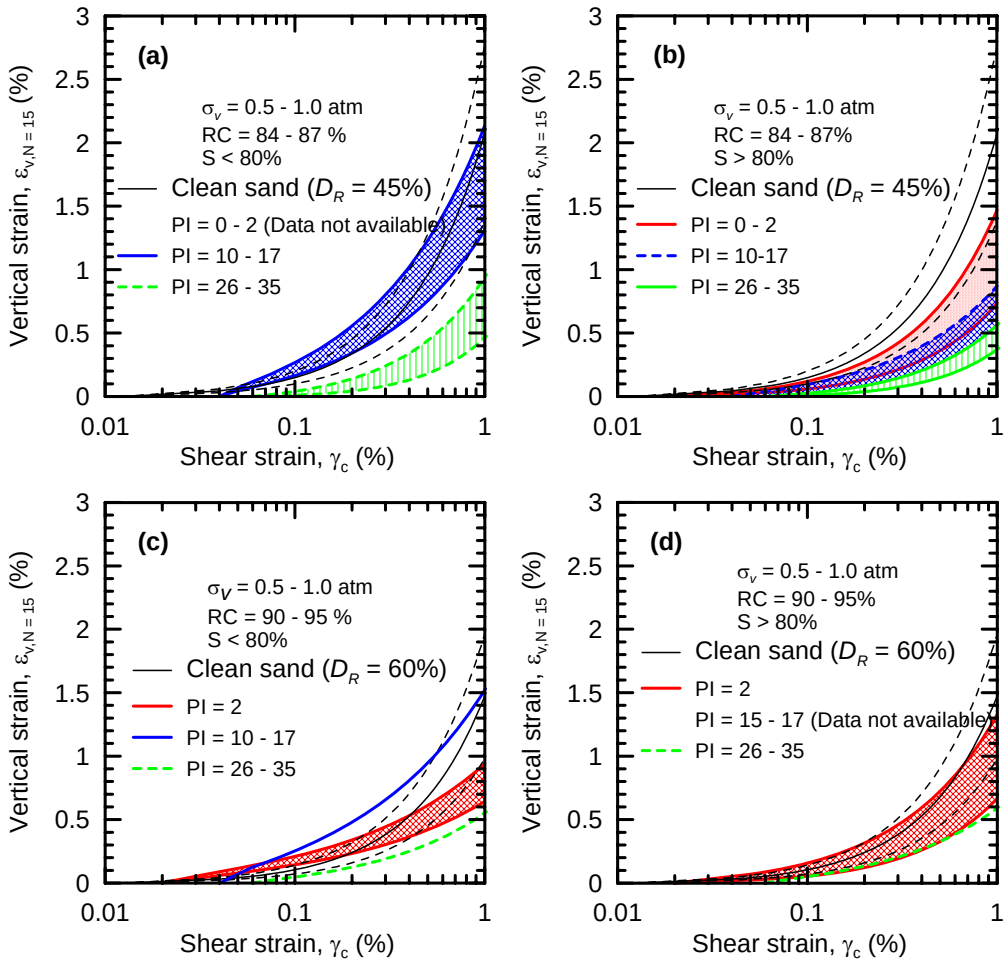

Figure 5.19. Seismic compression behavior of fine grained soils with measurable plasticity.

To develop the aforementioned guidelines, the test results are grouped based on plasticity index (PI), as-compacted relative compaction, and as-compacted degree of saturation. The grouping by PI is into the categories of nearly non-plastic (PI=0-2), marginal plasticity (PI=10-17) and high plasticity (PI=26-35). Many of the plastic soils tested to date exhibit only marginal dependence of vertical strains on relative compaction (RC), so only two RC groupings are made (84-87% and 90-95% modified Proctor). The segregation by as-compacted saturation

distinguishes materials having a clod structure (compaction on the dry side of the line of optimums, $S < 80\%$) from materials having more nearly a continuum structure (compaction on the wet side of optimum, $S > 80\%$)

Based on the above groupings, results for all tests on NC fine-grained, plastic soils are showed in Figure 5.19. Also shown for reference purposes is the mean ± *COV* of the clean sands model at a comparable RC (using empirical equation of Lee and Singh, 1971, to convert D_r to RC). The band of results shown for a given PI represents the scatter of the available data, which may be artificially high in some cases because of variable confining vertical stresses used in the tests.

Figures 5.19 (a) and (c) show results for materials dry of the line of optimums. There is a strong dependence of vertical strains on PI for these samples. The largest strains for low PI materials are comparable to those for clean sands. Figure 5.19(b) and (d) show similar results for materials compacted wet of the line of optimums. The vertical strains are significantly smaller, showing the strong effect of soil structure. As seen by comparing Figures 5.19(a) and (c) or (b) and (d), the effect of RC is relatively modest. A few caveats with respect to the use of Figure 5.19 should be noted:

- the results apply for NC materials (no ageing)
- the results apply for materials with large fines contents (to the point that fines dominate the soil behavior); the transitional effects of gradually increasing fines content have not been investigated
- the results apply for variable vertical loads, and no correction factors for the effects of vertical stress have been developed for fine-grained soils

6 SUMMARY

6.1 SCOPE OF RESEARCH

Seismic compression is defined as the accrual of contractive volumetric strains in unsaturated soils during strong shaking from earthquakes, and has been recognized as a major cause of seismically induced damage (i.e., Stewart et al., 2001, 2004; Wartman et al., 2003). As a result, there has been an increasing demand within the engineering profession for seismic compression analysis procedures as evidenced by the California Geological Survey's (CGS) recent requirement that analysis of seismic compression be included as part of the design process for critical projects such as school and hospital structures (CGS, 2004).

Existing methods for estimating seismic compression susceptibility include the Tokimatsu and Seed (1987) and Stewart and Whang (2003) procedures. However, these two procedures are based on laboratory test data for clean sands by Silver and Seed (1971) and soils with high fines content (FC ~ 50%) and low to moderate plasticity by Whang et al. (2004). Consequently, those analysis procedures remain limited in their applicability, because they only apply for a few specific soil characteristics. Accordingly, there is a major research need for laboratory testing to develop relations between shear strain demand and number of strain cycles to volumetric strains (termed a volumetric strain material model) that cover a broad range of soil types.

One of the central tasks of this research was to enhance the Digitally Controlled Simple Shear (DCSS) apparatus at UCLA for high quality dynamic soil testing. The principal recent

change to the device undertaken during the project period was the addition of a fully digital control system that has enhanced the device's control capabilities, particularly at high frequencies. This work is presented in Chapter 2 and Duku et al. (2007a).

A major component of the laboratory testing program involved developing a significantly enhanced database on the seismic compression of clean sands, and using this database to identify the critical factors affecting seismic compression of sand. A volumetric strain material model for sand was developed based on the data that accounts for the most critical controlling parameters. This work is presented in Chapter 3 and Duku et al. (2007b).

Additional laboratory work conducted as part of the present project involved testing compacted soils with fines. Testing was performed with non-plastic silty fines, and the effects of fines content and various compaction conditions was evaluated. This work is presented in Chapter 4 and Whang et al. (2005). Testing was also performed on samples with plastic fines. Test results were compiled for normally consolidated specimens, which were synthesized with previous test results to develop preliminary recommendations for seismic compression analysis of such soils. Testing was also performed on aged soils that experienced pseudo-overconsolidation to evaluate the effects of ageing on seismic compression susceptibility. This work is presented in Chapter 5 and Duku et al. (2006).

6.2 RESEARCH FINDINGS AND RECOMMENDATIONS

A state-of-the-art cyclic simple shear apparatus for soil testing has been developed at UCLA. The device is capable of uni-directionally commanding a sinusoidal signal with amplitude $\mu <$ 0.2 mm with the smallest errors at large displacements being approximately 1% in MIMO-PID control mode; negligible cross-coupling effects is observed when testing is conducted bi-

directionally. The device is also capable of reproducing strong earthquake motions; however, the tracking of weak motions is dominated by noise with zero mean and standard deviation = 0.00027 mm.

Our investigation of the seismic compression of clean sands involved the testing of 14 different clean sand materials. Compositional factors, saturation, frequency, mineralogy, and ageing were found to be insignificant. Factors that were found to be significant include relative density (D_R) and confining stress. Stress history was found to be insignificant over the range of normal pressures where compacted fills are typically overconsolidated. Based on these findings, a volumetric strain material model was developed for seismic compression analysis of clean sands.

The investigation of seismic compression behavior of non-plastic silty sands was conducted using materials with a range of as-compacted saturations (S), fines contents ($10 \leq FC \leq 50\%$), and relative compactions (RC). The effect of intermediate $S \approx 30\%$ was found to decrease vertical strains relative to values for dry ($S = 0\%$) and high saturation ($S \geq 60\%$) conditions, which produced similar amounts of vertical strains. The observed variation with saturation is likely related to matric suction in the soil, which is maximized at low saturation level ($S = 30\%$), and decreases towards zero or increases towards 60%. The effect of increasing non-plastic FC is to monotonically increase the seismic compression susceptibility when using constant RC as a basis for comparison. This result occurs in part because of the highly contractive nature of the non-plastic fines used in the present investigation. Other studies have found the opposite trend for soils with plastic fines; hence, fines plasticity seems to plays a major role in determining seismic compression susceptibility of high fines content soils.

The investigation of seismic compression behavior of soils with plastic fines was conducted using five medium to high plasticity materials. The soils were tested at a range of *RC*, *S*, and vertical stress. In addition, three of the materials were tested in such a way that the seismic compression of normally consolidated and pseudo-overconsolidated (i.e., aged) samples with otherwise similar characteristics could be compared. The results for normally consolidated soils show a strong decrease of seismic compression with increasing PI, significantly lower seismic compression potential for soils compacted wet of the line of optimums ($S > 80\%$), and only a modest effect of relative compaction. Ageing was found to significantly reduce the seismic compression potential of plastic soils but to not affect non-plastic soils.

REFERENCES

Alpan, I. (1967). "The empirical evaluation of the coefficient K_o and K_{oR}," *Soil and Foundation*, VII (1), 31 – 40.

Airey, D.W. and Wood, D.M. (1987). "An evaluation of direct simple shear tests on clay," *Geotechnique*, 37(1), 25-35

Amer, M.I., Kovacs, W.D., and Aggour, M.S. (1987). "Cyclic simple shear size effects," *Journal of Geotechnical Engineering*, 113(7), 693-707

American Society for Testing and Materials (ASTM D422). (2001). *Standard test method for particle-size analysis of soils*, ASTM, West Conshohocken, Pa.

American Society for Testing and Materials (ASTM D4253). (2001). *Standard test methods for maximum index density and unit weight of soils using a vibratory table*, ASTM, West Conshohocken, Pa.

American Society for Testing and Materials (ASTM D4254). *Standard test methods for minimum index density and unit weight of soils and calculation of relative density*, ASTM, West Conshohocken, Pa.

American Society for Testing and Materials (ASTM D5298-03). *Standard Test Method for Measurement of Soil Potential (Suction) Using Filter Paper*, ASTM, West Conshohocken, Pa.

Brandon, T.L., Duncan, J.M., and Gardner, W.S. (1990). "Hydrocompression settlement of deep fills," *J. Geotech. Engrg.*, ASCE, 116(10), 1536-1548.

Bray, J.D., Sancio, R.B., Riemer, M.F. and Durgunoglu, T. (2004). "Liquefaction Susceptibility of Fine-Grained Soils," *11th International Conf. On Soil Dynamics and Earthquake Engineering and 3rd International Conf. On Earthquake Geotechnical Engineering,* Berkeley, CA, Jan. 7-9, in press.

Bhatia, S., Schwab, J., and Ishibashi, I. (1985). "Cyclic simple shear, torsional shear, and triaxial – a comparative study," *Advances in the Art of Testing Soils under Cyclic Conditions,* Proceedings of a session sponsored by the Geotech. Engrg. Div., ASCE Convention, Detroit, 232-285

Bjerrum, L. and Landva, A. (1966). "Direct simple shear tests on a Norwegian quick clay," *Geotechnique*, 16(1), 1-20

Boulanger, R.W. (2003). "High overburden stress effects in liquefaction analyses," *J. Geotech. & Geoenv. Engrg.*, ASCE, 129 (12), 1071-1082.

Boulanger, R.W., Chan, C.K., Seed, H.B., Seed, R.B., and Sousa, J. (1993). "A low-compliance bi-directional cyclic simple shear apparatus," *Geotechnical Testing Journal*, ASTM, 16(1), 36-45

Budhu, M. (1985). "Lateral stresses observed in two simple shear apparatus," *Soils and Foundations*, 27(2), 31-41

Budhu, M., and Britto, A. (1987). "Numerical analysis of soils in simple shear devices," *Soils and Foundations*, 27(2), 31-41

California Geological Survey, CGS (2004). "Engineering geology and seismology for public schools and hospitals in California," Report to Accompany California Geological Survey Note 48 Checklist, Robert H. Sydnor (ed.).

Chang S. W., Bray, J. D., and Seed, R. B (1996). "Engineering implications of ground motions from the Northridge Earthquake," *Bull. Seism. Soc. Am.,* 86 (1B), S270-S288.

Cho, G., Dodds, J., and Santamarina, J. C. (2006). "Particle shape effects of packing density, stiffness, and strength: Natural and crushed sands," *J. Geotech. Engrg. Div.*, ASCE, 132(5), 591-602.

Chu, H.-H. and Vucetic, M. (1992). "Settlement of compacted clay in a cyclic direct simple shear device," *Geotech. Testing J.,* 15(4), 371-379.

Conte, J.P. and Trombetti, T.L. (2000). "Linear dynamic modeling of a uni-axial servo-hydraulic shaking table system," *Earthquake Engineering Structural Dynamics*, 29: 1375-1404

DeGroot, D.J., Ladd, C.C. and Germaine, J.T. (1996). "Undrained multidirectional direct simple shear behavior of cohesive soil," *Journal of Geotech. Engrg*., ASCE, 122(2), 91-98

Doroudian, M. and Vucetic, M., (1995). "A direct simple shear device for measuring small-strain behavior," *Geotechnical Testing Journal*, ASTM, 18(1), pp. 69-85.

Duku. P.M. (2007). "Seismic compression of soils with plastic and non-plastic fines." Ph.D. Thesis, University of California, Los Angeles.

Duku, P.M., Stewart, J.P., Whang, D.H., and Venugopal, R. (2007). "Digitally Controlled Simple Shear Apparatus for Dynamic Soil Testing," *Geotechnical Testing Journal*, ASTM, in press.

Duku, P.M., Stewart, J.P., and Whang, D.H. (2006). "Effects of post-compaction ageing on seismic compression of fine-grained soils," *GeoShanghai International Confereence*, Shanghai, China, June 6-8.

Duncan J. M., Williams G. W., Sehn A. L., and Seed R. B. (1991). "Estimation of earth pressure due to compaction," *J. Geotech. Engrg*., ASCE, 117 (12), 1833 – 1847.

Dyvik, R., Berre, T., Lacasse, S., and Raadim, B. (1987). "Comparison of truly undrained and constant volume direct simple shear tests," *Geotechnique*, 37, 3-10.

Dyvik, R., Zimmie, T. F., and Floess, C. H. L. (1981). "Lateral stress measurements in direct simple shear device," *Laboratory shear strength of Soil*, ASTM STP 740, 191-206.

Elgamal, A., Yang, Z., Lai, T., Kutter, B. L., and Wilson, D. W. (2005). "Dynamic response of saturated sand in laminated centrifuge container," *Journal of Geotech. and Geoenvg. Engrg.*, ASCE, 131(3), pp. 598-609.

Finn, W. D. L. (1981). "Liquefaction potential: developments since 1976," *Proc. 1st Int. Conf. Recent Adv. Geotech. Earthquake Engrg. Soil Dyn., St. Louis* 2. 655-681.

Franklin, F. G., Powell, J. D. and Workman, L. M. (1990) *Digital Control of Dynamic Systems, 2nd Edition,* Addison-Wesley, pp. 430-480.

Harder, L.F., Jr., and Boulanger, R.W. (1997). "Application of K_σ and K_α correction factors," *Proc., NCEER Workshop on Evaluation of Liquefaction Resistance of Soils, Rep. No. NCEER-97-0022*, National Center for Earthquake Engineering Research, SUNY Buffalo, N.Y., 167-190.

Hazirbaba, K. and Rathje, E.M. (2004). "A comparison between in situ and laboratory measurements of pore water pressure generation," *13th World Conference on Earthquake Engineering*, Vancouver, Canada, August. Paper No. 1220

Hsu, C.-C. and Vucetic, M. (2004). "Volumetric threshold shear strain for cyclic settlement," *J. Geotech. & Geoenv. Engrg.*, ASCE, 130 (1), 58-70.

Houston, S.L., Houston, W.N., and Spadola, D.J. (1988). "Prediction of field collapse of soils due to wetting," *J. Geotech. Engrg.*, ASCE, 114 (1), 40-58.

Idriss, I.M., and Boulanger, R. W. (2003). "Estimating K_α for use in evaluating cyclic resistance of sloping ground," *Proceedings of 8th US-Japan Workshop on Earthquake Resistant Design of Lifeline Facilities and Countermeasures against Liquefaction*, Hamada, O'Rourke, and Bardet, eds., Report MCEER-03-0003, MCEER, SUNNY, Buffalo, N.Y., 449-468.

Ishihara, K., and Koseki, J., (1989). "Discussion on the cyclic shear strength of fines-containing sands." *Proc. of the Eleventh Inter. Conf. on Soil Mechanics and Foundation Engrg.*, Rio de Janiero, Brazil, 101-106.

Ishihara, K., and Takatsu, H. (1979). "Effects of overconsolidation and K_0 conditions on the liquefaction characteristics of sands," *Soils and Found*ations, 19(4), 59-68.

Ishihara K. and Nagase, H. (1988). "Multi-directional irregular loading tests on sand," *Soil Dynamics and Earthquake Engineering*, 7(4), 201-212

Ishihara, K. and Yamazaki, F. (1980). "Cyclic simple shear tests on saturated sand in multi-directional loading," *Soils and Foundations*, 20 (1)

Jafazadeh, R. and Yanagisawa, E. (1998). "Behavior of saturated sand models in multi-directional shaking table tests," *Eleventh World Conference on Earthquake Engineering*, Pergamon, Elsevier, Paper No. 1049

Jaky, J. (1944). "The coefficient of earth pressure at rest," *Journal of the Society of Hungarian Architects and Engineers*, 78(22), 355-358.

Kokusho, T., Hara, T., and Hiraoko, R. (2004). "Undrained shear strength of granular soils with different particle gradations," *J. of Geotech. & Geoenvr. Engrg.*, ASCE, 130 (6), 621-629.

Kusakabe, S., Morio, S., Okabayashi, T., Fujii, T., and Hyodo, M. (1999). "Development of

a simplified simple shear apparatus and its application to various liquefaction tests," *Journal of Geotechnical Engineering*, JSCE, 617 (III/46), 299-304. In Japanese.

Kutter, B. L. (1995). "Recent advances in centrifuge modeling of seismic shaking," *3rd International Conference on Recent Advances in Geotechnical Earthquake Engineering and Soil Dynamics,* St. Louis, Missouri, April. Vol. 2, 927-940.

Ladd, R.S. (1974). "Specimen preparation and liquefaction of sands." *J. Geotech. Engrg. Div.,* ASCE, 100(10), 1180-1184.

Lawson, A.C., ed. (1908). "Minor geologic effects of the earthquake," *California earthquake of April 18, 1906,* Publ. 87, Vol. 1, Part 2, Carnegie Institute of Washington, D.C., 384-409.

Lawton, E., Fragaszy, R.J., and Hardcastle, J.H. (1989). "Collapse of compacted clayey sand" *J. Geotech. Engrg.,* ASCE, 115 (9), 1252-1266.

Lee, K.L., and Fitton, J.A., (1968). "Factors affecting the cyclic loading strength of soil." *Vibration Effects of Earthquakes on Soils and Foundations,* ASCE STP 450, 71-95.

Lee, K. L., and Focht, J. A. (1975). "Liquefaction potential of Ekofisk tank in North Sea," *J. of the Geotech. Engrg. Division*, ASCE, 100(1), 1-18.

Lee, K. L., and Singh, A. (1971). "Compaction of granular soils," *Proceedings of the 9th Annual Engineering Geology and Soils Engineering Symposium*, Idaho Department of Highways, Boise, Idaho.

Lefebvre, G. and Pfender, P. (1996). "Strain rate and preshear effects in cyclic resistance of soft clay," *Journal of Geotech. Engrg.*, ASCE, 122(1), 21-26

Lucks, A.S., Christian, J.T., Brandow, G.E. and Hoeg, K. (1972). "Stress conditions in NGI simple shear test," *J. Soil Mech. Found. Div*., ASCE, 98(1), 155-160.

Martin, G. R, Finn, W. D. L., and Seed, H. B. (1975). “Fundamentals of liquefaction under cyclic loading,” *J. of the Geotech. Engrg. Division*, ASCE, 101(5), 423-438.

McClure, F.E. (1973). *Performance of single family dwellings in the San Fernando earthquake of February 9, 1971*. NOAA, U.S. Dept. of Commerce, May.

Mulilis, P.J., Seed, H.B., Chan, C., Mitchell, J.K., and Arulanandan, K. (1977). “Effect of sample preparation on sand liquefaction.” *J. of the Geotech. Engrg. Div.*, ASCE, ï ð í (2), 91-109.

National Research Council, NRC (1985). *Liquefaction of soils during earthquakes*, Committee on Earthquake Engineering, Commission on Engineering and Technical Systems, National Academy Press.

Ohara, S., and Matsuda, H. (1988). “Study on the settlement of saturated clay layer induced by cyclic shear,” *Soils and Foundations*, Japanese Society of Soil Mechanics and Foundation Engrg., 28(3), 103-113.

Polito, C.P. (1999) “The effects of nonplastic and plastic fines on the liquefaction of sandy soils.” *PhD Thesis*. Virginia Polytechnic Institute and State University, Blacksburg, VA.

Polito, C. P., and Martin, J. R. (2001). “Effects of nonplastic fines on the liquefaction resistance of sands,” *J. Geotech. & Geoevn. Engrg.*, ASCE, 127(5), 408-415.

Pyke, R., Seed, H.B., Chan, C.K. (1975). “Settlement of sands under multidirectional shaking,” *J. Geotech. Engrg.*, ASCE, 101 (4), 379-398.

Riemer, M.F. and Seed, R.B. (1997). “Factors affecting apparent position of steady-state line,” *Journal of Geotech. Engrg.*, ASCE, 123(3), 281-288

Saada, A.S., Fries, G. and Ker, C.C. (1982). “An evaluation of laboratory testing techniques in soil mechanics,” *Soils and Foundations*, 23(2), 381-395

Shahnazari and Towhata (2001). “Torsion shear tests on cyclic stress-dilatancy relationship of sand,” *Soils and Foundation*, Japanese Geotechnical Society, 42(1), 105-119.

Sheahan, T.C., C.C. Ladd and Germaine, J.T. (1996) “Rate dependent undrained shear behavior of saturated clay,” *Journal of Geotechnical Engineering*, ASCE, 122(2), 99-108.

Shen, C.K., Sadigh, K. and Herrmann, L.R. (1978). “An analysis of NGI simple shear apparatus for cyclic load testing,” *Dynamic Geotechnical Testing*, STP 654, ASTM, Philadelphia, PA, 148-162

Tokimatsu, K. and Seed, H.B. (1987). “Evaluation of settlements in sands due to earthquake shaking.” *J. Geotech. Engrg.*, ASCE, 113(8), 861-878.

Seed, B. H., Pyke, R. M., and Martin, G. R. (1977). “Effect of multidirectional shaking on pore pressure development in sands,” *J. of the Geotech. Engrg. Division*, ASCE, 104(1), 27-43.

Silver, M.L. and Seed, H.B. (1971). “Volume changes in sands due to cyclic loading,” *J. Soil Mech. & Found. Div.*, ASCE, 97 (9), 1171-1182.

Stamatopoulos, C. A., Balla, L. N., and Stamatopoulos, A. C. (2004). “Earthquake-induced settlement as a result of densification, measured in laboratory tests,” *13th World Conference on Earthquake Engineering*, Vancouver, B.C., Canada.

Stewart, J.P., Bray, J.D., McMahon, D.J., Smith, P.M., and Kropp, A.L. (2001). “Seismic performance of hillside fills,” *J. Geotech. & Geoenv. Engrg.*, ASCE, 127 (11), 905-919.

Stewart, J.P., Smith, P.M., Whang, D.H., and Bray, J.D. (2004). "Seismic compression of two compacted earth fills shaken by the 1994 Northridge earthquake," *J. Geotech. & Geoenv. Engrg.*, ASCE, 130 (5), 461-476.

Stewart, J.P., and Whang, D.H. (2003). "Simplified procedure to estimate ground settlement from seismic compression in compacted soils," *Proc. of the 2003 Pacific Conference on Earthquake Engrg.*, New Zealand Society for Earthquake Engrg., Paper No. 046

Tatsuoka, F., and Silver, M.L. (1981). "Undrained stress-strain behavior of sand under irregular loading," *Soils and Foundations*, 21(1), 51-66

Thevanayagagam, S. (1998). "Effect of fines and confining stress on undrained shear strength of silty sands," *J. Geotech. & Geoenv. Engrg.*, ASCE, 124 (6), 479 – 491.

Tokimatsu, K. and Seed, H.B. (1987). "Evaluation of settlements in sands due to earthquake shaking." *J. Geotech. Engrg.*, ASCE, 113(8), 861-878.

Tsukamoto, Y., Ishihara, K., Sawada, S., and Kanno, T. (2004) "Residual deformation characteristics of partially saturated sandy soils subjected to seismic excitation," *11th International Conf. on Soil Dynamics and Earthquake Engineering*, Vol. 1, 694-701.

Vaid, Y.P., Sivathayalan, S., and Stedman, D. (1999). "Influence of specimen reconstitution method on the undrained response of sand." *Geotechnical Testing Journal*, ASTM, 2(3), 187-195.

Van Overschee, P. and De Moor, B. (1995), "A unifying theorem for three subspace system identification algorithms," *Automatica*, 31(12), pp. 1853-1864.

Vucetic, M. and Lacasse, S. (1982). "Specimen size effect in simple shear test," *Journal of Geotech. Engrg.* Div., ASCE, 108(12), 1567-1585

Wartman, J., Rodriguez-Marek, A., Repetto, P.C., Keefer, D.K., Rondinel, E., Zegarra-Pellane, J., and Baures, D. (2003). "Ground failure," *Earthquake Spectra*, 19(S1), 35-56.

Wilson, D. W., Boulanger, R. W., Feng, X., Hamann, B., Jeremic, B., Kutter, B. L., MA, K., Santamarina, C., Sprott, K. S., Velinsky, S. A., Weber, G., and Ben Yoo, S. J. (2004).

"The NEES geotechnical centrifuge at UC Davis" *13th World Conference on Earthquake Engineering*, Vancouver, Canada, August. Paper No. 2497.

Whang, D. (2001). "Seismic compression of compacted fills." *Ph.D. Thesis*, University of California, Los Angeles.

Whang, D.W., Stewart, J.P., and Bray, J.D. (2004). "Effect of compaction conditions on the seismic compression of compacted fill soils," *Geotechnical Testing Journal*, ASTM, 27(4), 371-379

Whang, D.H., Moyneur, M.S., Duku, P.M., and Stewart, J.P. (2005). "Seismic compression behavior of non-plastic silty sands," *Proceedings of an International Symposium on Advanced Experimental Unsaturated Soil Mechanics*, A. Tarantino, E. Romero, and Y.J. Cui (eds.), Trento, Italy, June 27-29, A.A. Balkema Publishers, pp 257-263.

Whang, D.H., Stewart, J.P., and Bray, J.D. (2004). "Effect of compaction conditions on the seismic compression of compacted fill soils," *Geotechnical Testing Journal*, ASTM, 27(4), 1-9.

Yamamuro, J. A., and Wood, F. M. (2004). "Effect of depositional method on the undrained behavior and microstructure of sand and silt," *Soil Dynamic and Earthquake Engineering*, Elsevier, 24, 751-760.

Yasuda, S., Wakamatsu, K., and Nagase, H., (1994). "Liquefaction of artificially filled silty sands." *Ground Failures Under Seismic Compression*, Geotech. Special Publication No. 44, ASCE, 91-104.

Youd, T. L. (1972). "Compaction of sands by repeated shear straining," *J. Soil Mech. & Found. Div.*, ASCE, 98 (7), 709-725.

Youd, T. L., and Craven, T. N. (1975). “Lateral stress in sands during cyclic loading,” *Journal of Geotech. Engrg. Division*, ASCE, 101 (GT2), 217-221.

Zettler, T.E., Frost, J.D., and DeJong, J.T. (2000). “Shear-induced changes in HDPE geomembrane surface topography,” *Geosynthetics International*, Vol. 7(3), 243-267.

Zlatovic, S. and Ishihara, K. (1997). *On the influence of nonplastic fines on residual strength*, Earthquake Geotechnical Engineering, Balkema, Rotterdam